Numerical Methods for the Continuation of Invariant Tori

A Thesis
Presented to
The Academic Faculty

by

Bryan Rasmussen

In Partial Fulfillment
of the Requirements for the Degree
Doctor of Philosophy

School of Mathematics
Georgia Institute of Technology
December 2003

Numerical Methods for the Continuation of Invariant Tori

Approved by:

Luca Dieci, Advisor	Guillermo Goldsztein
Konstantin Mischaikow	Andrzej Szymczak
Evans Harrell	

Date Approved: November 4, 2003

To Amanda and our child

ACKNOWLEDGEMENTS

First and foremost, the author thanks his advisor for being available for frequent discussions about hyperbolicity, Fréchet derivatives, and other minutiae. Thanks also go to the School of Mathematics at Georgia Tech for supporting the author financially with a teaching assistantship for two years, and to the National Science Foundation (and hence the taxpayers of the U. S.) for supporting the author on a research assistantship for the rest of his time here. Finally, the author thanks his wife, Amanda.

TABLE OF CONTENTS

LIST OF TABLES

LIST OF FIGURES

LIST OF SYMBOLS

A, B, etc.	Matrices, unless otherwise specified.
$\mathbf{x}$, $\mathbf{y}$, etc.	Vectors, unless otherwise specified.
a, b, etc.	Scalar parameters, unless otherwise specified.
$A, \mathbf{x} > a$	Component-wise $> a$.
$A, \mathbf{x} \geq a$	Component-wise $\geq a$.
$A >_p 0$	Matrix A is positive definite.
$A \geq_p 0$	Matrix A is positive semi-definite.
$\mathbb{R}^n$	n-dimensional real space.
$\mathcal{C}^k$	The space of k-continuously-differentiable functions.
S^n	n-dimensional sphere.
T^p	p-dimensional torus ($S^1 \times S^1 \times \cdots \times S^1$, p times).
$\widetilde{T}^p$	Discrete p-dimensional torus.
x_i	i^{th} component of vector $\mathbf{x}$, or i^{th} element of list $\mathbf{x}$.
$(x_i)_j$	i^{th} component of i^{th} element of a list.
$x^{(i)}$	i^{th} iteration of a discrete transformation.
$\mathbf{x}_{\phi_i}$	Partial derivative of $\mathbf{x}$ with respect to ϕ_i
$\dot{x}$	Time-derivative of x.
A^T	Transpose of matrix A.
$\mathcal{S}^\perp$	Orthogonal complement of space, $\mathcal{S}$.
$\|\bullet\|$	Euclidian vector or matrix norm.
$\|\bullet\|_e$	Special vector or matrix norm, defined in Chapter 3.
$\|\bullet\|_\infty$	Infinity vector or matrix norm ($\|\mathbf{x}\|_\infty = \max_i \|x_i\|$).
$\mathcal{T}_\mathbf{x}$, $\mathcal{N}_\mathbf{x}$	Tangent and normal spaces to a manifold at a point $\mathbf{x}$.

$D_{\boldsymbol{\phi}}$	(possibly partial) Jacobian with respect to $\boldsymbol{\phi}$.
G^t	Hadamard graph transform.
I_n	$\mathbb{R}^n$ identity matrix.
J	Jacobian matrix.
L	Lipschitz constant.
M	Manifold, bounding constant, or preconditioner.
N	Number of points.
$\mathcal{O}$	Order.
P	Permutation matrix.
R_θ	Rotation matrix by angle θ.
m	Maximum curvature.
n	Dimension of a space.
p	Dimension of a manifold.
q	Co-dimension of an embedded manifold $(n-p)$.
t	Time.
$\mathcal{V}$	Vertices of a box.
$\mathcal{W}$	Tangent directions at center of a box.
$\mathbf{y}$	Periodic solution vector, or a general vector.
θ	Generic angular coordinate.
$\hat{\mathbf{x}}$, $\overline{\mathbf{x}}$	Mappings, $T^p :\to \mathbb{R}^n$, representing a torus.
$\mathbf{r}$	Function, $T^p \to \mathbb{R}^q$, representing radial-toroidal coordinates.
$\mathbf{n}$, $\overline{\mathbf{n}}$	Normal vectors.
$\hat{Q}$, $\overline{Q}$	Orthogonal matrices.
$\boldsymbol{\Phi}$	Vector field on a real or complex space.
$\boldsymbol{\rho}$	Vector of radial-toroidal coordinates.
$\boldsymbol{\phi}$	Vector of angular-toroidal coordinates.
$\Pi_{\mathcal{S}}$	Orthogonal projection operator onto the space $\mathcal{S}$.

κ_p	Condition number with respect to p-norm.
λ	Scalar bifurcation parameter.
τ	Period.
ν, σ	Lyapunov-type numbers of a manifold.
$f'(t)$	Differentiation with respect to a single variable, t.

SUMMARY

This thesis is concerned with numerical techniques for resolving and continuing closed, compact invariant manifolds in parameter-dependent dynamical systems with specific emphasis on invariant tori under flows. In the first part, we review several numerical methods of continuing invariant tori and concentrate on one choice called the "orthogonality condition". We show that the orthogonality condition is equivalent to another condition on the smooth level and show that they both descend from the same geometrical relationship. Then we show that for hyperbolic, periodic orbits in the plane, the linearization of the orthogonality condition yields a scalar system whose characteristic multiplier is the same as the non-unity multiplier of the orbit. In the second part, we demonstrate that one class of discretizations of the orthogonality condition for periodic orbits represents a natural extension of collocation. Using this viewpoint, we give sufficient conditions for convergence of a periodic orbit. The stability argument does not extend to higher-dimensional tori, however, and we prove that the method is unconditionally unstable for some common types of two-tori embedded in $\mathbb{R}^3$ with even numbers of points in both angular directions. In the third part, we develop several numerical examples and demonstrate that the convergence properties of the method and discretization can be quite complicated. In the fourth and final part, we extend the method to the general case of p-tori in $\mathbb{R}^n$ in a different way from previous implementations and solve the continuation problem for a three-torus embedded in $\mathbb{R}^8$.

CHAPTER I

INTRODUCTION AND BACKGROUND

1.1 Motivation and Scope

The invariant manifolds of a dynamical system impart a great deal of information about the system as a whole. Often, when trying to piece together a general picture of the effect of a flow or map, the first items to find are the location, classification, and stability of invariant manifolds that the system admits. As computers have become faster and more robust, a need has developed for new numerical algorithms that can approximate invariant manifolds quickly and accurately.

Invariant tori in particular are one of the most commonly observed closed manifolds in dynamical systems. The appearance and breakdown of tori seems to be related to the onset of chaos in some physical situations, making invariant tori interesting objects for study.

Examples of flow-invariant tori abound in the literature. Just to name three, Matsumoto et al. [25] demonstrate how chaos develops through torus breakdown in an electrical circuit, Valkering et al [37] prove the existence of an invariant torus in two capacitively coupled Josephson junctions, and Langford numerically approximates an invariant torus in fluid-flow equations [22]. Langford also shows how an invariant torus can form through an interaction between a Hopf bifurcation and a simple steady-state bifurcation [23].

This thesis comprises three tasks related to the approximation of invariant tori: First, examine some of the current methods for continuing and approximating invariant tori in dynamical systems in order to understand the fundamental geometric conditions behind them. Second, modify one of the methods and examine some of its

convergence properties. Third, use that technique to continue several tori, including a 3-torus that arises in an indirectly coupled system of oscillators.

While invariant tori can appear in discrete dynamical systems (*i.e.*, maps), the focus of this thesis is on flows. Of course, numerical algorithms that work for discrete maps can, in theory, work for flows as well, since the solution map of the flow for a fixed time step is itself a diffeomorphism, but algorithms specifically designed for flows are potentially more efficient because they avoid direct integration in time.

1.2 Problem Definition

This thesis considers the system of ordinary differential equations given by

$$\dot{\mathbf{x}} = \mathbf{\Phi}(\mathbf{x}, \lambda) \qquad ; \qquad \mathbf{x} \in \mathbb{R}^n \ , \tag{1.1}$$

where λ is a scalar parameter and $\mathbf{\Phi}$ is a $\mathcal{C}^1$ vector field. Let $\boldsymbol{\varphi}^t$ be the solution operator of Equation (1.1). In other words, if $\mathbf{x}(t)$ is the solution of Equation (1.1) with initial condition, $\mathbf{x}(0) = \mathbf{x}_0$, then $\boldsymbol{\varphi}^t(\mathbf{x}_0, \lambda) = \mathbf{x}(t)$. A closed, compact manifold M is *invariant* under the flow defined by Equation (1.1) at a parameter value λ_0 if $\boldsymbol{\varphi}^t(M, \lambda_0) = M$ for all $t \in \mathbb{R}$.

When searching numerically for an invariant torus embedded in an ambient real space, the first task is to guess a "nearby" (see below) $\mathcal{C}^1$ torus embedded in $\mathbb{R}^n$ through the injective mapping $\overline{\mathbf{x}} : T^p \to \mathbb{R}^n$, where T^p is the abstract p-torus. The word "torus" may appear in many contexts from now on – it may refer to an abstract torus T^p, to the image of an embedding $T^p \to \mathbb{R}^n$, or to the embedding itself.

In practice, $\overline{\mathbf{x}}$ is usually just a previously-calculated invariant torus at a preceding parameter value λ_0, while the new invariant torus corresponds to an updated parameter value $\lambda = \lambda_0 + \Delta\lambda$. The origin of $\overline{\mathbf{x}}$ is irrelevant for computational purposes, however, so any reasonable initial guess will work.

In addition to $\overline{\mathbf{x}}$ itself, it is necessary to supply a $\mathcal{C}^1$, moving orthonormal system of vectors,

$\{\overline{\mathbf{n}}_1(\boldsymbol{\phi}), \overline{\mathbf{n}}_2(\boldsymbol{\phi}), \ldots, \overline{\mathbf{n}}_q(\boldsymbol{\phi})\}$ that span the normal plane of the image of $\overline{\mathbf{x}}$ at $\boldsymbol{\phi} \in T^p$. Let the $n \times q$ matrix $\overline{Q}$ hold the normal system in its columns,

$$\overline{Q}(\boldsymbol{\phi}) = \begin{pmatrix} \overline{\mathbf{n}}_1(\boldsymbol{\phi}) & \overline{\mathbf{n}}_2(\boldsymbol{\phi}) & \cdots & \overline{\mathbf{n}}_q(\boldsymbol{\phi}) \end{pmatrix}. \tag{1.2}$$

This gives rise to a local coordinate system. Every $\mathbf{x}$ near the image of $\overline{\mathbf{x}}$ corresponds to a unique pair, $(\boldsymbol{\phi}, \boldsymbol{\rho})$, through the equation

$$\mathbf{x} = \overline{\mathbf{x}}(\boldsymbol{\phi}) + \overline{Q}(\boldsymbol{\phi})\boldsymbol{\rho}, \tag{1.3}$$

where $\boldsymbol{\rho} \in \mathbb{R}^q$.

Let $\hat{\mathbf{x}} : T^p \to \mathbb{R}^n$ denote the unknown invariant torus. In local coordinates the torus has the form

$$\hat{\mathbf{x}}(\boldsymbol{\phi}) = \overline{\mathbf{x}}(\boldsymbol{\phi}) + \overline{Q}(\boldsymbol{\phi})\mathbf{r}(\boldsymbol{\phi}), \tag{1.4}$$

where $\mathbf{r} : T^p \to \mathbb{R}^q$.

Now it is possible to define an ambiguous term used above. Stating that $\overline{\mathbf{x}}$ is "near" $\hat{\mathbf{x}}$ – or simply that $\overline{\mathbf{x}}$ is "nearby" – is exactly the same as stating that the parameterization in Equation (1.4) is possible with unique $\mathbf{r}(\boldsymbol{\phi})$.

1.3 Persistence of Solutions

The first question to ask before embarking on a numerical search for a branch of tori is whether such a branch exists. Fortunately, theoretical results do guarantee continuation under certain assumptions. The discussion below borrows notation from Dieci and Lorenz [11], and it includes results for attracting tori. Similar results hold for repelling tori or tori of mixed hyperbolicity [41]. The original result is due to Fenichel [13].

Let M be a closed, compact, connected, $\mathcal{C}^k$ p-manifold that is invariant under the flow of Equation (1.1) at some parameter value λ_0. Let $\mathcal{T}_{\mathbf{x}}$ and $\mathcal{N}_{\mathbf{x}}$ denote the tangent and normal spaces of M respectively at $\mathbf{x} \in M$, and let $\Pi_{\mathcal{N}_{\mathbf{x}}} : \mathbb{R}^n \to \mathbb{R}^n$ denote the orthogonal projection operator onto $\mathcal{N}_{\mathbf{x}}$.

At any given point, $\mathbf{x} \in M$, let $\nu(\mathbf{x})$ be a number,

$$\nu(\mathbf{x}) = \limsup_{t\to\infty} \left\| \Pi_{\mathcal{N}_\mathbf{x}} \left(D_\mathbf{x}\boldsymbol{\varphi}^t \left(\boldsymbol{\varphi}^{-t}(\mathbf{x}) \right) \right) \right\|^{1/t} \ , \tag{1.5}$$

where $\|\bullet\|$ is the standard operator norm based on the Euclidian two-norm in $\mathbb{R}^n$. If $\nu(\mathbf{x}) < 1$, then there exists another number,

$$\sigma(\mathbf{x}) = \limsup_{t\to\infty} \frac{-\ln \|D_\mathbf{x}\boldsymbol{\varphi}^{-t}(\mathbf{x})\|}{\ln \|\Pi_{\mathcal{N}_\mathbf{x}} \left(D_\mathbf{x}\boldsymbol{\varphi}^t \left(\boldsymbol{\varphi}^{-t}(\mathbf{x}) \right) \right)\|} \ . \tag{1.6}$$

The two quantities $\nu(\mathbf{x})$ and $\sigma(\mathbf{x})$ are known as *Lyapunov-type numbers*, and they determine if the manifold persists under small perturbations of λ.

Note that the operator in Equation (1.5) maps $\mathcal{N}_{\boldsymbol{\varphi}^{-t}(\mathbf{x})}$ to $\mathcal{N}_\mathbf{x}$ and that the operator in the numerator of Equation (1.6) maps $\mathcal{T}_\mathbf{x}$ to $\mathcal{T}_{\boldsymbol{\varphi}^{-t}(\mathbf{x})}$. Moreover, the former operator describes forward time progression of normal vectors under the linearized flow, while the latter describes the backward time progression of tangent vectors, again under linearized flow.

The conclusion, therefore, is that $\sigma(\mathbf{x})$ represents a ratio of attractivity toward $\mathbf{x}$ from within M to attractivity toward $\mathbf{x}$ from outside M. This ratio should be small to ensure persistence of the invariant manifold.

The *global* Lyapunov-type numbers are suprema. If $\nu(\mathbf{x}) < 1$ for all $\mathbf{x} \in M$, then

$$\nu(M) = \sup_{\mathbf{x}\in M} \nu(x) \tag{1.7}$$

$$\sigma(M) = \sup_{\mathbf{x}\in M} \sigma(x) \ . \tag{1.8}$$

As long as the global ratio of attractivities is relatively small it is possible to continue M smoothly, as the following theorem states.

Theorem 1.1 (Fenichel) *Let M be a closed, compact, connected, $\mathcal{C}^k$ p-manifold that is invariant under the flow of Equation (1.1) at some parameter value λ_0. If $\nu(M) < 1$ and $\sigma(M) < 1/k$, and if $\Delta\lambda$ is sufficiently small, then there is a unique, $\mathcal{C}^k$ manifold that is invariant under the flow at $\lambda_0 + \Delta\lambda$ and is diffeomorphic to M.*

The restrictions on ν and σ listed above are sometimes called the "gap condition" [35].

The proof of this theorem is not included here. Essentially, the proof shows that for the given conditions on ν and σ, the Hadamard graph transform is a contraction mapping on the space of embeddings, and thus it converges to the new torus. (See Section 1.4.2 for an explanation of the graph transform.) The full proof requires a small perturbation of the original problem, which makes the details somewhat abstruse.

Wiggins [41] provides a more accessible discussion than the original proof [13]. Wiggins' book contains more illustrations and background information, as well as other useful results about the continuation of invariant manifolds. Dieci and Lorenz discuss how to track Lyapunov-type numbers numerically in some specific cases [11].

1.4 Previous Methods

A voluminous collection of numerical algorithms for continuing invariant manifolds has accumulated in the literature since the 1960's. This thesis concentrates on methods that have shown promise specifically for the continuation of invariant tori.

The methods examined here descend from one of three fundamental conditions: the PDE condition, the graph transform convergence condition, and the orthogonality condition. By far, the most popular numerical techniques to date have relied on either the PDE condition or the graph transform. As shown in [10], the graph transform actually represents the method of characteristics applied to the PDE condition, but implementation of the two techniques is fundamentally different, so this review considers them separately.

The orthogonality condition is the less common of the three conditions in the literature, but as results in Chapter 2 show, it is equivalent to the PDE condition in a very straightforward way on the smooth level.

Techniques based on the PDE and orthogonality conditions are examples of what Moore calls "direct methods" [28], since the torus is a solution to a given system of equations. Graph transform techniques are examples of "indirect methods," since they rely on attractivity properties of tori to generate an approximation.

1.4.1 PDE Condition

Dieci et al. propose in [12] that for a torus of the form of Equation (1.4) to be invariant, it must satisfy a particular first-order, hyperbolic PDE. The development of the PDE is straightforward.

Assume that the vector field in Equation (1.1) has a representation in the local $(\boldsymbol{\phi}, \boldsymbol{\rho})$ coordinate system, which is to say that $\boldsymbol{\Phi}$ looks like the following system:

$$\boldsymbol{\Phi}(\boldsymbol{\phi}, \boldsymbol{\rho}) = \begin{pmatrix} \dot{\boldsymbol{\phi}}(\boldsymbol{\phi}, \boldsymbol{\rho}) \\ \dot{\boldsymbol{\rho}}(\boldsymbol{\phi}, \boldsymbol{\rho}) \end{pmatrix} . \tag{1.9}$$

The Implicit Function Theorem [18, 20] guarantees that such a partition always exists locally, but it may be difficult to calculate, and $\dot{\boldsymbol{\phi}}$ and $\dot{\boldsymbol{\rho}}$ may not have a closed-form expansion.

The PDE condition is now a simple consequence of the fact that $\mathbf{r}(\boldsymbol{\phi})$ in Equation (1.4) is a pure function of $\boldsymbol{\phi}$, which is a function of time for a given initial condition. Taking the total derivative of $\mathbf{r}$ with respect to time yields

$$(D_{\boldsymbol{\phi}}\mathbf{r})\,\dot{\boldsymbol{\phi}}(\boldsymbol{\phi}, \mathbf{r}(\boldsymbol{\phi})) = \dot{\boldsymbol{\rho}}(\boldsymbol{\phi}, \mathbf{r}(\boldsymbol{\phi})) \ . \tag{1.10}$$

This is a first-order, hyperbolic system of PDE in $\boldsymbol{\phi}$, which is easy to see in component form:

$$\sum_{i=1}^{p} \left[\frac{\partial \mathbf{r}}{\partial \phi_i}(\boldsymbol{\phi}, \mathbf{r}(\boldsymbol{\phi})) \right] \dot{\phi}_i(\boldsymbol{\phi}, \mathbf{r}(\boldsymbol{\phi})) = \dot{\boldsymbol{\rho}}(\boldsymbol{\phi}, \mathbf{r}(\boldsymbol{\phi})) \ . \tag{1.11}$$

If the $\boldsymbol{\phi}$ coordinates on T^p are τ-periodic, then any $\mathbf{r}$ that satisfies the PDE above with the periodic boundary condition $\mathbf{r}(0, 0, \ldots, 0) = \mathbf{r}(\tau, \tau, \ldots, \tau)$ represents an invariant torus through Equation (1.4).

Direct solution of the PDE has two immediate and obvious difficulties. First, it requires a partition of the vector field as in Equation (1.9). While numerical schemes can estimate $\dot{\boldsymbol{\phi}}$ and $\dot{\boldsymbol{\rho}}$ (*e.g.*, by multivariate cubic spline interpolation on $\overline{\mathbf{x}}$), such schemes can be costly, so most examples of direct solution apply to cases where one can obtain the partition explicitly.

Dieci et al. first use a modified leapfrog discretization [12] to solve the PDE and continue an invariant torus in a system of coupled planar oscillators. Later, multi-grid and upwind solutions [7, 8] become the focus of investigation of the same problem.

More recent approaches have used Fourier expansions for direct solution of Equation (1.10). The basic idea of these spectral techniques is to write $\mathbf{r}$ as a summed series of periodic functions in $\boldsymbol{\phi}$ and then solve for the coefficients. Fourier techniques seem to work very well for both smooth and non-smooth tori, but again they require a partition of the vector field. The best references for the spectral method applied to invariant tori are [14], [26], and [36].

1.4.2 Graph Transform Techniques

As discussed above, the PDE condition is intrinsically related to graph transform techniques through the method of characteristics [10], but practical implementation of the two methods is completely different.

The greatest advantage of graph transform techniques is that, although they are equivalent to solving the PDE, they do not require formulation of the PDE (along with with its cryptic $\dot{\boldsymbol{\phi}}$ and $\dot{\boldsymbol{\rho}}$ functions), so they can apply to a much wider class of problems. They do, however, have their own limitations, notably a longer computation time, at least in the ways in which they have previously been implemented.

Graph transform methods follow Fenichel's proof of the continuation of tori in [13]. Given that the Hadamard graph transform is a contraction on the space of $\mathcal{C}^k$, torus-embedding functions when the Lyapunov-type numbers satisfy the gap condition as

in Section 1.3, one suspects that a numerical version of the transform might help to identify invariant tori. Indeed, this is the case, but discrete implementation can be complicated and costly.

Consider a dynamical system with solution operator $\boldsymbol{\varphi}^t$. Assume that $\hat{\mathbf{x}}^{(i)} : T^p \to \mathbb{R}^n$ is $\mathcal{C}^k$ and near an invariant torus and that the gap condition holds. Then for a fixed $t > 0$, the Hadamard graph transform G^t is an operator that maps $\hat{\mathbf{x}}^{(i)}$ to a new $\mathcal{C}^k$ function, $\hat{\mathbf{x}}^{(i+1)}$, such that the image of $\hat{\mathbf{x}}^{(i+1)}$ is the image of $\hat{\mathbf{x}}^{(i)}$ integrated forward under the flow for a fixed time. In other words, G^t satisfies

$$\text{image}\left[G^t(\hat{\mathbf{x}}^{(i)})\right] = \text{image}\left[\hat{\mathbf{x}}^{(i+1)}\right] = \boldsymbol{\varphi}^t(\text{image}\left[\hat{\mathbf{x}}^{(i)}\right]) \ . \tag{1.12}$$

The gap condition ensures that G^t is a contraction mapping on the space of $\mathcal{C}^k$ torus-embedding functions. In theory, then, all one has to do is to iterate G^t repeatedly, and the sequence $\left\{\hat{\mathbf{x}}^{(i)}\right\}$ will converge to a function that represents the invariant torus.

In practice, one must first convert the continuous graph transform into a discrete operation that is representable in a computer. The discrete representation of a function, $\hat{\mathbf{x}}^{(i)} : T^p \to \mathbb{R}^n$ is actually an ordered collection of $\mathbb{R}^n$ points, where each one corresponds to a particular $\boldsymbol{\phi} \in T^p$. It is generally useful to fix the discretization of T^p, so the points of $\hat{\mathbf{x}}^{(i+1)}$ will correspond to the same $\boldsymbol{\phi}$'s. Thus, $\hat{\mathbf{x}}^{(i)}$ and $\hat{\mathbf{x}}^{(i+1)}$ are really functions,

$$\hat{\mathbf{x}}^{(i)}, \hat{\mathbf{x}}^{(i+1)} : \widetilde{T}^p \to \mathbb{R}^n \ , \tag{1.13}$$

where $\widetilde{T}^p$ is a *discrete* torus, that is any collection of distinct points in T^p, usually ordered to simplify numerical calculations.

Now the problem is to find the "best" Euclidian distribution of points for $\hat{\mathbf{x}}^{(i+1)}$, given that the image of $\hat{\mathbf{x}}^{(i+1)}$ must be the integrated image of $\hat{\mathbf{x}}^{(i)}$. There are many possible definitions of "best", but one reasonable way to proceed is to force $\hat{\mathbf{x}}^{(i+1)}(\boldsymbol{\phi}_0)$ to be in the normal space to the image of $\hat{\mathbf{x}}^{(i)}$ at $\hat{\mathbf{x}}^{(i)}(\boldsymbol{\phi}_0)$ for any fixed $\boldsymbol{\phi}_0 \in \widetilde{T}^p$. That

is to say,

$$\left(\hat{\mathbf{x}}^{(i+1)}(\boldsymbol{\phi}_0) - \hat{\mathbf{x}}^{(i)}(\boldsymbol{\phi}_0)\right)^T \left[D_{\boldsymbol{\phi}}\hat{\mathbf{x}}^{(i)}(\boldsymbol{\phi}_0)\right] = \mathbf{0} \qquad \forall \boldsymbol{\phi}_0 \in \widetilde{T}^p \ . \tag{1.14}$$

The derivative in Equation (1.14) is really a numerical approximation, since the functions are only defined on discrete points. Regardless of how one specifies the normal direction on the image of $\hat{\mathbf{x}}^{(i)}$, it is still necessary to choose an order of operation of the graph transform to enforce Equation (1.14). The literature contains examples of two possible choices.

In the *boundary value problem* (BVP) approach, one interpolates on the image of $\hat{\mathbf{x}}^{(i)}$ and then solves, as the name implies, a boundary value problem. The process works in two steps:

First, some sort of interpolation (*e.g.*, cubic splines) generates a continuous version of the discrete image of $\hat{\mathbf{x}}^{(i)}$. If this interpolated object is denoted $M^{(i)}$, then for fixed $t > 0$, the BVP to solve at each $\boldsymbol{\phi}_0 \in \widetilde{T}^p$ is

$$\left(\boldsymbol{\varphi}^t(\mathbf{c}) - \mathbf{c}\right)^T \left[D_{\boldsymbol{\phi}}\hat{\mathbf{x}}^{(i)}(\boldsymbol{\phi}_0)\right] = \mathbf{0} \qquad \text{where} \qquad \mathbf{c} \in M^{(i)} \ . \tag{1.15}$$

Dieci and Lorenz first use this version of the graph transform to continue invariant tori in [10]. It has the advantage of stability near torus breakdown, but it is very slow.

In the *initial value problem* (IVP) approach, the process is reversed: First, integrate each $\hat{\mathbf{x}}^{(i)}(\boldsymbol{\phi}_0)$ forward under the flow by a fixed time t and *then* interpolate and re-distribute the points in Euclidian space to satisfy Equation (1.14).

Reichelt uses an IVP approach in [35]. He also borrows an extra re-parameterization algorithm from [29] to "beautify" the torus representation after a long continuation process has skewed it. His results show that the IVP method is much faster than the BVP method, but it is not as stable near breakdown. Figure 1.1 contrasts the two approaches pictorially.

Regardless of their style of implementation, all graph transform methods suffer

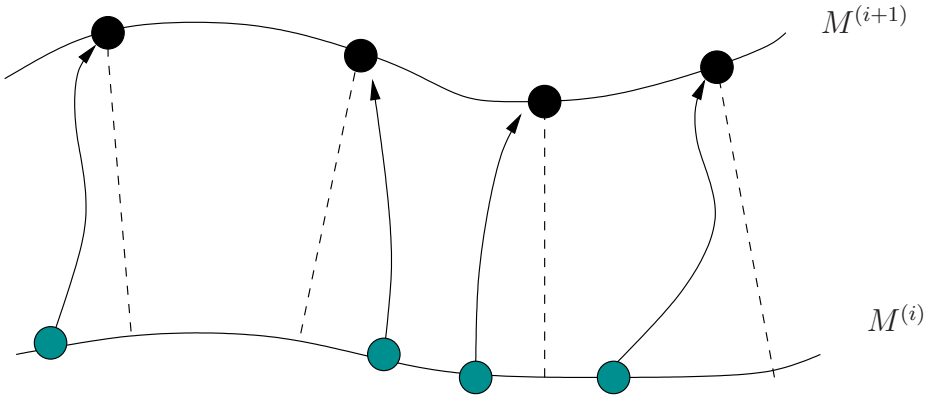

Boundary Value Approach

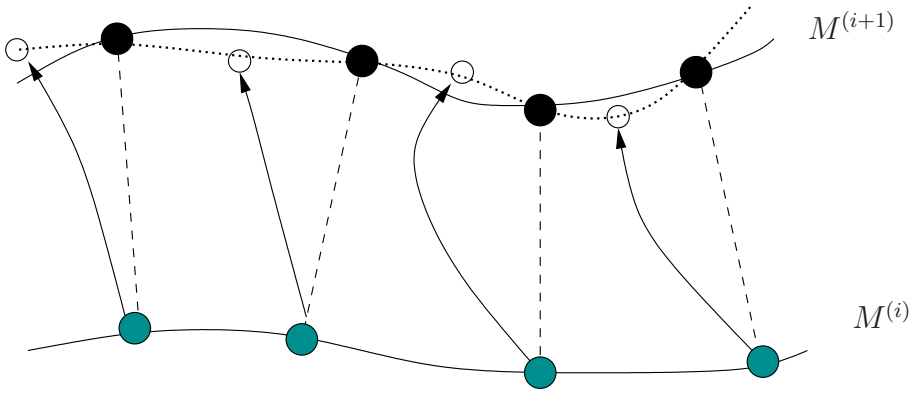

Initial Value Approach

Figure 1.1: Two Approaches to the Graph Transform

from two drawbacks: 1) they are slow, since the graph transform converges only linearly, and 2) they require a splitting of the stable and unstable sections of the normal bundle.

The second drawback occurs because the graph transform relies on attractivity of the torus in order to show convergence. Clearly, it is easy to adapt the algorithm to tori of mixed hyperbolicity by running time backwards in some parts of the space and forwards in other parts, but this requires foreknowledge of stable and unstable sections of the normal bundle. A comprehensive discussion of graph transform methods, including their applicability to tori with both stable and unstable directions, is available in [6] and [31].

1.4.3 Orthogonality Condition

In 1995 and 1996, Moore [29] proposed a different method for resolving invariant tori, along with an extension of the method to connecting orbits [27]. The method seems at first to avoid both of the obstacles inherent in the first two conditions, in that it does not require an explicit form for $\dot{\boldsymbol{\phi}}$ and $\dot{\boldsymbol{\rho}}$, nor does it rely on a linearly-convergent graph transform technique.

The *orthogonality condition* relies on purely geometrical reasoning. It says that for a manifold M to be invariant under the vector field, $\boldsymbol{\Phi}$, then the projection of $\boldsymbol{\Phi}$ onto the normal plane of M must be zero. Written symbolically,

$$\Pi_{\mathcal{N}_{\mathbf{x}}} \boldsymbol{\Phi}(\mathbf{x}) = \mathbf{0}, \quad \forall \mathbf{x} \in M \ . \tag{1.16}$$

If M has dimension p and is embedded in $\mathbb{R}^n$, then the projection operator $\Pi_{\mathcal{N}_{\mathbf{x}}}$ has a p-dimensional kernel. It is necessary to restrict the manifold further in order to have a unique solution to Equation (1.16).

Let $\hat{\mathbf{x}}$ be a torus as defined in Section 1.2, and let $\{\mathbf{n}_1(\boldsymbol{\phi}), \mathbf{n}_2(\boldsymbol{\phi}), \ldots, \mathbf{n}_q(\boldsymbol{\phi})\}$ be a moving, $\mathcal{C}^1$, orthonormal system that spans the normal space $\mathcal{N}_{\hat{\mathbf{x}}(\boldsymbol{\phi})}$ at any $\boldsymbol{\phi} \in T^p$.

Define

$$Q(\boldsymbol{\phi}) = \begin{pmatrix} \mathbf{n}_1(\boldsymbol{\phi}) & \mathbf{n}_2(\boldsymbol{\phi}) & \dots & \mathbf{n}_q(\boldsymbol{\phi}) \end{pmatrix} . \tag{1.17}$$

Equation (1.16) simplifies to q linearly independent equations,

$$Q(\boldsymbol{\phi})^T \boldsymbol{\Phi}\left(\hat{\mathbf{x}}(\boldsymbol{\phi})\right) = \mathbf{0}, \quad \forall \boldsymbol{\phi} \in T^p \, . \tag{1.18}$$

This is the orthogonality condition. If $\hat{\mathbf{x}}$ has the form of Equation (1.4), then q equations at each $\boldsymbol{\phi}$ provide enough information to solve for $\hat{\mathbf{x}}$.

Numerically, then, the most pressing question is how to calculate Q. All possibilities rely on some estimate of a derivative, as the normal plane has the form,

$$\mathcal{N}_{\hat{\mathbf{x}}(\boldsymbol{\phi})} = \operatorname{span}\left\{ \frac{\partial \hat{\mathbf{x}}\left(\boldsymbol{\phi}\right)}{\partial \phi_1}, \frac{\partial \hat{\mathbf{x}}\left(\boldsymbol{\phi}\right)}{\partial \phi_2}, \dots, \frac{\partial \hat{\mathbf{x}}\left(\boldsymbol{\phi}\right)}{\partial \phi_p} \right\}^{\perp} , \tag{1.19}$$

In fact, the original paper [29] only includes expansions for limit cycles and two-tori, so $p \leq 2$. The extension is natural, though.

As discussed in Section 3.2, many finite-difference templates for the partial derivatives are available, but only a few of them work. Moreover, while there are canonical representations for normal vectors to the derivatives in $\mathbb{R}^2$ and $\mathbb{R}^3$ ($\pi/2$ rotation and cross product respectively), higher-dimensional examples are not so straightforward. Chapter 3 describes how to calculate Q for two special cases, and Chapter 5 describes how to calculate Q in general. The only type of discretization that seems to work consistently is a class of discretizations called "box schemes."

In the original paper [29], Moore does not calculate the normal space in Equation (1.19) explicitly, preferring instead to use a quasi-Newton iteration to find the β's in the following equation, which is analogous to Equation (1.18):

$$\boldsymbol{\Phi}\left(\hat{\mathbf{x}}(\boldsymbol{\phi})\right) = \beta_1 \frac{\partial \hat{\mathbf{x}}\left(\boldsymbol{\phi}\right)}{\partial \phi_1} + \beta_2 \frac{\partial \hat{\mathbf{x}}\left(\boldsymbol{\phi}\right)}{\partial \phi_2} + \dots + \beta_p \frac{\partial \hat{\mathbf{x}}\left(\boldsymbol{\phi}\right)}{\partial \phi_p}, \tag{1.20}$$

where again, $p \leq 2$ in the original paper. This approach eliminates the need for an explicit Jacobian in Newton's method.

Computing the Jacobian numerically is neither difficult nor computationally intensive if programmed correctly, however, and moreover all methods must at some point compute the original normal vectors, $\overline{Q}$, so this thesis concentrates on a more direct approach using a full linear expansion and direct development of the normal vectors. The most difficult aspects of this are the above-mentioned calculation of Q, and – in higher dimensions – the solution of the linear system in Newton's method as discussed in Chapter 5.

Two very important issues that Moore does not address in [29] are the consistency and convergence of methods based on the orthogonality condition. Without such results, it is possible that the discrete problem may not have a unique, isolated solution or that the solutions do not converge to the smooth invariant torus as the spacing between points shrinks. One of the main goals of this thesis is to provide some of these results.

Chapter 2 demonstrates full consistency between the orthogonality condition and PDE method on the smooth level. This thesis does contain some convergence results for periodic orbits in Chapter 3, but unfortunately the convergence properties of the orthogonality condition with box schemes are quite complicated, and consistent, proven instability occurs in some very common cases. Therefore, while the orthogonality condition appears clearly superior in terms of computation time and ease of adaptability, it is subject to instability in some examples. A few illustrative examples appear in Chapter 4.

Finally, note that the orthogonality condition is not specific to tori. It is possible in theory to apply it to any closed manifold embedded in real or complex space, as long as the points on the surface have a suitable ordering and a trivial, well-understood normal bundle. Previous research has applied geometrical methods to several different types of manifolds [24, 27, 28, 29, 30], in particular as an alternative to standard methods (*e.g.*, [5, 38]) of computing connecting orbits.

1.5 Parameterization Issues

Moore does make one other important contribution to the theory of numerical continuation of tori in that he develops a parameterization technique for two-tori [29].

For a simple curve in $\mathbb{R}^n$, arc length distribution will generally ensure that the graph in Euclidian space is the best possible picture for the given number of points, although some applications may call for other distributions, such as a weighted distribution toward areas of higher curvature. With two-tori, however, there is no canonical distribution of points. Moore addresses this problem in [29] and proposes an algorithm for re-distributing points quasi-conformally, which is one possible natural extension of arc length. Reichelt uses that re-parameterization as part of the graph transform [35], and it seems to work well for two-tori, but no one has yet extended it to higher-dimensional manifolds.

This thesis does not discuss the re-parameterization issue in detail, but rather uses easier methods to distribute points when such methods are available. A robust and inexpensive re-parameterization technique for general p-tori would be a significant contribution to the field of computational geometry.

CHAPTER II

SMOOTH ANALYSIS OF ORTHOGONALITY CONDITION

This chapter demonstrates how the orthogonality condition given in Equation (1.18) is related to the PDE condition, and how it preserves characteristic multipliers through linearization around periodic orbits. It also contains some basic results that outline properties of the local toroidal coordinate system used frequently.

It should come as no surprise that the PDE and orthogonality conditions are equivalent on a basic level. In fact, one can make a general argument for equivalence by considering the situation where only one, isolated invariant torus exists near some fixed $\overline{\mathbf{x}}$. If the torus is invariant if and only if it satisfies both conditions, then the conditions must be somehow equivalent. (The terms "near" and "nearby" are in the sense of Section 1.2.)

Nevertheless, it is a useful exercise to step through the algebraic connections that lead from one condition to another. This exercise, which has not appeared in the literature before now, clarifies the relationship between the vector field and the mysterious $\dot{\boldsymbol{\phi}}$ and $\dot{\boldsymbol{\rho}}$ quantities in Equation (1.9).

Another useful exercise is to reduce the problem to the simplest possible type of torus: a periodic orbit in the plane. The linearized orthogonality condition should preserve certain hyperbolicity properties, as indeed some calculations in Section 2.3 indicate that it does.

2.1 Equivalence of PDE and Orthogonality Conditions

The fundamental equation that links the two conditions is

$$\frac{d}{dt}\hat{\mathbf{x}}(\boldsymbol{\phi}) = \boldsymbol{\Phi}\left(\hat{\mathbf{x}}(\boldsymbol{\phi})\right). \tag{2.1}$$

The left hand side of this equation is difficult to interpret. If $\boldsymbol{\phi}$ is a function of time up to some initial condition, then there exists a total derivative of $\hat{\mathbf{x}}$ with respect to time, $d\hat{\mathbf{x}}(\boldsymbol{\phi})/dt = D_{\boldsymbol{\phi}}\hat{\mathbf{x}}(\boldsymbol{\phi})\dot{\boldsymbol{\phi}}$. The total derivative should at any given $\boldsymbol{\phi} \in T^p$ be equal to the vector field evaluated at $\hat{\mathbf{x}}(\boldsymbol{\phi})$ if and only if $\hat{\mathbf{x}}$ defines an invariant torus.

That Equation (2.1) is an invariance condition is not immediately obvious, but it does actually relate the PDE and orthogonality conditions, as the following proposition shows.

Proposition 2.1 *Let $\overline{\mathbf{x}} : T^p \to \mathbb{R}^n$ be an injective, $\mathcal{C}^1$ mapping with $\overline{Q}$, $\boldsymbol{\phi}$, and $\boldsymbol{\rho}$ defined as in Equation (1.3). Let $\hat{\mathbf{x}} : T^p \to \mathbb{R}^n$ be an injective, $\mathcal{C}^1$ mapping of the form in Equation (1.4), and let $Q : T^p \to \mathbb{R}^n \times \mathbb{R}^q$ be a $\mathcal{C}^1$ mapping such that at any $\boldsymbol{\phi}$, $Q(\boldsymbol{\phi})$ is orthogonal and its columns span the normal space to the image of $\hat{\mathbf{x}}$ at $\boldsymbol{\phi}$.*

Then $\hat{\mathbf{x}}$ satisfies Equation (1.10) if and only if it satisfies Equation (1.18).

Proof

Write the vector field and the left hand side of Equation (2.1) in terms of the local toroidal coordinate system. The left hand side is

$$\begin{aligned}\frac{d}{dt}\hat{\mathbf{x}}(\boldsymbol{\phi}) &= \left(D_{\boldsymbol{\phi}}\hat{\mathbf{x}}(\boldsymbol{\phi})\right)\dot{\boldsymbol{\phi}} \\ &= \left[\left(D_{\boldsymbol{\phi}}\overline{\mathbf{x}}(\boldsymbol{\phi})\right) + \left(D_{\boldsymbol{\phi}}\overline{Q}(\boldsymbol{\phi})\boldsymbol{\rho}\right)_{\boldsymbol{\rho}=\mathbf{r}(\boldsymbol{\phi})} + \overline{Q}(\boldsymbol{\phi})\left(D_{\boldsymbol{\phi}}\mathbf{r}(\boldsymbol{\phi})\right)\right]\dot{\boldsymbol{\phi}},\end{aligned} \tag{2.2}$$

and the vector field evaluated at a point $\hat{\mathbf{x}}\left(\boldsymbol{\phi}\right)$, is

$$\boldsymbol{\Phi}\left(\hat{\mathbf{x}}(\boldsymbol{\phi})\right) = \left[\left(D_{\boldsymbol{\phi}}\overline{\mathbf{x}}(\boldsymbol{\phi})\right)\dot{\boldsymbol{\phi}} + \left(D_{\boldsymbol{\phi}}\overline{Q}(\boldsymbol{\phi})\boldsymbol{\rho}\right)_{\boldsymbol{\rho}=\mathbf{r}(\boldsymbol{\phi})}\dot{\boldsymbol{\phi}} + \overline{Q}(\boldsymbol{\phi})\dot{\boldsymbol{\rho}}\right]. \tag{2.3}$$

Equations (2.2) and (2.3) combine to form,

$$\frac{d}{dt}\hat{\mathbf{x}}(\boldsymbol{\phi}) = \boldsymbol{\Phi}\left(\hat{\mathbf{x}}(\boldsymbol{\phi})\right) + \overline{Q}(\boldsymbol{\phi})\left(\left(D_{\boldsymbol{\phi}}\mathbf{r}(\boldsymbol{\phi})\right)\dot{\boldsymbol{\phi}} - \dot{\boldsymbol{\rho}}\right) \ . \tag{2.4}$$

Multiplying both sides by Q^T and noting that $Q^T d\hat{\mathbf{x}}(\boldsymbol{\phi})/dt = \mathbf{0}$ gives.

$$Q^T\boldsymbol{\Phi}\left(\hat{\mathbf{x}}(\boldsymbol{\phi})\right) + Q^T\overline{Q}(\boldsymbol{\phi})\left(\left(D_{\boldsymbol{\phi}}\mathbf{r}(\boldsymbol{\phi})\right)\dot{\boldsymbol{\phi}} - \dot{\boldsymbol{\rho}}\right) = \mathbf{0} \ . \tag{2.5}$$

Thus, if $\hat{\mathbf{x}}$ satisfies the PDE condition, then it satisfies the orthogonality condition. Conversely, if $\hat{\mathbf{x}}$ satisfies the orthogonality condition, and if $Q^T\overline{Q}$ has full rank, then $\hat{\mathbf{x}}$ satisfies the PDE condition. But the fact that $\hat{\mathbf{x}}$ is parameterizable in the local toroidal coordinate system with a $\mathcal{C}^1$-smooth $\mathbf{r}(\boldsymbol{\phi})$ implies that $Q^T\overline{Q}$ has full rank, so the proof is done. □

One immediate consequence of the above proposition is the overall equivalence condition that links everything to Equation (2.1).

Proposition 2.2 *Let $\overline{\mathbf{x}}$, $\hat{\mathbf{x}}$, $\overline{Q}$, and Q be as in Proposition 2.1 above. Then $\hat{\mathbf{x}}$ satisfies the PDE and orthogonality conditions if and only if it satisfies Equation (2.1).*

Proof

From Equation (2.4), it is obvious that if $\hat{\mathbf{x}}$ satisfies the PDE condition, then it satisfies Equation (2.1). Conversely, one may obtain the PDE or orthogonality conditions by multiplying both sides of Equation (2.1) by $\overline{Q}^T$ or Q^T respectively. □

The two propositions above enforce the notion that there is really only one geometrical condition available: Equation (2.1). If $\hat{\mathbf{x}}$ has a parameterization of the form in Equation (1.4), then it is necessary to eliminate p equations from the n equations represented in Equation (2.1), and the PDE and orthogonality conditions represent two different ways of doing that.

2.2 Basic Results on the Coordinate System

This section contains two geometrical observations that improve the overall understanding of the local toroidal coordinate system used frequently in this thesis. The

first observation elucidates the relationship between a section of the tangent bundle of an arbitrary function and the time derivative of an angular coordinate.

Proposition 2.3 *Let* $\hat{\mathbf{x}}$, $\overline{\mathbf{x}}$, *and* $\overline{Q}$ *be as in Proposition 2.1, and let the vector field satisfy*

$$\mathbf{\Phi}\left(\hat{\mathbf{x}}(\boldsymbol{\phi})\right) = \left(D_{\boldsymbol{\phi}}\hat{\mathbf{x}}(\boldsymbol{\phi})\right)\mathbf{c}(\boldsymbol{\phi}) \ , \tag{2.6}$$

where $\mathbf{c} : T^p \to \mathbb{R}^p$ *is a* $\mathcal{C}^1$ *mapping. Then* $\mathbf{c}(\boldsymbol{\phi}) = \dot{\boldsymbol{\phi}}\left(\boldsymbol{\phi}, \mathbf{r}(\boldsymbol{\phi})\right)$.

Proof

Expanding the definition of $D_{\boldsymbol{\phi}}\hat{\mathbf{x}}(\boldsymbol{\phi})$ and substituting Equation (2.3) for the vector field yields

$$\begin{aligned}\left(D_{\boldsymbol{\phi}}\overline{\mathbf{x}}(\boldsymbol{\phi})\right)\dot{\boldsymbol{\phi}} + \left(D_{\boldsymbol{\phi}}\overline{Q}\boldsymbol{\rho}\right)_{\boldsymbol{\rho}=\mathbf{r}(\boldsymbol{\phi})}\dot{\boldsymbol{\phi}} + \overline{Q}\dot{\boldsymbol{\rho}} = \\ \left[\left(D_{\boldsymbol{\phi}}\overline{\mathbf{x}}(\boldsymbol{\phi})\right) + \left(D_{\boldsymbol{\phi}}\overline{Q}\boldsymbol{\rho}\right)_{\boldsymbol{\rho}=\mathbf{r}(\boldsymbol{\phi})} + \overline{Q}\left(D_{\boldsymbol{\phi}}\mathbf{r}(\boldsymbol{\phi})\right)\right]\mathbf{c}(\boldsymbol{\phi}).\end{aligned} \tag{2.7}$$

This converts to a matrix equation.

$$\begin{pmatrix} \left(\left(D_{\boldsymbol{\phi}}\overline{\mathbf{x}}(\boldsymbol{\phi})\right) + \left(D_{\boldsymbol{\phi}}\overline{Q}\boldsymbol{\rho}\right)_{\boldsymbol{\rho}=\mathbf{r}(\boldsymbol{\phi})}\right) & \overline{Q} \end{pmatrix} \begin{pmatrix} \mathbf{c} - \dot{\boldsymbol{\phi}} \\ \left(D_{\boldsymbol{\phi}}\mathbf{r}(\boldsymbol{\phi})\right) - \dot{\boldsymbol{\rho}} \end{pmatrix} = \mathbf{0}. \tag{2.8}$$

Note that $\left(D_{\boldsymbol{\phi}}\overline{\mathbf{x}}(\boldsymbol{\phi})\right) + \left(D_{\boldsymbol{\phi}}\overline{Q}\boldsymbol{\rho}\right)_{\boldsymbol{\rho}=\mathbf{r}(\boldsymbol{\phi})}$ has full rank because $\overline{\mathbf{x}}$ is nearby, so Equation (2.8) proves the proposition and recovers the PDE condition as a bonus. □

The next proposition has to do with the term on the left-hand side of the fundamental condition, Equation (2.1).

Proposition 2.4 *Let* $\hat{\mathbf{x}}$ *and* Q *be as in Proposition 2.1, and suppose that* $\hat{\mathbf{x}}$ *defines a torus that is invariant under the flow given by the vector field* $\mathbf{\Phi}$. *Then*

$$\frac{d}{dt}\hat{\mathbf{x}}(\boldsymbol{\phi}) = \Pi_{\mathcal{T}_{\hat{\mathbf{x}}(\boldsymbol{\phi})}}\mathbf{\Phi}\left(\hat{\mathbf{x}}(\boldsymbol{\phi})\right) \qquad \forall \boldsymbol{\phi} \in T^p \ , \tag{2.9}$$

where $\Pi_{\mathcal{T}_{\hat{\mathbf{x}}(\boldsymbol{\phi})}}$ *represents the projection onto the tangent space of the image of* $\hat{\mathbf{x}}$ *at* $\hat{\mathbf{x}}(\boldsymbol{\phi})$.

Proof

This is geometrically clear, but one can make an algebraic argument by noting that for any given $\boldsymbol{\phi} \in T^p$, $\boldsymbol{\Phi}\left(\hat{\mathbf{x}}(\boldsymbol{\phi})\right) = \left(\Pi_{\mathcal{T}_{\hat{\mathbf{x}}(\boldsymbol{\phi})}} + \Pi_{\mathcal{N}_{\hat{\mathbf{x}}(\boldsymbol{\phi})}}\right) \boldsymbol{\Phi}\left(\hat{\mathbf{x}}(\boldsymbol{\phi})\right)$, and that the invariance of $\hat{\mathbf{x}}$ means that it satisfies Equations (1.16) and (2.1). □

The converse of Proposition 2.4 does not hold – just because a function $\hat{\mathbf{x}}$ satisfies Equation (2.9) does not imply that it is an invariant torus. A simple counterexample exists in the planar system of equations in polar coordinates,

$$\begin{aligned} \dot{r} &= r(\lambda - r^2) \\ \dot{\theta} &= 1 \ . \end{aligned} \tag{2.10}$$

This system has an attracting limit cycle centered at the origin with a radius of $\sqrt{\lambda}$. (Multiplying the first line by -1 makes the limit cycle unstable.)

Let $\lambda = 1$ and $\overline{\mathbf{x}}(\theta) = (\cos\theta, \sin\theta)$ in Cartesian coordinates, and let $\hat{\mathbf{x}}(\theta) = 2\,(\cos\theta, \sin\theta)$.

Obviously, $\hat{\mathbf{x}}$ is not an invariant torus, yet a calculation yields.

$$\Pi_{\mathcal{T}_{\hat{\mathbf{x}}(\theta)}} \boldsymbol{\Phi}\left(\hat{\mathbf{x}}(\theta)\right) = 2 \begin{pmatrix} -\sin\theta \\ \cos\theta \end{pmatrix} = \left(D_\theta \hat{\mathbf{x}}(\theta)\right) \dot{\theta} = \frac{d}{dt}\hat{\mathbf{x}}(\theta) \ . \tag{2.11}$$

Given these results, it is reasonable to ask if Equation (2.9) is trivially satisfied for any $\hat{\mathbf{x}}$. Another example shows that this is not the case and that the left hand side of Equation (2.9) is not always easy to quantify.

Consider again the vector field in Equation (2.10) with the same $\overline{\mathbf{x}}$, but now let $\hat{\mathbf{x}}(\theta) = (0.1 + \sin\theta)\,(\cos\theta, \sin\theta)$. Note that $d\hat{\mathbf{x}}(\theta)/dt = (d\hat{\mathbf{x}}(\theta)/d\theta)\,\dot{\theta} = d\hat{\mathbf{x}}(\theta)/d\theta$, and calculate

$$\frac{d}{d\theta}\hat{\mathbf{x}}(\theta) = \begin{pmatrix} 0.1\cos^2\theta - \sin\theta\,(1 + 0.1\sin\theta) \\ 0.1\cos\theta\sin\theta + \cos\theta \end{pmatrix} \ . \tag{2.12}$$

The vector field expands out as

$$\boldsymbol{\Phi}\left(\hat{\mathbf{x}}(\theta)\right) = (1 + 0.1\sin\theta) \begin{pmatrix} \cos\theta - \sin\theta - (1 + 0.1\sin\theta)^2\cos\theta \\ \cos\theta + \sin\theta - (1 + 0.1\sin\theta)^2\sin\theta \end{pmatrix} \ . \tag{2.13}$$

Rather than calculate the projection explicitly, just notice that

$$\Pi_{\mathcal{T}_{\hat{\mathbf{x}}(\theta)}} \mathbf{\Phi}\left(\hat{\mathbf{x}}(\theta)\right) = \left(\frac{\left(d\hat{\mathbf{x}}(\theta)/d\theta\right)^T \mathbf{\Phi}\left(\hat{\mathbf{x}}(\theta)\right)}{\left(d\hat{\mathbf{x}}(\theta)/d\theta\right)^T \left(d\hat{\mathbf{x}}(\theta)/d\theta\right)} \right) \frac{d}{d\theta}\hat{\mathbf{x}}(\theta) \ . \tag{2.14}$$

The coefficient on the right-hand side of the above equation is not always one (for example, at $\theta = 0$), so Equation (2.9) does not hold for all θ.

In conclusion, note that the functions $\dot{\boldsymbol{\phi}}$, $\dot{\boldsymbol{\rho}}$, and $(d\hat{\mathbf{x}}(\boldsymbol{\phi})/dt)$, while well-defined in a theoretical sense, are not always easy to calculate – even in reduced and simplified systems. Thus, numerical methods that calculate these quantities are generally not as robust as those that do not.

2.3 Linearization around Planar Periodic Orbits

Equivalence between the orthogonality and PDE conditions indicates that methods based on the orthogonality condition are at least as consistent as those based on the PDE, which is an important result. Further exploration shows that the orthogonality condition applied to periodic orbits in the plane preserves hyperbolicity properties of the orbit.

Let $\overline{\mathbf{x}}(t)$ be a periodic solution of Equation (1.1) of minimal period τ. Then there is a linear variational equation associated with the solution:

$$\dot{\mathbf{y}} = D\mathbf{\Phi}\left(\overline{\mathbf{x}}(t)\right)\mathbf{y}. \tag{2.15}$$

This is a linear, periodically forced system, so for each fundamental matrix solution $Y(t)$, it admits a *monodromy matrix* through the relationship $Y(t+\tau) = Y(t)M$. The eigenvalues of all such monodromy matrices are identical, and for a hyperbolic orbit, they are 1, μ_1, μ_2, ..., μ_{n-1}, where each of the μ_i's has modulus either strictly greater than or less than 1 [18]. These are the "characteristic multipliers" of the orbit.

In the plane, there are obviously only two characteristic multipliers associated with a periodic orbit: 1 and μ. The primary claim of this section is that linearization

of the orthogonality condition about a hyperbolic periodic orbit in the plane preserves the non-unity multiplier, μ.

The linearized orthogonality condition with small perturbation ρ has the form,

$$\left[D_r \mathbf{n}(\phi)^T \mathbf{\Phi}\left(\mathbf{x}(\phi)\right)\right] \rho = 0, \tag{2.16}$$

where ϕ is an arbitrary angular coordinate that parameterizes the curve. Since $\mathbf{x}(\phi) = \overline{\mathbf{x}}(\phi) + r(\phi)\overline{\mathbf{n}}(\phi)$ and $\mathbf{n}(\phi) = R_{\pi/2}\mathbf{x}_\phi / \left\|\mathbf{x}_\phi\right\|$, where $R_{\pi/2}$ is a $\pi/2$ rotation, this reduces to

$$\mathbf{n}(\phi)^T D\boldsymbol{\phi}\left(\mathbf{x}(\phi)\right)\overline{\mathbf{n}}(\phi)\rho + \frac{\mathbf{\Phi}\left(\mathbf{x}(\phi)\right)^T}{\left\|\mathbf{x}_\phi\right\|} R_{\pi/2}\left(\frac{d\mathbf{x}_\phi}{dr} - \frac{\left(\left(d\mathbf{x}_\phi/dr\right)^T \mathbf{x}_\phi\right)\mathbf{x}_\phi}{\mathbf{x}_\phi^T \mathbf{x}_\phi}\right)\rho = 0, \tag{2.17}$$

which is to say,

$$\mathbf{n}(\phi)^T D\boldsymbol{\phi}\left(\mathbf{x}(\phi)\right)\overline{\mathbf{n}}(\phi)\rho + \frac{\mathbf{\Phi}\left(\mathbf{x}(\phi)\right)^T}{\left\|\mathbf{x}_\phi\right\|} R_{\pi/2}\mathbf{n}(\phi)\mathbf{n}(\phi)^T \frac{d\mathbf{x}_\phi}{dr}\rho = 0. \tag{2.18}$$

If $\hat{\mathbf{x}}(\phi)$ is the exact periodic solution, then the vector field lies in the tangent plane at every point, so $\mathbf{\Phi}\left(\hat{\mathbf{x}}(\phi)\right)^T R_{\pi/2}\mathbf{n}(\phi) = \pm\left\|\mathbf{\Phi}\left(\hat{\mathbf{x}}(\phi)\right)\right\|$, where the sign is negative if $\mathbf{\Phi}\left(\hat{\mathbf{x}}(\phi)\right)$ lies in the same direction as $\hat{\mathbf{x}}_\phi(\phi)$ and positive otherwise. The local coordinate system indicates that $\hat{\mathbf{x}}_\phi = \overline{\mathbf{x}}_\phi + r_\phi\overline{\mathbf{n}} + r\overline{\mathbf{n}}_\phi$, so $\left(d\mathbf{x}_\phi/dr\right)\rho = \rho_\phi\overline{\mathbf{n}} + \rho\overline{\mathbf{n}}_\phi$.

These two relationships added into Equation (2.18) give the linearized problem about the exact solution,

$$\rho_\phi = \frac{\mathbf{n}^T}{\mathbf{n}^T\overline{\mathbf{n}}}\left(\pm\frac{\left\|\hat{\mathbf{x}}_\phi(\phi)\right\|}{\left\|\mathbf{\Phi}\left(\hat{\mathbf{x}}(\phi)\right)\right\|} D\mathbf{\Phi}\left(\hat{\mathbf{x}}(\phi)\right)\overline{\mathbf{n}}(\phi) - \overline{\mathbf{n}}_\phi\right)\rho. \tag{2.19}$$

If ϕ ranges from 0 to ϕ_1, then the "characteristic multiplier" associated with this equation is simply $\rho(\phi_1)$, with the initial condition $\rho(0) = 1$. A standard result about local coordinate systems ties the linearized problem to the characteristic multipliers of the variational problem.

Proposition 2.5 *Let $\overline{\mathbf{x}}(t)$ be an isolated periodic solution of Equation (1.1), let $\overline{Q}(t)$ be a moving orthonormal system in the graph of $\overline{\mathbf{x}}$, and let the characteristic multipliers of the associated variational system in Equation (2.15) be* 1, μ_1, μ_2, ..., μ_{n-1}.

Then the characteristic multipliers of the system,

$$\mathbf{z}_t = \overline{Q}(t)^T \left[-\overline{Q}_t(t) + D\mathbf{\Phi}\left(\overline{\mathbf{x}}(t)\right) \overline{Q}(t) \right] \mathbf{z}, \tag{2.20}$$

are μ_1, μ_2, ..., μ_{n-1}.

A proof of this and similar results is available in standard texts [18], so it is not included here.

One important fact to note is that in the plane, $\overline{\mathbf{n}}(t)^T \overline{\mathbf{n}}_t(t) = 0$. Also, if $\overline{\mathbf{x}}$ is the exact solution, then $\|\overline{\mathbf{x}}_\phi(\phi)\| \,/\, \|\mathbf{\Phi}(\overline{\mathbf{x}}(\phi))\| = \pm dt/d\phi$.

Thus, Equation (2.19) taken with $\hat{\mathbf{x}} = \overline{\mathbf{x}}$ and $\mathbf{n} = \overline{\mathbf{n}}$ reduces to the form of Proposition 2.5. It must be true that Equation (2.19) admits a characteristic multiplier $\pm\mu$ if $\overline{\mathbf{x}}$ is the exact solution.

Given this result, two natural questions emerge:

- Does a similar result hold if the system is not planar?

The linearization above relies on the fact that $\mathbf{n} = R_{\pi/2}\mathbf{x}_\phi / \|\mathbf{x}_\phi\|$. Such a closed-form description of Q is not available in general, so this question likely does not have a straightforward answer.

- Does Equation (2.19) admit characteristic multiplier $\pm\mu$ if $\overline{\mathbf{x}}$ is *not* the exact solution?

A limiting argument (as $\overline{\mathbf{x}} \to \hat{\mathbf{x}}$ in the $\mathcal{C}^1$ sense) follows easily, but numerical experiments indicate something stronger – that the multiplier does not change as long as $\overline{\mathbf{x}}$ is sufficiently close to the exact solution. This is reasonable, since the underlying attractivity structure of the orbit *should* persist irrespective of the coordinate system.

CHAPTER III

DISCRETIZATION OF ORTHOGONALITY CONDITION: SPECIAL CASES

Because of the obfuscated nature of $\dot{\boldsymbol{\phi}}$ and $\dot{\boldsymbol{\rho}}$, and because of the inherent limitations in the graph transform method (most notably the need for integration of the differential equation and the need to split the normal bundle into attracting and repelling spaces), numerical methods based on the orthogonality condition show the most promise for finding higher-dimensional invariant tori under flows. The orthogonality condition does have its own difficulties, however, particularly in the choice of normal vectors and the possibility of multiple solutions to the discrete equations. Numerical experimentation shows that many natural discretizations will lead to instability in the numerical solution, especially in higher dimensions.

This chapter gives sufficient conditions for convergence of the discrete orthogonality condition as applied to a hyperbolic, periodic orbit. The proof applies to several possible discretizations, as long as the instantaneous normal vectors – irrespective of computation method – are normal to the line segment between subsequent points on the orbit. The proof relies on inherent interchangeability between mid-point collocation and the orthogonality condition as applied to hyperbolic, periodic orbits, which indicates that the orthogonality condition represents a natural extension of collocation to higher-dimensional manifolds, plus a re-normalization rule.

This chapter also outlines two special cases in which the normal vectors have a canonical representation: 1) A periodic orbit in the plane, where the normal vector is a rotation of the tangent vector; and 2) a two-torus embedded in $\mathbb{R}^3$, where the

normal vector is a cross-product of the two tangent vectors. Finally, it contains a proof of ill-conditioning for a class of examples of two-tori in $\mathbb{R}^3$, which indicates that the convergence properties of the orthogonality condition are complicated and are not amenable to analysis. Chapter 5 proposes one technique for computing normal vectors for general p-tori embedded in $\mathbb{R}^n$.

3.1 Stability of Method for Periodic Orbits

Whether computing periodic orbits or higher-dimensional tori, the process always starts with an initial guess, $\overline{\mathbf{x}}$, and the method leads to a solution that is referenced to the initial guess via a local coordinate transformation.

Let $\widetilde{T} = \{\phi_1, \phi_2, \ldots, \phi_N\}$ be an ordered set of distinct points in S^1 (which is to say, T^1). Let $\overline{\mathbf{x}}(\phi) : S^1 \to \mathbb{R}^n$ be the nearby initial guess with requisite normal vectors, $\overline{Q}(\phi)$, as in Section 1.2, so the solution is an invariant, discrete "torus" of the form

$$\hat{\mathbf{x}}(\phi_i) = \overline{\mathbf{x}}(\phi_i) + \overline{Q}(\phi_i)\mathbf{r}\left(\phi_i\right), \qquad i = 1, 2, \ldots, N. \tag{3.1}$$

The $\mathbf{r}\left(\phi_i\right)$ give the invariant torus, where each $\mathbf{r}\left(\phi_i\right)$ is in $\mathbb{R}^{n-1}$.

To shorten the notation, let $\mathbf{y}_i = \mathbf{y}\left(\phi_i\right)$, where $\mathbf{y}$ can be $\overline{\mathbf{x}}$, $\hat{\mathbf{x}}$, $\mathbf{r}$, or $\overline{Q}$, so Equation (3.2) becomes

$$\hat{\mathbf{x}}_i = \overline{\mathbf{x}}_i + \overline{Q}_i\mathbf{r}_i, \qquad i = 1, 2, \ldots, N. \tag{3.2}$$

Some definitions will help to formalize the language. The following definitions are more general than necessary in the current section, but they will be useful later.

Definition 3.1 *The pair* $\left[\overline{\mathbf{x}}, \overline{Q}\right]$ *is a* reference p-torus *if* $\overline{\mathbf{x}} : T^p \to \mathbb{R}^n$ *is* $\mathcal{C}^2$ *and invertible with full-rank first derivative, and* $\overline{Q} : T^p \to \mathbb{R}^{n\times q}$, $q = n - p$, *is a* $\mathcal{C}^1$ *mapping such that at every* $\boldsymbol{\phi} \in T^p$, $\overline{Q}(\boldsymbol{\phi})$ *is a matrix whose orthonormal columns span the normal space to the image of* $\overline{\mathbf{x}}$ *at* $\overline{\mathbf{x}}(\boldsymbol{\phi})$.

In the special case of $p = 1$, the term "reference curve" replaces "reference 1-torus". The term "reference curve" may apply to the pair described above, to the

mapping $\overline{\mathbf{x}}$, or to the image of that mapping in the plane. By convention, a reference curve $\overline{\mathbf{x}}$ is said to be "close in the $\mathcal{C}^1$ sense" to a closed, $\mathcal{C}^1$-smooth, non-self-intersecting curve $\mathbf{y}$ in $\mathbb{R}^n$ if $\mathbf{y}$ admits a parameterization of the form $\mathbf{y}(\phi) = \overline{\mathbf{x}}(\phi) + \overline{Q}(\phi)\mathbf{r}(\phi)$, and the $\mathcal{C}^1$ norm of the difference, $\mathbf{y} - \overline{\mathbf{x}}$, is small. This definition extends naturally if $\mathbf{y}$ and $\overline{\mathbf{x}}$ are tori instead of curves. The next two definitions formalize the language of discrete points on the initial guess.

Definition 3.2 *A* skeleton *on a reference p-torus is a set,* $\left[\overline{\mathbf{x}}_{i_1,i_2,\ldots,i_p}\overline{Q}_{i_1,i_2,\ldots,i_p}\right]$, $i_k = 1, 2, \ldots, N_k$, $k = 1, 2, \ldots, p$, *such that the angles* $\boldsymbol{\phi}_{i_1,i_2,\ldots,i_p} = \left(\phi_{i_1}, \phi_{i_2}, \ldots, \phi_{i_p}\right)$ *represent a lexicographically ordered set of distinct points in* T^p, $\overline{\mathbf{x}}_{i_1,i_2,\ldots,i_p} = \overline{\mathbf{x}}\left(\boldsymbol{\phi}_{i_1,i_2,\ldots,i_p}\right)$, *and* $\overline{Q}_{i_1,i_2,\ldots,i_p} = \overline{Q}\left(\boldsymbol{\phi}_{i_1,i_2,\ldots,i_p}\right)$. *It is called a* δ*-skeleton for some* $\delta > 0$ *if the minimum arc-length distance along the surface of the graph of* $\overline{\mathbf{x}}$ *between neighboring points is less than* δ *everywhere.*

Given a skeleton on the initial guess, the desired solution comes entirely from a set of q-vectors, through Equation (3.2), and the solution $\hat{\mathbf{x}}$ should be close to the skeleton in a discrete sense approximating $\mathcal{C}^1$. The next definition is an attempt to extend the idea of $\mathcal{C}^1$ closeness to discrete solutions.

Definition 3.3 *Let* $\left[\overline{\mathbf{x}}_{i_1,i_2,\ldots,i_p}, \overline{Q}_{i_1,i_2,\ldots,i_p}\right]$ *be a skeleton on a reference p-torus. An* α-update *is a collection of real q-vectors,* $\left\{\mathbf{r}_{i_1,i_2,\ldots,i_p}\right\}$, *that satisfies two conditions:*

1. $\left\|\mathbf{r}_{i_1,i_2,\ldots,i_p}\right\| < \alpha$, *and*
2. $\left\|\mathbf{r}_{i_1,i_2,\ldots,i_p} - \mathbf{r}_{i'_1,i'_2,\ldots,i'_p}\right\| < \alpha\Delta s$, *where* Δs *is the minimum arc length distance between* $\overline{\mathbf{x}}_{i_1,i_2,\ldots,i_p}$ *and* $\overline{\mathbf{x}}_{i'_1,i'_2,\ldots,i'_p}$ *taken along the surface of the image of* $\overline{\mathbf{x}}$, *and* $\overline{\mathbf{x}}_{i_1,i_2,\ldots,i_p}$ *and* $\overline{\mathbf{x}}_{i'_1,i'_2,\ldots,i'_p}$ *are neighbors in the lexicographic ordering.*

By convention, the term "α-update" occasionally applies to the updated torus $\hat{\mathbf{x}}$, rather than the $\mathbf{r}$'s.

Whereas $\overline{Q}$ varies smoothly and is available everywhere on the surface of the graph of $\overline{\mathbf{x}}$, Equation (1.18) requires *instantaneous*, smoothly varying normal vectors. The choice of discretizations essentially reduces to a choice about how to calculate those vectors on the graph of $\hat{\mathbf{x}}$.

Normal vectors should always be orthogonal to the derivative, $d\hat{\mathbf{x}}/d\phi$, so one obvious place to start is to consider the mid-points. To simplify the algebraic operations, let $\hat{\mathbf{x}}_- = \hat{\mathbf{x}}_{i+1} - \hat{\mathbf{x}}_i$ and $\hat{\mathbf{x}}_{1/2} = \left(\hat{\mathbf{x}}_{i+1} + \hat{\mathbf{x}}_i\right)/2$. (Note that the notation suppresses the assumed index, i.) The derivative $d\hat{\mathbf{x}}/d\phi$ should be roughly in the same direction as $\hat{\mathbf{x}}_-$ at the half point. The results of this section apply to a class of discretizations with instantaneous normal vectors according to box schemes. The term "box scheme" has already appeared several times in this thesis, but the following is a more exact definition in the case of a periodic orbit. The definition extends in later sections to general p-tori in $\mathbb{R}^n$.

Definition 3.4 *Let* $\left[\overline{\mathbf{x}}_i, \overline{Q}_i\right]$ *be a skeleton on a reference curve. The skeleton is equipped with a* box scheme *if there exists* $\alpha > 0$ *such that for any* α*-update* $\hat{\mathbf{x}}$ *and every* i *there is a rule for finding a unique* $n \times q$ *matrix,* $Q_{1/2}$*, whose orthonormal columns are orthogonal to* $\hat{\mathbf{x}}_-$*. In addition,* $Q_{1/2}$ *must vary smoothly with* $\hat{\mathbf{x}}_-$*.*

Given a reference curve with a box scheme, Equation (1.18) has the representation,

$$Q_{1/2}^T \mathbf{\Phi}\left(\hat{\mathbf{x}}_{1/2}\right) = \mathbf{0}, \tag{3.3}$$

Later sections show how to calculate $Q_{1/2}$ in various circumstances, but the results in this section apply to any discretization scheme where $Q_{1/2}$ satisfies these properties.

The key to proving that the solutions of the discrete problem are isolated when applied to hyperbolic, periodic orbits is to recognize that all discretizations of the above form are equivalent to collocation using the "mid-point rule" with a particular choice of phase condition. Previous, well-established results then give closeness estimates.

Among other applications, collocation works on boundary-value problems of the form,

$$\begin{aligned} \dot{\mathbf{x}} &= \mathbf{\Phi}(\mathbf{x}) \\ \mathbf{g}(\mathbf{x}(0), \mathbf{x}(\tau)) &= 0, \end{aligned} \tag{3.4}$$

where $\mathbf{g}$ is the boundary condition, and τ might be the (unknown, minimal) period of a periodic orbit.

The driving idea behind collocation is to ensure that the vector field is in the same direction as the derivative $\dot{\mathbf{x}}$ at "ghost points" between the grid points of a particular discretization [2]. The particular case of interest is the mid-point rule, where

$$\hat{\mathbf{x}}_{-} - h_i \mathbf{\Phi}\left(\hat{\mathbf{x}}_{1/2}\right) = 0 \qquad \text{for all } i = 1, 2, \ldots, N, \tag{3.5}$$

where $h_i = t_{i+1} - t_i$. Immediately one sees that this is very close to the development in Equation (3.3), except that collocation normalizes by time instead of arc length. The translation of a time normalization into an arc-length normalization is the key to relating collocation with a mid-point rule to the orthogonality condition with a box scheme.

Collocation has a long history in numerical analysis, and its convergence properties are well-studied. Many of the proofs of convergence rely on a certain level of differentiability, plus a global Lipschitz condition, as in the following definition.

Definition 3.5 *The vector field $\mathbf{\Phi}$ is $\mathcal{C}^k_{\text{Lip}}$ in a neighborhood if it is $\mathcal{C}^k$ in the neighborhood, and if there exists $L > 0$ such that for all $\mathbf{y}$, $\mathbf{z}$ in the neighborhood and all non-negative collections of integers $s_1, s_2, ..., s_n$ such that $\sum_{i=1}^{n} s_i = u \leq k$, the following Lipschitz condition holds:*

$$\left\| \frac{\partial^u \mathbf{\Phi}(\mathbf{y})}{\partial x_1^{s_1} \partial x_2^{s_2} \cdots \partial x_n^{s_n}} - \frac{\partial^u \mathbf{\Phi}(\mathbf{z})}{\partial x_1^{s_1} \partial x_2^{s_2} \cdots \partial x_n^{s_n}} \right\| < L \left\| \mathbf{y} - \mathbf{z} \right\|$$

A typical convergence result is the following theorem [2, 9].

Theorem 3.1 *Let* $\mathbf{\Phi}$ *be* $\mathcal{C}^2_{\text{Lip}}$*, and let* $\mathbf{x}^*$ *be a solution of the system in Equation (3.4) such that* $\mathbf{x}^*$ *is isolated in a tubular neighborhood of radius* ρ_0*. Then there exists an* $h_0 > 0$ *and a* $\rho \leq \rho_0$ *such that for all mid-point collocation discretizations of Equation (3.4) with* $\max_i h_i \leq h_0$*, there exists a unique discrete solution* $\hat{\mathbf{x}}$ *of the collocation equations in a tubular neighborhood of* $\mathbf{x}$ *of radius* ρ*. Moreover,*

$$\|\hat{\mathbf{x}}_i - \mathbf{x}^*(t_i)\| = \mathcal{O}\left(h^2\right) \qquad \text{for all } \; i = 1, 2, \ldots, N. \tag{3.6}$$

No proof is included here. For a more general theorem with a proof, see [2].

The case under consideration is a hyperbolic, periodic orbit, which is to say an orbit whose only multiplier on the unit circle is 1. Theorem 3.1 does not apply directly to this situation because the period, τ, and hence the mesh, is unknown. The addition of a trivial equation in the vector field and an extra boundary condition changes the system into one to which classical collocation theory applies. Namely, Equation (3.4) becomes

$$\begin{aligned} \dot{\mathbf{x}} &= \tau \mathbf{\Phi}(\mathbf{x}) \\ \dot{\tau} &= 0 \\ \mathbf{x}(0) - \mathbf{x}(1) &= 0 \\ \sigma(\mathbf{x}) &= 0, \end{aligned} \tag{3.7}$$

where σ is a scalar condition known as the *phase condition*.

Many different types of phase conditions can make the problem well-posed. If $\overline{\mathbf{x}}$ is a reference curve with a skeleton, then one reasonable choice is to let $\sigma(\mathbf{x}) = (\mathbf{x}(0) - \overline{\mathbf{x}}_1)^T \overline{\mathbf{x}}'_1$, where the prime indicates differentiation with respect to ϕ, so $\overline{\mathbf{x}}'_1$ is a tangent vector to the graph of $\overline{\mathbf{x}}$ at $\overline{\mathbf{x}}_1$. This phase condition is valid as long as it satisfies a transversality condition [9], $D\sigma(\mathbf{x}^*)\mathbf{\Phi}(\mathbf{x}^*) \neq 0$, which reduces to $\mathbf{\Phi}(\mathbf{x}^*(0))^T \overline{\mathbf{x}}'_1 \neq 0$. Under such circumstances Theorem 3.1 applies to Equation (3.7).

All the machinery is in place now to draw the connection between collocation and the orthogonality condition for hyperbolic, periodic orbits.

Corollary 3.1 *Let* $\mathbf{\Phi}$ *be* $\mathcal{C}^2_{\text{Lip}}$*, and let* $\mathbf{x}^*$ *be an isolated solution of the system in Equation (3.7). Then for any reference curve,* $\left[\overline{\mathbf{x}}, \overline{Q}\right]$*, sufficiently close to* $\mathbf{x}^*$ *in the* $\mathcal{C}^1$ *sense, there exists* $\delta > 0$ *such that for any* δ*-skeleton on* $\left[\overline{\mathbf{x}}, \overline{Q}\right]$ *equipped with a box scheme, there exists a unique discrete solution* $\{\hat{\mathbf{x}}_i\}$*,* $i = 1, 2, \ldots, N$ *of the orthogonality equations (Equation (3.3)). Moreover, there exist* $0 = t_1 < t_2 < \cdots < t_N < \tau$ *such that*

$$\|\hat{\mathbf{x}}_i - \mathbf{x}^*(t_i)\| = \mathcal{O}\left(\max_i \|\hat{\mathbf{x}}_-\|^2\right) = \mathcal{O}\left(\delta^2\right) \qquad \text{for all } i = 1, 2, \ldots, N. \tag{3.8}$$

Proof

Let $\left[\overline{\mathbf{x}}_i, \overline{Q}_i\right]$, $i = 1, 2, \ldots, N$, be a δ-skeleton with small δ on a reference curve. As long as the reference curve is sufficiently close to the solution of Equation (3.7) in the $\mathcal{C}^1$-sense, it is possible to expand Equation (3.7) into $nN + N$ differential equations with $nN + N$ boundary conditions [2, 3]. The expansion is

$$\begin{aligned}
\dot{\mathbf{x}}_i &= (t_{i+1} - t_i)\,\tau \mathbf{\Phi}(\mathbf{x}_i), \qquad i = 1, 2, \ldots, N \\
\dot{\tau} &= 0 \\
\dot{t}_i &= 0, \qquad i = 2, 3, \ldots, N \\
\mathbf{x}_i(1) - \mathbf{x}_{i+1}(0) &= 0, \qquad i = 1, 2, \ldots, N \\
(\mathbf{x}_i(0) - \overline{\mathbf{x}}_i)^T \overline{\mathbf{x}}_i' &= 0,
\end{aligned} \tag{3.9}$$

with the convention that $t_1 = 0$, $t_{N+1} = 1$, and $i + 1 = 1$, when $i = N$. This system admits a unique solution if and only if Equation (3.7) does, since the t_i's are the times at which the periodic orbits intersect the subsequent normal spaces.

Consider the mid-point collocation discretization of Equation (3.9) where the mesh is $\{0, 1\}$. The discrete version of Equation (3.9) is

$$\begin{aligned}
\hat{\mathbf{x}}_- - \tau(t_{i+1} - t_i)\,\mathbf{\Phi}\left(\hat{\mathbf{x}}_{1/2}\right) &= 0 \\
(\hat{\mathbf{x}}_i - \overline{\mathbf{x}}_i)^T \overline{\mathbf{x}}'_i &= 0.
\end{aligned} \tag{3.10}$$

Theorem 3.1 says that if δ is sufficiently small – and thus N is sufficiently large – then there is a unique solution to Equation (3.10). That solution also satisfies

Equation (3.7), so Theorem 3.1 says that the solution is accurate to order h^2, where $h = \max_i (t_{i+1} - t_i) / \tau$.

Of course, $\{\hat{\mathbf{x}}_i\}$ is a solution if and only if the vector field is in the same direction as $\hat{\mathbf{x}}_-$ at each i (up to sign), which occurs if and only if the projection in Equation (3.3) is zero, so $\{\hat{\mathbf{x}}_i\}$ is also a solution to the discrete equations of the orthogonality condition. Conversely, any solution to the discrete equations of the orthogonality condition is also a solution to Equation (3.10) with $h_i = \|\hat{\mathbf{x}}_-\| / \left(\tau \left\|\mathbf{\Phi}\left(\hat{\mathbf{x}}_{1/2}\right)\right\|\right)$. The solution to Equation (3.10) is therefore unique (with unique t_i's).

The order equivalency between $\|\hat{\mathbf{x}}_-\|$ and δ is simply a restatement of closeness constraints. As long as the solution to the discrete orthogonality equations is an α-update with sufficiently small α (guaranteed if the reference curve is close to the real orbit in the $\mathcal{C}^1$ sense), then there exists a constant, C such that $\|\hat{\mathbf{x}}_-\| < C \|\overline{\mathbf{x}}_-\|$, and moreover C is independent of the skeleton for sufficiently small δ. This fact completes the proof. □

The next obvious question to ask is if a similar line of reasoning ensures isolated solutions near other types of "one-tori", for example hetero- or homoclinic orbits. Unfortunately, the presence of fixed points or other closed sub-manifolds can lead to instability in the orthogonality equations. See Sections 4.1.3 and 4.2.3 for examples.

Yet another question is how the concept of a box scheme applies to general p-dimensional tori. The following definition extends the definition of a box scheme to two-tori.

Definition 3.6 *Let* $\left[\overline{\mathbf{x}}_{i,j}\overline{Q}_{i,j}\right]$, $i = 1, 2, \ldots, N_i$, $j = 1, 2, \ldots, N_j$ *be a skeleton on a reference 2-torus. The skeleton is equipped with a* box scheme *if there exists* $\alpha > 0$ *such that for any* α*-update* $\hat{\mathbf{x}}$ *and every* $\{i, j\}$ *there is a rule for finding a unique* $n \times (n-2)$ *matrix,* $Q_{1/2}$*, whose orthonormal columns are orthogonal to the vectors,* $\hat{\mathbf{x}}_-^{(1)} = (\hat{\mathbf{x}}_{i+1,j} + \hat{\mathbf{x}}_{i+1,j+1} - \hat{\mathbf{x}}_{i,j+1} - \hat{\mathbf{x}}_{i,j}) /2$*, and* $\hat{\mathbf{x}}_-^{(2)} = (\hat{\mathbf{x}}_{i+1,j+1} + \hat{\mathbf{x}}_{i,j+1} - \hat{\mathbf{x}}_{i+1,j} - \hat{\mathbf{x}}_{i,j}) /2$*. In addition,* $Q_{1/2}$ *must vary smoothly with* $\hat{\mathbf{x}}_-^{(1)}$ *and* $\hat{\mathbf{x}}_-^{(2)}$*.*

Chapter 5 extends the notion of the box scheme to general p-tori, although the reader can probably discern at this point what the tangent vectors must be if the torus is p-dimensional. The primary difficulty is not in determining tangent directions, but rather in specifying $Q_{1/2}$, given those tangent directions.

Irrespective of the choice of rule for calculating $Q_{1/2}$, all applications of the orthogonality condition to skeletons with a box scheme result in the same basic sparsity pattern in the Jacobian, as outlined in the following definition.

Definition 3.7 *A matrix, J, is said to be* periodic, block bi-diagonal *if it has the form,*

$$J = \begin{pmatrix} A_1 & B_1 & 0 & \cdots & 0 & 0 \\ 0 & A_2 & B_2 & \cdots & 0 & 0 \\ \vdots & \vdots & \vdots & \ddots & \vdots & \vdots \\ 0 & 0 & 0 & \cdots & A_{N-1} & B_{N-1} \\ B_N & 0 & 0 & \cdots & 0 & A_N \end{pmatrix}, \tag{3.11}$$

where all of the blocks are square and are of the same dimension. In the special case that all the blocks are scalar, J is said to be periodic bi-diagonal.

If a periodic orbit is embedded in $\mathbb{R}^n$, then a box scheme yields a periodic, block bi-diagonal Jacobian whose blocks are full and have dimension $(n-1) \times (n-1)$.

3.2 Box Schemes in Two Special Cases

In two particular cases, there is a canonical representation for a normal vector given a representative tangent vector, and hence there is only one natural way to build a box scheme.

3.2.1 Limit Cycle in the Plane

If the limit cycle happens to be embedded in the plane, calculating $\overline{Q}$ and $Q_{1/2}$ is as simple as rotating the tangent by 90 degrees.

Let $\left[\overline{\mathbf{x}}_i, \overline{Q}_i\right]$, $i = 1, 2, \ldots, N$ be a skeleton on a reference curve. The canonical instantaneous normal vector up to sign is,

$$\mathbf{n}(\phi) = R_{\pi/2} \frac{d}{d\phi} \hat{\mathbf{x}}(\phi), \tag{3.12}$$

where $R_{\pi/2}$ is a $\pi/2$ rotation matrix:

$$R_{\pi/2} = \begin{pmatrix} 0 & 1 \\ -1 & 0 \end{pmatrix}. \tag{3.13}$$

It may be worthwhile to normalize $\mathbf{n}$ if there is a compelling reason to use unit vectors, but this may not be necessary in all circumstances. The natural choice of $\mathbf{n}$ and the definitions of $\hat{\mathbf{x}}_{1/2}$ and $\hat{\mathbf{x}}_-$ in previous sections transform Equation (3.3) into

$$\mathbf{\Phi}\left(\hat{\mathbf{x}}_{1/2}\right)^T R_{\pi/2} \hat{\mathbf{x}}_- / \left\|\hat{\mathbf{x}}_-\right\| = 0, \qquad i = 1, 2, \ldots, N. \tag{3.14}$$

This represents a valid box scheme, as in Definition 3.4. The definition $\hat{\mathbf{x}}(\phi_i) = \overline{\mathbf{x}}(\phi_i) + r_i \mathbf{n}(\phi_i)$ turns this into a system in $\{r_i\}$:

$$\mathbf{\Phi}\left(\frac{\overline{\mathbf{x}}_{i+1} + \overline{\mathbf{x}}_i + r_{i+1}\overline{\mathbf{n}}_{i+1} + r_i \overline{\mathbf{n}}_i}{2}\right)^T R_{\pi/2} \frac{\overline{\mathbf{x}}_{i+1} - \overline{\mathbf{x}}_i + r_{i+1}\overline{\mathbf{n}}_{i+1} - r_i \overline{\mathbf{n}}_i}{\left\|\overline{\mathbf{x}}_{i+1} - \overline{\mathbf{x}}_i + r_{i+1}\overline{\mathbf{n}}_{i+1} - r_i \overline{\mathbf{n}}_i\right\|} = 0. \tag{3.15}$$

(The collection $\{r_i\}$ represents an *update*.)

Solving this system with a root-finding routine such as Newton's method gives the r_i and hence the invariant torus. In summary, the algorithm progresses as follows:

Algorithm 3.1 *Solving for S^1 in $\mathbb{R}^2$.*

1. Start with a given λ, an ordered sequence of points $\{\phi_1, \phi_2, \ldots, \phi_N\} \in S^1$, and a nearby torus given by $\overline{\mathbf{x}} : S^1 \to \mathbb{R}^2$.

2. Calculate the normal directions, $\overline{\mathbf{n}}_i$, $i = 1, 2, \ldots, N$. For example, use the equation

$$\overline{\mathbf{n}}_i = R_{\pi/2} \frac{\overline{\mathbf{x}}(\phi_{i+1}) - \overline{\mathbf{x}}(\phi_{i-1})}{\left\|\overline{\mathbf{x}}(\phi_{i+1}) - \overline{\mathbf{x}}(\phi_{i-1})\right\|}. \tag{3.16}$$

3. Use Newton's method to solve the system given by applying the fundamental equation (*e.g.*, Equation (3.15)) at every $i = 1, 2, \ldots, N$.

4. The unknowns are a list of numbers, $\{r_i\}$. The calculated torus is $\hat{\mathbf{x}}(\phi_i) = \overline{\mathbf{x}}(\phi_i) + r_i\overline{\mathbf{n}}(\phi_i)$.

5. If desired, re-distribute the points according to arc length to get a better parameterization. This gives a new $\hat{\mathbf{x}}$.

6. Update $\lambda = \lambda + \Delta\lambda$, set $\overline{\mathbf{x}} = \hat{\mathbf{x}}$ and $r_i = 0$, $\forall\ i$ (or some other initial guess for the Newton iterations), and go back to Step 2.

The Jacobian introduced through the above choice of box scheme comprises some interesting properties. One is the relationship between the entries of the Jacobian and the non-unity multiplier.

First, one should note that the Jacobian structure is periodic bi-diagonal and looks like

$$J = \begin{pmatrix} a_1 & b_1 & 0 & \cdots & 0 & 0 \\ 0 & a_2 & b_2 & \cdots & 0 & 0 \\ \vdots & \vdots & \vdots & \ddots & \vdots & \vdots \\ 0 & 0 & 0 & \cdots & a_{N-1} & b_{N-1} \\ b_N & 0 & 0 & \cdots & 0 & a_N \end{pmatrix}, \tag{3.17}$$

where N is the number of points on the skeleton. The a's and b's grow large as $\delta \to 0$, but their product remains bounded and in fact approaches the characteristic multiplier of the linearized orthogonality condition.

Proposition 3.1 *Let $[\overline{\mathbf{x}}_i, \overline{\mathbf{n}}_i]$, $i = 1, 2, \ldots, N$, be a δ-skeleton on a reference curve in the plane, and let $\mathbf{x}^*(\phi) = \overline{\mathbf{x}}(\phi) + r(\phi)\overline{\mathbf{n}}(\phi)$ be an isolated, hyperbolic, periodic solution to Equation (1.1) where the vector field is $\mathcal{C}^2_{\text{Lip}}$. Let μ_1 be the characteristic multiplier of the system that results from linearizing the orthogonality condition about*

the periodic orbit (i.e., Equation (2.19) with $\mathbf{x}^*$ *in place of* $\hat{\mathbf{x}}$*). If the Jacobian, J, in Equation (3.17) is calculated at convergence, then*

$$\left| \prod_{i=1}^{N} b_i^{-1} a_i \right| = |\mu_1| + \mathcal{O}(\delta). \tag{3.18}$$

Proof

Let $\{\hat{\mathbf{x}}_i\}$ be the solution to the discrete orthogonality condition equations. Corollary 3.1 guarantees that there is a set of points on the graph of $\mathbf{x}^*$, say $\{\mathbf{x}_i^*\}$, such that $\|\hat{\mathbf{x}}_i - \mathbf{x}_i^*\| = \mathcal{O}(\delta^2)$. Let $\{\mathbf{n}_i^*\}$ be the corresponding normal directions.

Consider a center-difference approximation to the linearized orthogonality condition. The original condition is

$$\rho_\phi = \frac{\mathbf{n}^{*T}}{\overline{\mathbf{n}}^T \mathbf{n}^*} \left(\frac{\left\| \mathbf{x}_\phi^*(\phi) \right\|}{\mathbf{\Phi}\left(\mathbf{x}^*(\phi)\right) R_{\pi/2} \mathbf{n}^*(\phi)} D\mathbf{\Phi}\left(\mathbf{x}^*(\phi)\right) \overline{\mathbf{n}}(\phi) - \overline{\mathbf{n}}_\phi \right) \rho. \tag{3.19}$$

With the usual subscript notation, center difference approximations are

$$\rho(\phi) \approx \rho_{1/2} = (\rho_{i+1} + \rho_i)/2 \qquad \rho_\phi(\phi) \approx \rho_-/\Delta\phi = (\rho_{i+1} - \rho_i)/\Delta\phi \tag{3.20}$$

$$\mathbf{x}^*(\phi) \approx \mathbf{x}_{1/2}^* = \left(\mathbf{x}_{i+1}^* + \mathbf{x}_i^*\right)/2 \qquad \mathbf{x}_\phi^*(\phi) \approx \mathbf{x}_-^*/\Delta\phi = \left(\mathbf{x}_{i+1}^* - \mathbf{x}_i^*\right)/\Delta\phi \tag{3.21}$$

$$\mathbf{n}^*(\phi) \approx \mathbf{n}_{1/2}^* = \left(\mathbf{n}_{i+1}^* + \mathbf{n}_i^*\right)/2 \qquad \mathbf{n}_\phi^*(\phi) \approx \mathbf{n}_-^*/\Delta\phi = \left(\mathbf{n}_{i+1}^* - \mathbf{n}_i^*\right)/\Delta\phi \tag{3.22}$$

$$\overline{\mathbf{n}}(\phi) \approx \overline{\mathbf{n}}_{1/2} = (\overline{\mathbf{n}}_{i+1} + \overline{\mathbf{n}}_i)/2 \qquad \overline{\mathbf{n}}_\phi(\phi) \approx \overline{\mathbf{n}}_-/\Delta\phi = (\overline{\mathbf{n}}_{i+1} - \overline{\mathbf{n}}_i)/\Delta\phi, \tag{3.23}$$

which leads to a discrete approximation,

$$\frac{\rho_{i+1} - \rho_i}{\Delta\phi} = \frac{2\mathbf{n}_{1/2}^{*T}}{\left(\overline{\mathbf{n}}_{i+1} + \overline{\mathbf{n}}_i\right)^T \mathbf{n}_{1/2}^*} \left(\frac{\left\| \mathbf{x}_-^* \right\|/\Delta\phi}{\mathbf{\Phi}\left(\mathbf{x}_{1/2}^*\right) R_{\pi/2} \mathbf{n}_{1/2}^*} D\mathbf{\Phi}\left(\mathbf{x}_{1/2}^*\right) \overline{\mathbf{n}}_{1/2} - \frac{\overline{\mathbf{n}}_{i+1} - \overline{\mathbf{n}}_i}{\Delta\phi} \right) \frac{\rho_{i+1} + \rho_i}{2}. \tag{3.24}$$

Solving for ρ_{i+1} gives

$$\rho_{i+1} = \left(\frac{-\left\| \mathbf{x}_-^* \right\| \mathbf{n}_{1/2}^{*T} D\mathbf{\Phi}\left(\mathbf{x}_{1/2}^*\right) \overline{\mathbf{n}}_{1/2} + 2\mathbf{n}_{1/2}^{*T} \overline{\mathbf{n}}_i \mathbf{\Phi}\left(\mathbf{x}_{1/2}^*\right)^T R_{\pi/2} \mathbf{n}_{1/2}^*}{\left\| \mathbf{x}_-^* \right\| \mathbf{n}_{1/2}^{*T} D\mathbf{\Phi}\left(\mathbf{x}_{1/2}^*\right) \overline{\mathbf{n}}_{1/2} + 2\mathbf{n}_{1/2}^{*T} \overline{\mathbf{n}}_{i+1} \mathbf{\Phi}\left(\mathbf{x}_{1/2}^*\right)^T R_{\pi/2} \mathbf{n}_{1/2}^*} \right) \rho_i. \tag{3.25}$$

Because this is a center-difference approximation, the product $\prod_{i=2}^{N} \rho_{i+1}/\rho_i$ is an $\mathcal{O}(\delta)$ approximation to the characteristic multiplier. It therefore suffices to compare the coefficient in Equation (3.25) to the product of the a's and b's from the Jacobian. By definition,

$$a_i = \left[\frac{d}{dr_i}\mathbf{n}_{1/2}\mathbf{\Phi}\left(\hat{\mathbf{x}}_{1/2}\right)\right] \qquad \text{and} \qquad b_i = \left[\frac{d}{dr_{i+1}}\mathbf{n}_{1/2}\mathbf{\Phi}\left(\hat{\mathbf{x}}_{1/2}\right)\right]. \tag{3.26}$$

Explicit differentiation gives

$$\begin{aligned} a_i &= -\frac{\mathbf{n}_{1/2}^T\overline{\mathbf{n}}_i}{\|\hat{\mathbf{x}}_-\|}\mathbf{\Phi}\left(\hat{\mathbf{x}}_{1/2}\right)^T R_{\pi/2}\mathbf{n}_{1/2} + \frac{1}{2}\mathbf{n}_{1/2}^T D\mathbf{\Phi}\left(\hat{\mathbf{x}}_{1/2}\right)\overline{\mathbf{n}}_i, \text{and} \\ b_i &= \frac{\mathbf{n}_{1/2}^T\overline{\mathbf{n}}_{i+1}}{\|\hat{\mathbf{x}}_-\|}\mathbf{\Phi}\left(\hat{\mathbf{x}}_{1/2}\right)^T R_{\pi/2}\mathbf{n}_{1/2} + \frac{1}{2}\mathbf{n}_{1/2}^T D\mathbf{\Phi}\left(\hat{\mathbf{x}}_{1/2}\right)\overline{\mathbf{n}}_{i+1}, \end{aligned} \tag{3.27}$$

so

$$\frac{a_i}{b_i} = \frac{\|\hat{\mathbf{x}}_-\|\,\mathbf{n}_{1/2}^T D\mathbf{\Phi}\left(\hat{\mathbf{x}}_{1/2}\right)\overline{\mathbf{n}}_i - 2\mathbf{n}_{1/2}^T\overline{\mathbf{n}}_i\mathbf{\Phi}\left(\hat{\mathbf{x}}_{1/2}\right)^T R_{\pi/2}\mathbf{n}_{1/2}}{\|\hat{\mathbf{x}}_-\|\,\mathbf{n}_{1/2}^T D\mathbf{\Phi}\left(\hat{\mathbf{x}}_{1/2}\right)\overline{\mathbf{n}}_{i+1} + 2\mathbf{n}_{1/2}^T\overline{\mathbf{n}}_{i+1}\mathbf{\Phi}\left(\hat{\mathbf{x}}_{1/2}\right)^T R_{\pi/2}\mathbf{n}_{1/2}}. \tag{3.28}$$

The argument now reduces to a comparison of Equations (3.25) and (3.28).

The points $\{\mathbf{x}_i^*\}$ are chosen to satisfy $\left\|\hat{\mathbf{x}}_{1/2} - \mathbf{x}_{1/2}^*\right\| = \mathcal{O}(\delta^2)$ and $\left\|\mathbf{n}_{1/2} - \mathbf{n}_{1/2}^*\right\| = \mathcal{O}(\delta^2)$. These relationships, together with the fact that the vector field is $\mathcal{C}^2_{\text{Lip}}$, imply that

$$\mathbf{n}_{1/2}^T\overline{\mathbf{n}}_i\mathbf{\Phi}\left(\hat{\mathbf{x}}_{1/2}\right)^T R_{\pi/2}\mathbf{n}_{1/2} = \mathbf{n}_{1/2}^{*T}\overline{\mathbf{n}}_i\mathbf{\Phi}\left(\mathbf{x}_{1/2}^*\right)^T R_{\pi/2}\mathbf{n}_{1/2}^* + \mathcal{O}\left(\delta^2\right). \tag{3.29}$$

Although $\overline{\mathbf{n}}_{1/2}$ is only within order δ of $\overline{\mathbf{n}}_i$ and $\overline{\mathbf{n}}_{i+1}$, the differences $\|\hat{\mathbf{x}}_-\|$ and $\left\|\mathbf{x}_-^*\right\|$ are both of order δ themselves, so

$$\begin{aligned} \|\hat{\mathbf{x}}_-\|\,\mathbf{n}_{1/2}^T D\mathbf{\Phi}\left(\hat{\mathbf{x}}_{1/2}\right)\overline{\mathbf{n}}_{i+1} &= \left\|\mathbf{x}_-^*\right\|\mathbf{n}_{1/2}^T D\mathbf{\Phi}\left(\mathbf{x}_{1/2}^*\right)\overline{\mathbf{n}}_{1/2} + \mathcal{O}\left(\delta^2\right), \text{ and} \\ \|\hat{\mathbf{x}}_-\|\,\mathbf{n}_{1/2}^T D\mathbf{\Phi}\left(\hat{\mathbf{x}}_{1/2}\right)\overline{\mathbf{n}}_i &= \left\|\mathbf{x}_-^*\right\|\mathbf{n}_{1/2}^T D\mathbf{\Phi}\left(\mathbf{x}_{1/2}^*\right)\overline{\mathbf{n}}_{1/2} + \mathcal{O}\left(\delta^2\right). \end{aligned} \tag{3.30}$$

Equations (3.29) and (3.30) imply that $a_i/b_i = -\rho_{i+1}/\rho_i + \mathcal{O}(\delta^2)$. Because δ is order $1/N$,

$$\left|\prod_{i=1}^{N} a_i/b_i\right| = \left|\prod_{i=1}^{N} \rho_{i+1}/\rho_i\right| + \mathcal{O}(\delta), \tag{3.31}$$

which completes the proof. □

This proposition indicates not only that the product $\left|\prod_{i=1}^{N} a_i/b_i\right|$ is bounded well away from ± 1 – a sufficient condition for the Jacobian to be well-conditioned, as Proposition 3.3 will show later – but also that the product is closely related to a characteristic multiplier that indicates hyperbolicity. In other words, the convergence properties of the method are directly related to hyperbolicity properties of the torus itself in this particular case.

3.2.2 Two-Torus in $\mathbb{R}^3$

The algorithm for a two-torus in $\mathbb{R}^3$ also includes a canonical way to calculate the normal directions, in this case via cross products.

Let $\boldsymbol{\phi} = (\phi_1, \phi_2)$ be angular coordinates on T^2, and let $\boldsymbol{\phi}_{i,j} = ((\phi_1)_i, (\phi_2)_j)$, $i = 1, 2, \ldots, N_i$, $j = 1, 2, \ldots, N_j$, be the lexicographically bi-ordered set of distinct points in T^2,

$$\left\{ \begin{array}{llll} ((\phi_1)_1, (\phi_2)_1), & ((\phi_1)_1, (\phi_2)_2), & \ldots, & \left((\phi_1)_1, (\phi_2)_{N_j}\right), \\ ((\phi_1)_2, (\phi_2)_1), & ((\phi_1)_2, (\phi_2)_2), & \ldots, & \left((\phi_1)_2, (\phi_2)_{N_j}\right), \\ & & \vdots & \\ \left((\phi_1)_{N_i}, (\phi_2)_1\right), & \left((\phi_1)_{N_i}, (\phi_2)_2\right), & \ldots, & \left((\phi_1)_{N_i}, (\phi_2)_{N_j}\right) \end{array} \right\} .$$

Let $\overline{\mathbf{x}}(\boldsymbol{\phi})$ be a nearby torus with requisite normal vectors, $\overline{\mathbf{n}}(\boldsymbol{\phi})$, as in Section 1.2, so the solution is an invariant, discrete torus of the form,

$$\hat{\mathbf{x}}(\boldsymbol{\phi}_{i,j}) = \overline{\mathbf{x}}(\boldsymbol{\phi}_{i,j}) + r_{i,j}\overline{\mathbf{n}}(\boldsymbol{\phi}_{i,j}) \qquad (i,j) \in \{1, 2, \ldots, N_i\} \times \{1, 2, \ldots, N_j\} \ . \tag{3.33}$$

Notation is similar to the scalar case, where, if y represents $\hat{\mathbf{x}}$, $\overline{\mathbf{x}}$, ϕ, or $\overline{\mathbf{n}}$, then

$$y_{i,j} = y(\phi_{i,j}), \tag{3.34}$$

$$y_{-}^{(1)} = y_{i+1,j+1} - y_{i,j}, \tag{3.35}$$

$$y_{-}^{(2)} = y_{i+1,j} - y_{i,j+1}, \text{ and} \tag{3.36}$$

$$y_{1/2} = \left(y_{i,j} + y_{i+1,j} + y_{i,j+1} + y_{i+1,j+1}\right)/4. \tag{3.37}$$

Because the ambient space is $\mathbb{R}^3$, the cross product provides a normal vector up to sign:

$$\mathbf{n}(\boldsymbol{\phi}) = \frac{\hat{\mathbf{x}}_{\phi_1}(\boldsymbol{\phi}) \times \hat{\mathbf{x}}_{\phi_2}(\boldsymbol{\phi})}{\|\hat{\mathbf{x}}_{\phi_1}(\boldsymbol{\phi}) \times \hat{\mathbf{x}}_{\phi_2}(\boldsymbol{\phi})\|}. \tag{3.38}$$

Substituting this into Equation (1.18) reduces it to

$$\boldsymbol{\Phi}\left(\hat{\mathbf{x}}(\boldsymbol{\phi})\right)^T \frac{\hat{\mathbf{x}}_{\phi_1}(\boldsymbol{\phi}) \times \hat{\mathbf{x}}_{\phi_2}(\boldsymbol{\phi})}{\|\hat{\mathbf{x}}_{\phi_1}(\boldsymbol{\phi}) \times \hat{\mathbf{x}}_{\phi_2}(\boldsymbol{\phi})\|} = 0 \ , \tag{3.39}$$

which must apply at every $\boldsymbol{\phi}_{i,j}$.

It is now time to choose a discretization for the derivatives, which turns out to be a delicate task, since the choice of discrete representation for the derivatives, $\hat{\mathbf{x}}_{\phi_1}(\boldsymbol{\phi})$ and $\hat{\mathbf{x}}_{\phi_2}(\boldsymbol{\phi})$, affects the stability of the algorithm significantly.

The discretization investigated here is the natural generalization of the center-difference discretization for the one-torus. The approximations apply at the midpoints of boxes on the surface of the discrete torus.

$$\frac{\hat{\mathbf{x}}_{\phi_1}(\boldsymbol{\phi}) \times \hat{\mathbf{x}}_{\phi_2}(\boldsymbol{\phi})}{\|\hat{\mathbf{x}}_{\phi_1}(\boldsymbol{\phi}) \times \hat{\mathbf{x}}_{\phi_2}(\boldsymbol{\phi})\|} \approx \frac{\hat{\mathbf{x}}_{-}^{(1)} \times \hat{\mathbf{x}}_{-}^{(2)}}{\left\|\hat{\mathbf{x}}_{-}^{(1)} \times \hat{\mathbf{x}}_{-}^{(2)}\right\|}. \tag{3.40}$$

Again, the periodic conditions imply that $i+1 = 1$ when $i = N_i$ and $j+1 = 1$ when $j = N_j$. Equation (3.40) leads to a geometrically clear expression for the normal vector. Let $\mathbf{n}_{1/2}$ denote the updated normal vector at the center of the box (*i.e.*, $\mathbf{n}(\phi_{1/2})$), and

$$\mathbf{n}_{1/2} = \frac{\hat{\mathbf{x}}_{-}^{(1)} \times \hat{\mathbf{x}}_{-}^{(2)}}{\left\|\hat{\mathbf{x}}_{-}^{(1)} \times \hat{\mathbf{x}}_{-}^{(2)}\right\|}. \tag{3.41}$$

An easily verifiable identity shows that this is equivalent to an average of derivatives along the sides of the box:

$$\left(\hat{\mathbf{x}}_{-}^{(1)} \times \hat{\mathbf{x}}_{-}^{(2)}\right)/2 = \\ \frac{\left(\hat{\mathbf{x}}_{i+1,j+1} + \hat{\mathbf{x}}_{i,j+1} - \hat{\mathbf{x}}_{i+1,j} - \hat{\mathbf{x}}_{i,j}\right)}{2} \times \frac{\left(\hat{\mathbf{x}}_{i+1,j+1} + \hat{\mathbf{x}}_{i+1,j} - \hat{\mathbf{x}}_{i,j+1} - \hat{\mathbf{x}}_{i,j}\right)}{2}. \tag{3.42}$$

Thus, the discretization represents both an average between derivatives and a normal vector that comes from a cross product of diagonals on the box, and it therefore represents a box scheme as in Definition 3.6.

Equation (3.41), substituted into Equation (3.39), gives an expression in r that generates $N_i N_j$ equations.

$$\mathbf{\Phi}\left(\hat{\mathbf{x}}_{1/2}\right)^T \frac{\hat{\mathbf{x}}_-^{(1)} \times \hat{\mathbf{x}}_-^{(2)}}{\left\| \hat{\mathbf{x}}_-^{(1)} \times \hat{\mathbf{x}}_-^{(2)} \right\|} = 0 \ . \tag{3.43}$$

This is the fundamental equation for a two-torus embedded in $\mathbb{R}^3$. The solution algorithm is similar to Algorithm 3.1.

Algorithm 3.2 *Solving for T^2 in $\mathbb{R}^3$.*

1. Start with a given λ, a bi-ordered sequence of points as in Equation (3.32), and a nearby torus given by $\overline{\mathbf{x}} : T^2 \to \mathbb{R}^3$. In reality, $\overline{\mathbf{x}}$ is a collection of points in $\mathbb{R}^3$, not a smooth function.

2. Calculate the normal directions, $\overline{\mathbf{n}}_{i,j}$, $i = 1, 2, \ldots, N_i$, $j = 1, 2, \ldots, N_j$. For example, use the equation,

$$\overline{\mathbf{n}}_i = \frac{(\overline{\mathbf{x}}_{i+1,j+1} - \overline{\mathbf{x}}_{i-1,j-1}) \times (\overline{\mathbf{x}}_{i+1,j-1} - \overline{\mathbf{x}}_{i-1,j+1})}{\|(\overline{\mathbf{x}}_{i+1,j+1} - \overline{\mathbf{x}}_{i-1,j-1}) \times (\overline{\mathbf{x}}_{i+1,j-1} - \overline{\mathbf{x}}_{i-1,j+1})\|} \ . \tag{3.44}$$

3. Use Newton's method to solve the system given by applying the fundamental equation (*e.g.*, Equation (3.43)) at every point (i, j).

4. The torus at the solution is $\hat{\mathbf{x}}_{i,j} = \overline{\mathbf{x}}_{i,j} + r_{i,j}\overline{\mathbf{n}}_{i,j}$.

5. If desired, re-distribute the points to get a better parameterization. This gives a new $\hat{\mathbf{x}}$.

6. Update $\lambda = \lambda + \Delta\lambda$, set $\overline{\mathbf{x}} = \hat{\mathbf{x}}$ and $r_{i,j} = 0 \ \forall \ i, j$, and go back to Step 2.

The Jacobian for a two-torus in $\mathbb{R}^3$ is clearly periodic block-bi-diagonal with periodic bi-diagonal blocks, as in Definition 3.7. The next section contains a discussion of the stability of the method with this discretization as compared to other possibilities.

3.3 Stability of Method for Two-Torus in $\mathbb{R}^3$

As in the planar case, the most pressing questions are whether the system of equations given by Equation (3.43) is solvable, and if that solution is isolated. Unfortunately, the question is very complicated in higher dimensions, so much so that there is no general convergence proof for the orthogonalization technique with the box discretization.

For example, the method seems to be well-conditioned if the torus is hyperbolic, has no invariant sub-manifolds (*e.g.*, fixed points, periodic orbits), and the discretization *does not use an even number of points in the i and j directions*. This means that the orthogonality condition applied to a torus using a 39×39 discretization might be stable, while the same method applied to the same torus with a 40×40 discretization will be unconditionally unstable. Furthermore, if the torus contains a fixed point or a periodic orbit, then the method may or may not be stable, even if the discretization is not even-even.

Clearly, the convergence properties of the method are delicate and subtle. It is possible, however, to prove ill-conditioning in the case of an even-even discretization. Some of the concepts developed in the planar case carry over to higher-dimensional tori, but now there is no canonical distribution similar to arc length, so the general conditions for convergence do not have a simple definition of "reasonably well distributed".

In general, the Jacobian is poorly conditioned if the following are true:

1. The torus is $\mathcal{C}^2$-smooth.

2. The initial guess, $\overline{\mathbf{x}}$, is "good enough" in a discrete sense approximating the $\mathcal{C}^1$-norm.

3. The discretization points are close in the sense that, given two successive points in any direction, there exists a connecting path along the surface of the torus whose arc length does not exceed a given global maximum.

4. The discretization points are distributed in such a way that the boxes formed by their vertices are not overly elongated in a certain direction (although they may be skewed diagonally).

5. The discretization has an even number of points in both of the i and j directions.

These loosely worded conditions are nearly the same as in the proof of *well-conditioning* for periodic orbits, except for the extra complexity involved in discretely approximating a two-dimensional surface in $\mathbb{R}^3$.

Recall the terms *reference 2-torus*, *skeleton*, and *α-update* in Definitions 3.1, 3.2, and 3.3 respectively. The convention in this section is to refer to a "reference 2-torus" embedded in $\mathbb{R}^3$ simply as a "reference torus", denoted $[\overline{\mathbf{x}}, \overline{\mathbf{n}}]$. Also, i and j replace i_1, and i_2, so a skeleton has the form $[\{\overline{\mathbf{x}}_{i,j}\}, \{\overline{\mathbf{n}}_{i,j}\}]$, $i = 1, 2, \ldots, N_i$, $j = 1, 2, \ldots, N_j$. An α-update is a collection of scalars, since the codimension is one, so it has the form $\{r_{i,j}\}$.

Let $s_-^{(1)}$ denote the minimum arc length distance between $\overline{\mathbf{x}}_{i,j}$ and $\overline{\mathbf{x}}_{i+1,j+1}$ along the surface of of the image of $\overline{\mathbf{x}}$. Let $s_-^{(2)}$ denote the similar minimum arc length distance between $\overline{\mathbf{x}}_{i+1,j}$ and $\overline{\mathbf{x}}_{i,j+1}$. Note the suppression of the subscript in the notation – the assumption is always that the point of reference is (i, j).

Definition 3.8 *Let $\delta > 0$ and $1 \geq \kappa > 0$ be fixed. The set, $[\{\overline{\mathbf{x}}_{i,j}\}, \{\overline{\mathbf{n}}_{i,j}\}]$, $i = 1, 2, \ldots, N_i$, $j = 1, 2, \ldots, N_j$ is a δ, κ-*skeleton *on the reference torus, $[\overline{\mathbf{x}}, \overline{\mathbf{n}}]$, if it is a skeleton that satisfies three properties:*

1. $\max_{i,j} s_-^{(1)} < \delta$

2. $\max_{i,j} s_-^{(2)} < \delta$, *and*

3. $\max_{i,j} \sin\zeta < \kappa$, *where ζ is the angle between $\overline{\mathbf{x}}_-^{(1)}$ and $\overline{\mathbf{x}}_-^{(2)}$.*

The last condition ensures that the boxes of the skeleton do not become overly elongated. In particular,

$$\left\|\overline{\mathbf{x}}_{-}^{(1)} \times \overline{\mathbf{x}}_{-}^{(2)}\right\| / \left(\left\|\overline{\mathbf{x}}_{-}^{(1)}\right\| \left\|\overline{\mathbf{x}}_{-}^{(2)}\right\|\right) > \kappa. \tag{3.45}$$

The sparsity structure of the Jacobian is somewhat richer than in the planar case, and indeed the last property implying poor-conditioning – that an even number of discretization point be used in both directions – must be the result of linear algebraic considerations, not inherent properties of the torus.

The Jacobian for a two-torus in $\mathbb{R}^3$ using the discretization scheme described in the previous section is periodic, block bi-diagonal (as in Definition 3.7) with $N = N_i$. Moreover, each of the blocks A_i and B_i is $N_j \times N_j$ and is periodic bi-diagonal.

Let $f_{i,j} = \mathbf{\Phi}\left(\hat{\mathbf{x}}_{1/2}\right)^T \hat{\mathbf{x}}_{-}^{(1)} \times \hat{\mathbf{x}}_{-}^{(2)} / \left\|\hat{\mathbf{x}}_{-}^{(1)} \times \hat{\mathbf{x}}_{-}^{(2)}\right\|$ (so the goal of the Newton iteration is to solve the system $f_{i,j} = 0 \ \forall i, j$). The individual elements of A_i and B_i are as follows:

$$\begin{aligned}
(A_i)_{j,j} &= \frac{\partial f_{i,j}}{\partial r_{i,j}} &&= \mathbf{n}_{1/2}^T D\mathbf{\Phi}\left(\hat{\mathbf{x}}_{1/2}\right) \frac{\overline{\mathbf{n}}_{i,j}}{4} + \mathbf{\Phi}\left(\hat{\mathbf{x}}_{1/2}\right)^T \frac{\partial \mathbf{n}_{1/2}}{\partial r_{i,j}} \\
(A_i)_{j,j+1} &= \frac{\partial f_{i,j}}{\partial r_{i,j+1}} &&= \mathbf{n}_{1/2}^T D\mathbf{\Phi}\left(\hat{\mathbf{x}}_{1/2}\right) \frac{\overline{\mathbf{n}}_{i,j+1}}{4} + \mathbf{\Phi}\left(\hat{\mathbf{x}}_{1/2}\right)^T \frac{\partial \mathbf{n}_{1/2}}{\partial r_{i,j+1}} \\
(B_i)_{j,j} &= \frac{\partial f_{i,j}}{\partial r_{i+1,j}} &&= \mathbf{n}_{1/2}^T D\mathbf{\Phi}\left(\hat{\mathbf{x}}_{1/2}\right) \frac{\overline{\mathbf{n}}_{i+1,j}}{4} + \mathbf{\Phi}\left(\hat{\mathbf{x}}_{1/2}\right)^T \frac{\partial \mathbf{n}_{1/2}}{\partial r_{i+1,j}} \\
(B_i)_{j,j+1} &= \frac{\partial f_{i,j}}{\partial r_{i+1,j+1}} &&= \mathbf{n}_{1/2}^T D\mathbf{\Phi}\left(\hat{\mathbf{x}}_{1/2}\right) \frac{\overline{\mathbf{n}}_{i+1,j+1}}{4} + \mathbf{\Phi}\left(\hat{\mathbf{x}}_{1/2}\right)^T \frac{\partial \mathbf{n}_{1/2}}{\partial r_{i+1,j+1}},
\end{aligned} \tag{3.46}$$

where $j = 1, 2, \ldots, N_j$, and $j + 1$ is taken to be N_j-periodic.

The conditioning of the sums and/or differences of the block rows, $A_i \pm B_i$, determine invertibility properties of the Jacobian, so relationships between these derivatives are important in establishing a bound on the inverse norm of the whole matrix. A technical proposition helps to analyze these relationships.

Proposition 3.2 *Let $[\overline{\mathbf{x}}, \overline{\mathbf{n}}]$ be a reference torus. Then for any $\epsilon > 0$, there exist $\alpha, \delta > 0$, $1 \geq \kappa > 0$ such that for any δ, κ-skeleton, $[\{\overline{\mathbf{x}}_{i,j}\}, \{\overline{\mathbf{n}}_{i,j}\}]$, and for any*

α-update, $\{r_{i,j}\}$,

$$\left\| \frac{\partial \mathbf{n}_{1/2}}{\partial r_{i+1,j+1}} + \frac{\partial \mathbf{n}_{1/2}}{\partial r_{i,j}} \right\| < \epsilon, \ \textit{and}$$
$$\left\| \frac{\partial \mathbf{n}_{1/2}}{\partial r_{i+1,j}} + \frac{\partial \mathbf{n}_{1/2}}{\partial r_{i,j+1}} \right\| < \epsilon, \ \ \textit{for all} \ \ i = 1, 2, \ldots, N_i, \ j = 1, 2, \ldots, N_j.$$

Proof

It suffices to prove the first inequality because the proof of the second is essentially identical.

The proof of this proposition requires a few technical inequalities in order to bound terms in the expansion of the derivative. First, because $\overline{\mathbf{x}}$ is $\mathcal{C}^2$-smooth, there is a constant $C > 0$ such that for sufficiently small δ, $\left\| \overline{\mathbf{x}}_-^{(1,2)} \right\| \geq C s_-^{(1,2)}$.

The next bound is on the difference between subsequent normal vectors. Let $\boldsymbol{\gamma}$ be a curve parameterized in arc length along the surface of the graph of $\overline{\mathbf{x}}$ between $\overline{\mathbf{x}}_{i,j}$ and $\overline{\mathbf{x}}_{i+1,j+1}$ such that $\boldsymbol{\gamma}(0) = \overline{\mathbf{n}}_{i,j}$, $\boldsymbol{\gamma}(\Delta s) = \overline{\mathbf{n}}_{i+1,j+1}$. Then

$$\left\| \overline{\mathbf{n}}_-^{(1)} \right\| = \left\| \int_0^{\Delta s} \overline{\mathbf{n}}'(s) ds \right\|, \tag{3.47}$$

where $\overline{\mathbf{n}}'$ is the directional derivative with respect to arc length along the curve $\boldsymbol{\gamma}$. The fact that $\overline{\mathbf{x}}$ is a $\mathcal{C}^2$ function implies that the norm of the directional derivative is globally bounded by a constant, m, so

$$\left\| \overline{\mathbf{n}}_-^{(1)} \right\| \leq m s_-^{(1)} \qquad \text{and} \qquad \left\| \overline{\mathbf{n}}_-^{(2)} \right\| \leq m s_-^{(2)}. \tag{3.48}$$

(Recall that $s_-^{(1)}$ is the *shortest* arc length along the surface of the graph of $\overline{\mathbf{x}}$ between $\overline{\mathbf{x}}_{i,j}$ and $\overline{\mathbf{x}}_{i+1,j+1}$, and $s_-^{(2)}$ is the same between $\overline{\mathbf{x}}_{i+1,j}$ and $\overline{\mathbf{x}}_{i,j+1}$.)

The next ratio to bound is $\left\| \overline{\mathbf{x}}_-^{(1)} \right\| / \left\| \hat{\mathbf{x}}_-^{(1)} \right\|$. The largest possible value occurs when $\left\| \overline{\mathbf{n}}_-^{(1)} \right\|$ is at a maximum, and $r_{i+1,j+1} = r_{i,j} = \pm\alpha$. In this case,

$$\left\| \hat{\mathbf{x}}_-^{(1)} \right\| = \left\| \overline{\mathbf{x}}_-^{(1)} \pm \alpha \overline{\mathbf{n}}_-^{(1)} \right\| \geq \left\| \overline{\mathbf{x}}_-^{(1)} \right\| - \alpha \left\| \overline{\mathbf{n}}_-^{(1)} \right\| \geq \left\| \overline{\mathbf{x}}_-^{(1)} \right\| - \alpha m s_-^{(1)}. \tag{3.49}$$

A similar argument for $\overline{\mathbf{x}}_-^{(2)}$ applies, so

$$\left\| \hat{\mathbf{x}}_-^{(1,2)} \right\| / s_-^{(1,2)} \geq C - \alpha m \qquad \text{and} \qquad \left\| \overline{\mathbf{x}}_-^{(1,2)} \right\| / \left\| \hat{\mathbf{x}}_-^{(1,2)} \right\| \leq \alpha m / C. \tag{3.50}$$

Equations (3.48) and (3.50) together imply that

$$\left\|\overline{\mathbf{n}}_{-}^{(1,2)}\right\| / \left\|\hat{\mathbf{x}}_{-}^{(1,2)}\right\| \leq m/(C-\alpha m). \tag{3.51}$$

Another worst-case analysis bounds the reciprocal, $\left\|\hat{\mathbf{x}}_{-}^{(1)}\right\| / \left\|\overline{\mathbf{x}}_{-}^{(1)}\right\|$. The bound is

$$\begin{aligned}\left\|\hat{\mathbf{x}}_{-}^{(1)}\right\| / \left\|\overline{\mathbf{x}}_{-}^{(1)}\right\| &\leq \left(\left\|\overline{\mathbf{x}}_{-}^{(1)}\right\| + \left\|r_{i+1,j+1}\overline{\mathbf{n}}_{i+1,j+1} - r_{i,j}\overline{\mathbf{n}}_{i,j}\right\|\right) / \left\|\overline{\mathbf{x}}_{-}^{(1)}\right\| \\ &< 1 + \alpha s_{-}^{(1)} / \left\|\overline{\mathbf{x}}_{-}^{(1)}\right\| + \alpha \left\|\overline{\mathbf{n}}_{-}^{(1)}\right\| / \left\|\overline{\mathbf{x}}_{-}^{(1)}\right\| \end{aligned} \tag{3.52}$$

and, since a similar argument applies to $\overline{\mathbf{n}}_{-}^{(2)}$,

$$\left\|\hat{\mathbf{x}}_{-}^{(1,2)}\right\| / \left\|\overline{\mathbf{x}}_{-}^{(1,2)}\right\| \leq 1 + \alpha m/C + \alpha/C. \tag{3.53}$$

The final inequality constrains the normalization factors in the calculation of normal vectors. The ratio is

$$\begin{aligned}\frac{\left\|\overline{\mathbf{x}}_{-}^{(1)} \times \overline{\mathbf{x}}_{-}^{(2)}\right\|}{\left\|\hat{\mathbf{x}}_{-}^{(1)} \times \hat{\mathbf{x}}_{-}^{(2)}\right\|} &\leq \frac{\left\|\overline{\mathbf{x}}_{-}^{(1)} \times \overline{\mathbf{x}}_{-}^{(2)}\right\|}{\left(\begin{array}{r} \left\|\overline{\mathbf{x}}_{-}^{(1)} \times \overline{\mathbf{x}}_{-}^{(2)}\right\| - \left\|\overline{\mathbf{x}}_{-}^{(1)} \times \left(r_{i+1,j}\overline{\mathbf{n}}_{i+1,j} - r_{i,j+1}\overline{\mathbf{n}}_{i,j+1}\right)\right\| - \\ \left\|\left(r_{i+1,j+1}\overline{\mathbf{n}}_{i+1,j+1} - r_{i,j}\overline{\mathbf{n}}_{i,j}\right) \times \overline{\mathbf{x}}_{-}^{(2)}\right\| - \\ \left\|\left(r_{i+1,j+1}\overline{\mathbf{n}}_{i+1,j+1} - r_{i,j}\overline{\mathbf{n}}_{i,j}\right) \times \left(r_{i+1,j}\overline{\mathbf{n}}_{i+1,j} - r_{i,j+1}\overline{\mathbf{n}}_{i,j+1}\right)\right\| \end{array}\right)} \\ &\leq \frac{\left\|\overline{\mathbf{x}}_{-}^{(1)}\right\| \left\|\overline{\mathbf{x}}_{-}^{(2)}\right\|}{\left(\begin{array}{r} \kappa \left\|\overline{\mathbf{x}}_{-}^{(1)}\right\| \left\|\overline{\mathbf{x}}_{-}^{(2)}\right\| - \left\|\overline{\mathbf{x}}_{-}^{(1)}\right\| \left(\alpha s_{-}^{(2)} + \alpha \left\|\overline{\mathbf{n}}_{-}^{(2)}\right\|\right) - \\ \left\|\overline{\mathbf{x}}_{-}^{(2)}\right\| \left(\alpha s_{-}^{(1)} + \alpha \left\|\overline{\mathbf{n}}_{-}^{(1)}\right\|\right) - \\ \left(\alpha s_{-}^{(2)} + \alpha \left\|\overline{\mathbf{n}}_{-}^{(2)}\right\|\right) \left(\alpha s_{-}^{(1)} + \alpha \left\|\overline{\mathbf{n}}_{-}^{(1)}\right\|\right) \end{array}\right)}. \end{aligned} \tag{3.54}$$

The arc-length inequalities give

$$\left(\alpha s_{-}^{(1,2)} + \alpha \left\|\overline{\mathbf{n}}_{-}^{(1,2)}\right\|\right) / \left\|\overline{\mathbf{x}}_{-}^{(1,2)}\right\| \leq (\alpha m + \alpha)/C, \quad \text{so} \tag{3.55}$$

$$\frac{\left\|\overline{\mathbf{x}}_{-}^{(1)} \times \overline{\mathbf{x}}_{-}^{(2)}\right\|}{\left\|\hat{\mathbf{x}}_{-}^{(1)} \times \hat{\mathbf{x}}_{-}^{(2)}\right\|} \leq \frac{1}{\kappa - 2(\alpha m + \alpha)/C - (\alpha m + \alpha)^2/C^2}. \tag{3.56}$$

These inequalities will help to minimize pieces of the expansion of the equations of the proposition. Parsing the derivative yields

$$\frac{\partial \mathbf{n}_{1/2}}{\partial r_{i+1,j+1}} + \frac{\partial \mathbf{n}_{1/2}}{\partial r_{i,j}} = R_{\pi/2}\left(\frac{\partial}{\partial r_{i,j}} + \frac{\partial}{\partial r_{i+1,j+1}}\right)\frac{\hat{\mathbf{x}}_-^{(1)} \times \hat{\mathbf{x}}_-^{(2)}}{\left\|\hat{\mathbf{x}}_-^{(1)} \times \hat{\mathbf{x}}_-^{(2)}\right\|}$$

$$= R_{\pi/2}\frac{\overline{\mathbf{n}}_-^{(1)} \times \hat{\mathbf{x}}_-^{(2)}}{\left\|\hat{\mathbf{x}}_-^{(1)} \times \hat{\mathbf{x}}_-^{(2)}\right\|} - \frac{\left(\hat{\mathbf{x}}_-^{(1)} \times \hat{\mathbf{x}}_-^{(2)}\right)\left(\hat{\mathbf{x}}_-^{(1)} \times \hat{\mathbf{x}}_-^{(2)}\right)^T}{\left\|\hat{\mathbf{x}}_-^{(1)} \times \hat{\mathbf{x}}_-^{(2)}\right\|^3}\left(\overline{\mathbf{n}}_-^{(1)} \times \hat{\mathbf{x}}_-^{(2)}\right),$$

which can be written,

$$\frac{\partial \mathbf{n}_{1/2}}{\partial r_{i+1,j+1}} + \frac{\partial \mathbf{n}_{1/2}}{\partial r_{i,j}} = R_{\pi/2}\Pi_{\mathcal{T}}\frac{\overline{\mathbf{n}}_-^{(1)} \times \hat{\mathbf{x}}_-^{(2)}}{\left\|\hat{\mathbf{x}}_-^{(1)} \times \hat{\mathbf{x}}_-^{(2)}\right\|}, \tag{3.57}$$

where $\Pi_{\mathcal{T}}$ is the projection onto the "tangent space at the half point," *i.e.*, the space spanned by $\hat{\mathbf{x}}_-^{(1)}$ and $\hat{\mathbf{x}}_-^{(2)}$. The strategy for minimizing this projection is 1) to show that the item being projected is bounded in norm, then 2) to show that it approaches the normal direction under the assumed constraints for the statement of the proposition.

Equation (3.56) gives the inequality,

$$\left\|\frac{\overline{\mathbf{n}}_-^{(1)} \times \hat{\mathbf{x}}_-^{(2)}}{\left\|\hat{\mathbf{x}}_-^{(1)} \times \hat{\mathbf{x}}_-^{(2)}\right\|}\right\| \leq \frac{\left\|\overline{\mathbf{n}}_-^{(1)}\right\|\left\|\hat{\mathbf{x}}_-^{(2)}\right\|}{\kappa\left\|\overline{\mathbf{x}}_-^{(1)}\right\|\left\|\overline{\mathbf{x}}_-^{(2)}\right\|\left(\kappa - 2\left(\alpha m + \alpha\right)/C - \left(\alpha m + \alpha\right)^2/C^2\right)}. \tag{3.58}$$

Application of Equation (3.53) refines the inequality and shows that a constant majorizes $\left\|\overline{\mathbf{n}}_-^{(1)} \times \hat{\mathbf{x}}_-^{(2)} / \left\|\hat{\mathbf{x}}_-^{(1)} \times \hat{\mathbf{x}}_-^{(2)}\right\|\right\|$.

Therefore, in order to show that the right-hand side of Equation (3.57) can be made arbitrarily small – and in doing so, prove the proposition – it suffices to show that the cross product $\overline{\mathbf{n}}_-^{(1)} \times \hat{\mathbf{x}}_-^{(2)}$ approaches the direction of $\mathbf{n}_{1/2}$ as $\alpha \to 0$ (for sufficiently small δ and sufficiently large κ). One way to accomplish this is to minimize

$\mathbf{n}_{1/2}^T \overline{\mathbf{n}}_-^{(1)} / \left\| \hat{\mathbf{x}}_-^{(1)} \right\|$, which is implied by minimizing four different items:

$$\begin{aligned} \left| \overline{\mathbf{n}}_{i,j}^T \hat{\mathbf{x}}_-^{(1)} \right| / \left\| \hat{\mathbf{x}}_-^{(1)} \right\|, \qquad & \left| \overline{\mathbf{n}}_{i,j}^T \hat{\mathbf{x}}_-^{(2)} \right| / \left\| \hat{\mathbf{x}}_-^{(2)} \right\|, \\ \left| \overline{\mathbf{n}}_{i+1,j+1}^T \hat{\mathbf{x}}_-^{(1)} \right| / \left\| \hat{\mathbf{x}}_-^{(1)} \right\|, \quad \text{and} \quad & \left| \overline{\mathbf{n}}_{i+1,j+1}^T \hat{\mathbf{x}}_-^{(2)} \right| / \left\| \hat{\mathbf{x}}_-^{(2)} \right\|. \end{aligned} \tag{3.59}$$

The argument is similar for all four quantities, so the following discussion only minimizes one of them. The top left term expands as

$$\begin{aligned} \frac{\left| \overline{\mathbf{n}}_{i,j}^T \hat{\mathbf{x}}_-^{(1)} \right|}{\left\| \hat{\mathbf{x}}_-^{(1)} \right\|} &= \frac{\left| \overline{\mathbf{n}}_{i,j}^T \overline{\mathbf{x}}_-^{(1)} + (r_{i+1,j+1} - r_{i,j}) \, \overline{\mathbf{n}}_{i,j}^T \overline{\mathbf{n}}_{i+1,j+1}^T + r_{i,j} \overline{\mathbf{n}}_{i,j}^T \overline{\mathbf{n}}_-^{(1)} \right|}{\left\| \overline{\mathbf{x}}_-^{(1)} \right\|} \frac{\left\| \overline{\mathbf{x}}_-^{(1)} \right\|}{\left\| \hat{\mathbf{x}}_-^{(1)} \right\|} \\ &\leq \left(\left| \overline{\mathbf{n}}_{i,j}^T \overline{\mathbf{x}}_-^{(1)} \right| / \left\| \overline{\mathbf{x}}_-^{(1)} \right\| + \alpha/C + \alpha m/C \right) \frac{\alpha m}{C}. \end{aligned} \tag{3.60}$$

The key to minimizing the right-hand side is to recognize that the direction of $\overline{\mathbf{x}}_-^{(1)} / \left\| \overline{\mathbf{x}}_-^{(1)} \right\|$ approaches the tangent space at as $\left\| \overline{\mathbf{x}}_-^{(1)} \right\| \to 0$. More precisely, for a fixed point, $\overline{\mathbf{x}}_{i,j}$, where the other vertices of the box ($\overline{\mathbf{x}}_{i,j+1}$, $\overline{\mathbf{x}}_{i+1,j}$, and $\overline{\mathbf{x}}_{i+1,j+1}$) vary,

$$\overline{\mathbf{n}}_{i,j} = \lim_{\left\| \overline{\mathbf{x}}_-^{(1,2)} \right\| \to 0} \frac{\overline{\mathbf{x}}_-^{(1)} \times \overline{\mathbf{x}}_-^{(2)}}{\left\| \overline{\mathbf{x}}_-^{(1)} \times \overline{\mathbf{x}}_-^{(2)} \right\|}, \tag{3.61}$$

where the limit is taken with the κ constraint of Equation (3.45).

Therefore, $\lim_{\delta \to 0} \left| \overline{\mathbf{n}}_{i,j}^T \overline{\mathbf{x}}_-^{(1)} \right| / \left\| \overline{\mathbf{x}}_-^{(1)} \right\| = 0$, which demonstrates that the right-hand side of Equation (3.60) shrinks to zero by restricting δ and α. As mentioned above, the rest of the items in Equation (3.59) have the same bound. This consequently minimizes Equation (3.57) and completes the proof. □

It is now relatively easy to show how the Jacobian becomes ill-conditioned when N_i and N_j are even numbers. Let $[\overline{\mathbf{x}}, \overline{\mathbf{n}}]$ be a reference torus, and let $[\{\overline{\mathbf{x}}_{i,j}\}, \{\overline{\mathbf{n}}_{i,j}\}]$ be a δ, κ-skeleton, with δ sufficiently small and κ sufficiently large. Assume that there is a tubular neighborhood of the graph of $\hat{\mathbf{x}}$ where the vector field is $\mathcal{C}^1_{\text{Lip}}$. Let J be the Jacobian at some α-update, and let the individual blocks be labeled as in Definition 3.7.

Equation (3.46) implies that for any $i = 1, 2, \ldots, N_i$,

$$A_i - B_i = \begin{pmatrix} c_{i,1} & c_{i,1} & 0 & \cdots & 0 & 0 \\ 0 & c_{i,2} & c_{i,2} & \cdots & 0 & 0 \\ \vdots & \vdots & \vdots & \ddots & \vdots & \vdots \\ 0 & 0 & 0 & \cdots & c_{i,N_j-1} & c_{i,N_j-1} \\ c_{i,N_j} & 0 & 0 & \cdots & 0 & c_{i,N_j} \end{pmatrix} + \begin{pmatrix} \varepsilon_{i,1} & \varepsilon'_{i,1} & 0 & \cdots & 0 & 0 \\ 0 & \varepsilon_{i,2} & \varepsilon'_{i,2} & \cdots & 0 & 0 \\ \vdots & \vdots & \vdots & \ddots & \vdots & \vdots \\ 0 & 0 & 0 & \cdots & \varepsilon_{i,N_j-1} & \varepsilon'_{i,N_j-1} \\ \varepsilon'_{i,N_j} & 0 & 0 & \cdots & 0 & \varepsilon_{i,N_j} \end{pmatrix}, \quad (3.62)$$

where

$$c_{i,j} = \mathbf{\Phi}\left(\hat{\mathbf{x}}_{1/2}\right)^T \left(\frac{\partial \mathbf{n}_{1/2}}{\partial r_{i,j}} - \frac{\partial \mathbf{n}_{1/2}}{\partial r_{i+1,j}}\right), \quad (3.63)$$

$$\varepsilon_{i,j} = \mathbf{n}_{1/2}^T D\mathbf{\Phi}\left(\hat{\mathbf{x}}_{1/2}\right) \frac{\overline{\mathbf{n}}_{i,j} - \overline{\mathbf{n}}_{i+1,j}}{4}, \text{ and} \quad (3.64)$$

$$\varepsilon'_{i,j} = \mathbf{n}_{1/2}^T D\mathbf{\Phi}\left(\hat{\mathbf{x}}_{1/2}\right) \frac{\overline{\mathbf{n}}_{i,j+1} - \overline{\mathbf{n}}_{i+1,j+1}}{4} + \mathbf{\Phi}\left(\hat{\mathbf{x}}_{1/2}\right)^T \left(\frac{\partial \mathbf{n}_{1/2}}{\partial r_{i,j+1}} - \frac{\partial \mathbf{n}_{1/2}}{\partial r_{i+1,j+1}} - \frac{\partial \mathbf{n}_{1/2}}{\partial r_{i,j}} + \frac{\partial \mathbf{n}_{1/2}}{\partial r_{i+1,j}}\right). \quad (3.65)$$

If N_j is even, then the first matrix on the right-hand side of Equation (3.62) has a null eigenvector (with N_j elements): $\mathbf{v} = \begin{pmatrix} 1 & -1 & 1 & \cdots & -1 \end{pmatrix}^T$. Hence, if $\varepsilon_{i,j}, \varepsilon'_{i,j} = 0$ for all i, j, and if N_i and N_j are even, then the Jacobian is singular with a null eigenvector (with $N_i \cdot N_j$ elements): $\begin{pmatrix} \mathbf{v}^T & -\mathbf{v}^T & \mathbf{v}^T & \cdots & -\mathbf{v}^T \end{pmatrix}^T$.

To show ill-conditioning, it therefore suffices to minimize all the $\varepsilon_{i,j}$ and $\varepsilon'_{i,j}$ using α, δ, and κ. The fact that the vector field is $\mathcal{C}^1_{\text{Lip}}$ gives a universal bound on the norm of $\mathbf{\Phi}\left(\hat{\mathbf{x}}_{1/2}\right)$ and $D\mathbf{\Phi}\left(\hat{\mathbf{x}}_{1/2}\right)$ for a sufficiently constrained update. Moreover, $\|\overline{\mathbf{n}}_{i,j} - \overline{\mathbf{n}}_{i+1,j}\|$ and $\|\overline{\mathbf{n}}_{i,j+1} - \overline{\mathbf{n}}_{i+1,j+1}\|$ and are of the same order as the arc length

between $\overline{\mathbf{x}}_{i,j}$ and $\overline{\mathbf{x}}_{i+1,j}$ and between $\overline{\mathbf{x}}_{i,j+}$ and $\overline{\mathbf{x}}_{i+1,j+1}$ respectively (as in Equation (3.48)). The limit $\delta \to 0$ therefore implies that $\varepsilon_{i,j} \to 0$ for all i, j.

Shrinking δ also causes the first term in the definition of $\varepsilon'_{i,j}$ to go to zero, and hence Lemma 3.2 implies that J becomes progressively more poorly conditioned as α, δ go to zero and κ remains near one.

The most obvious way to attempt to repair the ill-conditioning of the Jacobian is to force N_i and/or N_j to be odd. Unfortunately, this will not guarantee stability for many different types of tori.

Numerical experimentation has shown (in Chapter 4 for example) that if a torus is hyperbolic and contains no closed, invariant, sub-manifolds, then the method generally works well if N_i and/or N_j is odd. If the torus contains a periodic orbit or fixed point, however, then the method is not always stable. The variability between examples indicates that proving a general set of stability conditions for the method would be a very complicated task.

Thus, the only practical way to check stability at present is to monitor the condition number of the Jacobian directly on a case-by-case basis. For two-tori in $\mathbb{R}^3$, this is not too onerous, but the computation of condition numbers for higher-dimensional tori can take too much time. It is useful to have a short cut for evaluating the Jacobian that takes advantage of the structure of the matrix to minimize computation time.

The following proposition outlines a linear algebraic property of the Jacobian that helps to determine a bound on the inverse norm, but it does not appear to be tied intrinsically to any property of the torus.

Proposition 3.3 *Let J be a periodic, block bi-diagonal matrix as in Definition 3.7, and let m and n be positive real numbers. Assume that J satisfies one of the following conditions (where sums and differences are N-periodic, so $N+1$ is taken to be 1):*

Condition I: The B blocks are invertible, and

$$a) \quad \left\|B_i^{-1}A_iB_{i-1}^{-1}A_{i-1}\cdots B_k^{-1}\right\| \le m \quad \forall\, i=1,2,\ldots,N,\ k=i,i-1,\ldots,i+1$$

$$b) \quad \left\|\left(I-(-1)^N B_i^{-1}A_iB_{i-1}^{-1}A_{i-1}\cdots B_{i+1}^{-1}A_{i+1}\right)^{-1}\right\| \le n \quad \forall\, i=1,2,\ldots,N.$$

Condition II: The A blocks are invertible, and

$$a) \quad \left\|A_i^{-1}B_iA_{i+1}^{-1}B_{i+1}\cdots A_k^{-1}\right\| \le m, \quad i=1,2,\ldots,N,\ k=i,i+1,\ldots,i-1$$

$$b) \quad \left\|\left(I-(-1)^N A_i^{-1}B_iA_{i+1}^{-1}B_{i+1}\cdots A_{i-1}^{-1}B_{i-1}\right)^{-1}\right\| \le n, \quad i=1,2,\ldots,N.$$

Then $\|J^{-1}\| \le mnN$.

Proof

Let each block of the Jacobian be $N'\times N'$, and pick $\mathbf{y}\in\mathbb{R}^{NN'}$ such that $\|\mathbf{y}\|=1$. Let $\mathbf{y}$ be block partitioned, $\mathbf{y}=\begin{pmatrix}\mathbf{y}_1^T & \mathbf{y}_2^T & \cdots & \mathbf{y}_N^T\end{pmatrix}^T$, where each $\mathbf{y}_i$ has N' elements in it. Let $J\mathbf{y}=\mathbf{f}=\begin{pmatrix}\mathbf{f}_1^T & \mathbf{f}_2^T & \cdots & \mathbf{f}_N^T\end{pmatrix}^T$, where the block segments are the same size as for $\mathbf{y}$. If Condition I holds, then for all $i=1,2,\ldots,N$,

$$\begin{aligned}\mathbf{y}_i &= B_{i-1}^{-1}\mathbf{f}_{i-1} - B_{i-1}^{-1}A_{i-1}\mathbf{y}_{i-1}\\ &= B_{i-1}^{-1}\mathbf{f}_{i-1} - B_{i-1}^{-1}A_{i-1}B_{i-2}^{-1}\mathbf{f}_{i-2} + B_{i-1}^{-1}A_{i-1}B_{i-2}^{-1}A_{i-2}\mathbf{y}_{i-2}.\end{aligned} \tag{3.66}$$

Following this expansion to its natural end results in the expression,

$$\begin{aligned}\left(I-(-1)^N B_{i-1}^{-1}A_{i-1}B_{i-2}^{-1}A_{i-2}\cdots B_i^{-1}A_i\right)\mathbf{y}_i = \\ B_{i-1}^{-1}\mathbf{f}_{i-1} - B_{i-1}^{-1}A_{i-1}B_{i-2}^{-1}\mathbf{f}_{i-2}+\ldots \\ +(-1)^N B_{i-1}^{-1}A_{i-1}B_{i-2}^{-1}A_{i-2}\cdots A_{i+1}B_i^{-1}\mathbf{f}_i.\end{aligned} \tag{3.67}$$

By Condition I (a), the norm of the left-hand side obeys the inequality,

$$\left\|\left(I-(-1)^N B_{i-1}^{-1}A_{i-1}B_{i-2}^{-1}A_{i-2}\cdots B_i^{-1}A_i\right)\mathbf{y}_i\right\| \ge \|\mathbf{y}_i\|/n. \tag{3.68}$$

By Condition I (b), the norm of the right-hand side obeys the inequality,

$$\left\| \begin{array}{l} B_{i-1}\mathbf{f}_{i-1} - B_{i-1}^{-1}A_{i-1}B_{i-2}^{-1}\mathbf{f}_{i-2} + \ldots \\ \qquad + (-1)^N B_{i-1}^{-1}A_{i-1}B_{i-2}^{-1}A_{i-2}\cdots A_{i+1}B_i^{-1}\mathbf{f}_i \end{array} \right\| \\ \leq m\sum_{k=1}^{N} \|\mathbf{f}_i\| \leq m\sqrt{N}\,\|\mathbf{f}\|\,. \quad (3.69)$$

Thus, $\|\mathbf{f}\| \geq \|\mathbf{y}_i\| \,/\, \left(nm\sqrt{N}\right)$ for all $i = 1, 2, \ldots, N$. Since $\mathbf{y}$ is a unit vector, there exists some i such that $\|\mathbf{y}_i\| \geq 1/\sqrt{N}$, which implies that $\|\mathbf{f}\| \geq 1/\left(nmN\right)$ and implies the desired inequality.

If J satisfies Condition II but not Condition I, then there is an expansion equivalent to Equation (3.67), namely,

$$\left(I - (-1)^N A_i^{-1}B_iA_{i+1}^{-1}B_{i+1}\cdots A_{i-1}^{-1}B_{i-1}\right)\mathbf{y}_i = \\ A_i^{-1}\mathbf{f}_i - A_i^{-1}B_iA_{i+1}^{-1}\mathbf{f}_{i+1} + \ldots \\ + (-1)^N A_i^{-1}B_iA_{i+1}^{-1}B_{i+1}\cdots A_{i-1}^{-1}B_{i-1}\mathbf{f}_{i-1}. \quad (3.70)$$

The proof then proceeds in the same way as above. □

This proposition is useful because it provides a way to estimate the condition of the Jacobian by concentrating on sub-blocks instead of the whole matrix. It does *not* give a proof of non-singularity in terms of properties of the torus or discretization, as in Section 3.1, because – as mentioned above – general convergence conditions for the method are likely to be very complicated.

Proposition 3.3 explains in yet another way why even-even discretizations are unstable, while others may or may not be. For an even-even discretization, the operator chain, $B_{N_i}^{-1}A_{N_i}\cdots B_1^{-1}A_1$, generally has an eigenvalue near one, which violates condition I, b) in the statement of the proposition. Switching N_j to an odd number removes that eigenvalue, whereas switching N_i to an odd number changes the sign of $(-1)^{N_i}$. Either way, switching to at least one odd number in the discretization

might help to improve the condition number of the Jacobian and hence stabilize the method, although it does not do so in all cases. See Section 4.2 for examples.

Finally, a reasonable question to ask is how – or even whether –the odd/even difficulties encountered with a two-torus in $\mathbb{R}^3$ persist into the general method. The periodic block bi-diagonal structure of the Jacobian leads to one logical conjecture about the number of points necessary to have stability: For a p-torus with $N_1, N_1, \ldots, N_p$ discretization points in each angular direction, at least $p-1$ of the N_i's should be odd.

Such a choice allows all the top-level A and B (which are themselves periodic, block bi-diagonal) to be invertible, and it also satisfies the proper sign in Proposition 3.3. Numerical experimentation has shown that the conjecture is probably correct for the general method applied to two- and three-tori. See Chapter 5 for numerical results.

3.4 Alternate Discretizations

Given that changing the odd/even character of N_i and N_j does not necessarily stabilize the method for two-tori, the next logical step is to examine different discretizations. This thesis does not contain any analysis of the convergence properties of discretizations other than the box template, but some numerical experiments have shown that other discretizations are not necessarily better.

A *center-difference* discretization leads to $N_i \cdot N_j$ equations of the form,

$$f_{i,j} = \mathbf{\Phi}\left(\hat{\mathbf{x}}_{i,j}\right)^T \frac{\left(\hat{\mathbf{x}}_{i+1,j} - \hat{\mathbf{x}}_{i-1,j}\right) \times \left(\hat{\mathbf{x}}_{i,j+1} - \hat{\mathbf{x}}_{i,j-1}\right)}{\left\|\left(\hat{\mathbf{x}}_{i+1,j} - \hat{\mathbf{x}}_{i-1,j}\right) \times \left(\hat{\mathbf{x}}_{i,j+1} - \hat{\mathbf{x}}_{i,j-1}\right)\right\|}, \tag{3.71}$$

and the method requires that $f_{i,j} = 0$ for all i, j. The Jacobian for this discretization is *block, periodic, tri-diagonal* (the obvious extension of Definition 3.7), where the diagonal blocks are periodic tri-diagonal, and the off-diagonal blocks are diagonal. Each row contains five nonzero entries.

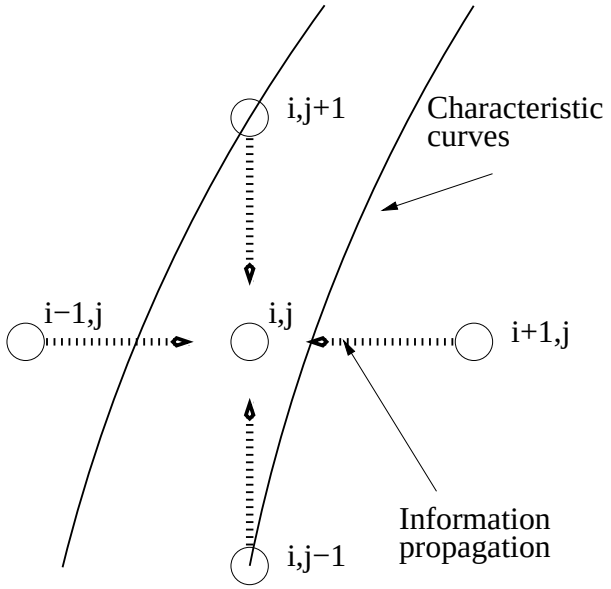

Figure 3.1: Center-Difference Template

Unfortunately, the method seems to be unconditionally unstable when applied to the torus of Section 4.2.1. This result makes sense if the template is considered as a discretization of the PDE in Equation (1.10). As mentioned in the discussion of graph transform techniques, the characteristic curves of the PDE are flow lines under the vector field. Then the center-difference discretization requires information to propagate across characteristic curves, which induces instability. See Figure 3.1 for a graphical representation.

It should be noted that the planar analogy to the center-difference discretization to Equation (3.71) *is* stable. That analogous discretization is

$$f_i = \mathbf{\Phi}\left(\hat{\mathbf{x}}_i\right)^T R_{\pi/2} \frac{\hat{\mathbf{x}}_{i+1} - \hat{\mathbf{x}}_{i-1}}{\left\|\hat{\mathbf{x}}_{i+1} - \hat{\mathbf{x}}_{i-1}\right\|}, \tag{3.72}$$

where $R_{\pi/2}$ is the usual $\pi/2$ rotation. This discretization is useful in breaking up cycles with equilibria into segments, as in Section 4.1.3.

Other variations of the discretization in Equation (3.71) include forward-forward, forward-backward, center-forward, etc. Some of the variations are stable for a while, when applied to the torus in Section 4.2.1, but none perform as well as the box

scheme.

One way to stabilize the method in some circumstances is to do away with the center point and use an average,

$$f_{i,j} = \mathbf{\Phi}\left(\frac{\hat{\mathbf{x}}_{i+1,j} + \hat{\mathbf{x}}_{i-1,j} + \hat{\mathbf{x}}_{i,j+1} + \hat{\mathbf{x}}_{i,j-1}}{4}\right)^T \frac{(\hat{\mathbf{x}}_{i+1,j} - \hat{\mathbf{x}}_{i-1,j}) \times (\hat{\mathbf{x}}_{i,j+1} - \hat{\mathbf{x}}_{i,j-1})}{\|(\hat{\mathbf{x}}_{i+1,j} - \hat{\mathbf{x}}_{i-1,j}) \times (\hat{\mathbf{x}}_{i,j+1} - \hat{\mathbf{x}}_{i,j-1})\|}, \quad (3.73)$$

which leads to a Jacobian of the same form, except that now there are only four nonzero entries in each row, since the diagonal is empty. This scheme is essentially just a box scheme, though, with a larger (and hence less accurate) box.

One other possibility is to modify the box scheme by changing the definition of the half-point. Previously, $\hat{\mathbf{x}}_{1/2} = (\hat{\mathbf{x}}_{i,j} + \hat{\mathbf{x}}_{i+1,j} + \hat{\mathbf{x}}_{i,j+1} + \hat{\mathbf{x}}_{i+1,j+1})/4$, but another reasonable definition is

$$\hat{\mathbf{x}}_{1/2} = (\overline{\mathbf{x}}_{i,j} + \overline{\mathbf{x}}_{i+1,j} + \overline{\mathbf{x}}_{i,j+1} + \overline{\mathbf{x}}_{i+1,j+1})/4 + (r_{i,j} + r_{i,j+1} + r_{i+1,j} + r_{i+1,j+1})(\overline{\mathbf{n}}_{i,j} + \overline{\mathbf{n}}_{i,j+1} + \overline{\mathbf{n}}_{i+1,j} + \overline{\mathbf{n}}_{i+1,j+1})/16. \quad (3.74)$$

As expected, this does not seem to change change the stability properties of the method significantly.

The final discretization explored here is the the use of triangularization to represent the two-dimensional surface in $\mathbb{R}^3$. Triangles have a distinct, unambiguous orientation and thus eliminate the need for averaging to obtain normal directions. When the triangles have vertices $\{\hat{\mathbf{x}}_{i,j}, \hat{\mathbf{x}}_{i+1,j}, \hat{\mathbf{x}}_{i,j+1}\}$, then the equations to be solved are of the form,

$$f_{i,j} = \mathbf{\Phi}\left(\frac{\hat{\mathbf{x}}_{i,j} + \hat{\mathbf{x}}_{i+1,j} + \hat{\mathbf{x}}_{i,j+1}}{3}\right)^T \frac{(\hat{\mathbf{x}}_{i+1,j} - \hat{\mathbf{x}}_{i,j}) \times (\hat{\mathbf{x}}_{i,j+1} - \hat{\mathbf{x}}_{i,j})}{\|(\hat{\mathbf{x}}_{i+1,j} - \hat{\mathbf{x}}_{i,j}) \times (\hat{\mathbf{x}}_{i,j+1} - \hat{\mathbf{x}}_{i,j})\|}. \quad (3.75)$$

Triangularization unfortunately seems to be less stable than the box scheme. In numerical experiments, the condition number of the Jacobian is much higher than with the box scheme, and the method only continues for a few λ-steps before breaking down due to instabilities.

CHAPTER IV

NUMERICAL RESULTS: SPECIAL CASES

This chapter contains some numerical results for Algorithms 3.1 and 3.2, specifically, computations for three different planar oscillators and three different two-tori embedded in $\mathbb{R}^3$. The behavior of the method in these situations illustrates some of the concepts developed in Chapter 3. It also indicates how complicated the general convergence conditions of the method may be.

4.1 Example: Limit Cycles in the Plane

The simplest types of "tori" are closed orbits in the plane. They are useful as preliminary tests of torus-approximation algorithms because they do not require much computation time or memory storage.

This section contains three examples of the orthogonality condition and Algorithm 3.1 applied to limit cycles in the plane. The first limit cycle is a smooth modification of a simple, attracting oscillator. The method performs well with or without arc length re-distribution. The second limit cycle is the classic van der Pol oscillator, which becomes pinched throughout the continuation process and thus demonstrates how arc length continuation can be very useful in the algorithm. The third limit cycle contains two fixed points. The method is unstable when applied to this example, but a different discretization can correct it.

4.1.1 Peanut Limit Cycle in the Plane

One particularly straightforward (but ultimately *too* straightforward) example is the vector field given in polar coordinates by Equation (2.10). That limit cycle does grow with increasing λ, but because it does not change shape, it is not a good test case for

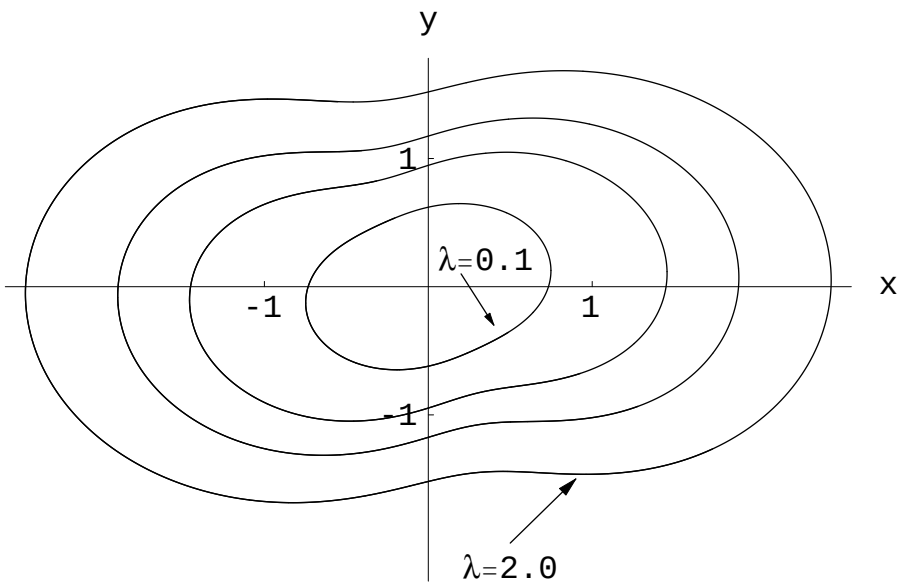

Figure 4.1: Peanut Limit Cycle

numerical algorithms.

Fortunately, one can modify the system to obtain a one-torus that distorts and becomes non-convex as it grows. Consider the system in polar coordinates,

$$\begin{aligned} \dot{r} &= r(\lambda - r^2) + 5\lambda \cos^2\theta \\ \dot{\theta} &= 1 \ . \end{aligned} \tag{4.1}$$

The system in Cartesian coordinates is

$$\begin{aligned} \dot{x}_1 &= x_1\left(\lambda - x_1^2 - x_2^2\right) + \frac{5\lambda x_1^3}{\left(x_1^2 + x_2^2\right)^{3/2}} - x_2 \\ \dot{x}_2 &= x_2\left(\lambda - x_1^2 - x_2^2\right) + \frac{5\lambda x_1^2 x_2}{\left(x_1^2 + x_2^2\right)^{3/2}} + x_1 \ . \end{aligned} \tag{4.2}$$

The addition of the second term in the $\dot{r}$ equation causes the limit cycle to pinch at the top and bottom as it grows. Eventually, the limit cycle begins to look like a peanut. Figure 4.1 shows the evolution of this stable limit cycle for $\lambda = 0.1$, 0.5, 1.0, and 2.0.

The following figures show the results of the algorithm applied to a 50-point grid where the parameter grows from $\lambda = 0.1$ to $\lambda = 2.0$ with a step size of 0.1. To start

the algorithm, the initial guess is

$$\overline{\mathbf{x}}(\phi_i) = \overline{\mathbf{x}}_i = 0.8 \begin{pmatrix} \cos(\phi_i) \\ \sin(\phi_i) \end{pmatrix} , \tag{4.3}$$

where $\phi_i = 2\pi i/50$, $i = 1, 2, \ldots, 50$.

The Jacobian in Newton's method comes from forward-differencing on r with a step size of 10^{-9}, and the cut off criterion for Newton's method is that the two-norm of the right-hand side of the correction be less than 0.001. In other words, if each Newton iteration is the solution of $J\mathbf{y} = \mathbf{f}$, and then the next $\mathbf{f}$ is evaluated at $\mathbf{x} + \mathbf{y}$, then the cut off criterion is that $\|\mathbf{f}\| < 0.001$.

Figures 4.2 and 4.3 show the continuation of the limit cycle with and without re-distributing via arc length respectively. The curves in Figure 4.2 represent the solution at convergence, but before re-distribution at that value of λ. The results in the two figures are nearly identical, with the only difference being the location of the points.

The estimated condition numbers of the Jacobian come from the one-norm estimation function "condest" in Matlab 6.0. The estimation procedure does use a pseudo-random seed, so it is not fully repeatable [19].

When the algorithm includes re-distribution at convergence at each λ step, the condition number (with respect to to the one-norm) of the (50×50) Jacobian ranges approximately from 3.7 to 23.8 and averages about 10. Without re-distribution, it ranges approximately from 12.1 to 27.1 and averages about 20.

The algorithm seems to be extremely robust and stable, converging to a reasonable approximation with no arc length re-distribution with as few as 20 points. Computation time is minimal.

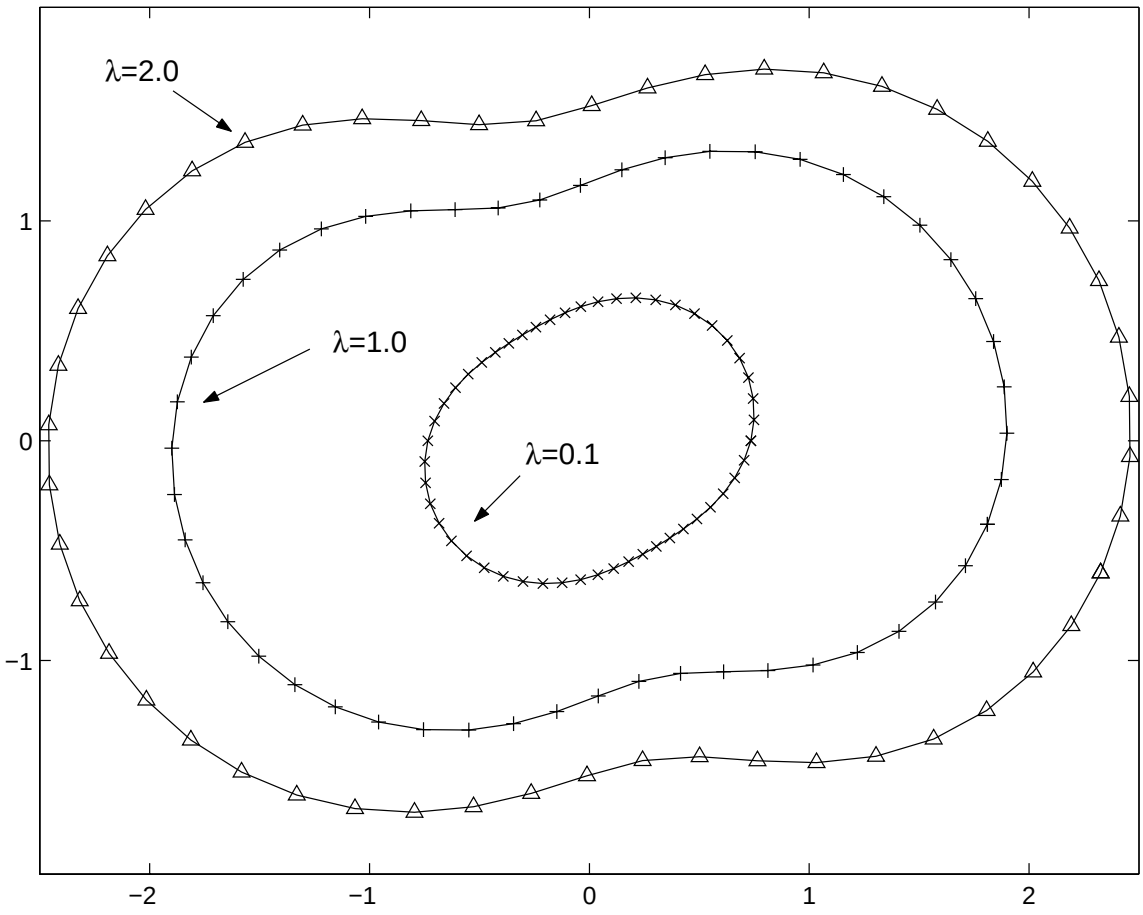

Figure 4.2: Continuation of Peanut Orbit with Re-distribution

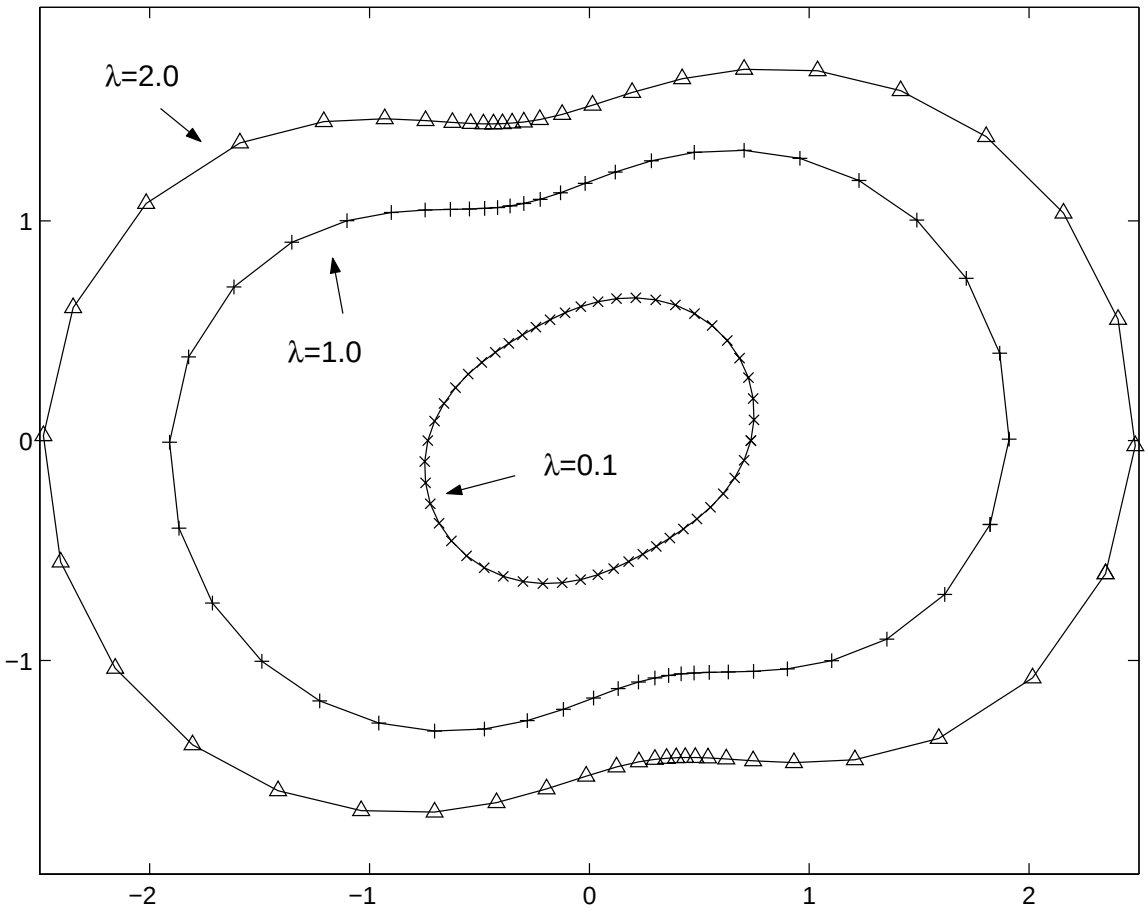

Figure 4.3: Continuation of Peanut Orbit without Re-distribution

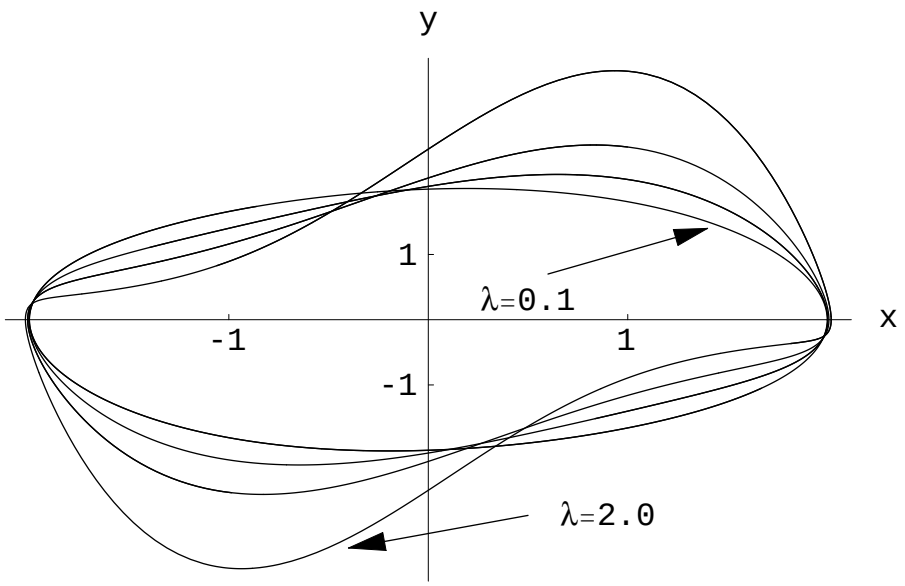

Figure 4.4: van der Pol Oscillator

4.1.2 van der Pol Oscillator

Another example of an attracting limit cycle in the plane is the familiar *van der Pol* oscillator,

$$\ddot{x} + \lambda\dot{x}(x^2 - 1) + x = 0, \tag{4.4}$$

which reduces to the first-order system,

$$\begin{aligned} \dot{x}_1 &= x_2 \\ \dot{x}_2 &= -x_1 + \lambda x_2 \left(1 - x_1^2\right). \end{aligned} \tag{4.5}$$

This system has an attracting periodic orbit for $\lambda > 0$ [18], so again it is possible to get a picture of the orbit from forward integration. Figure 4.4 shows the orbit for $\lambda = 0.1$, 0.5, 1.0, and 2.0.

The van der Pol oscillator becomes pinched and forms sharp corners much more than the orbit in the previous section. While this pinching may not indicate a loss of smoothness on the theoretical level, it does require a little more work in the discretization. As numerical results demonstrate, arc length re-distribution between steps can prevent breakdown in the discrete representation of the orbit.

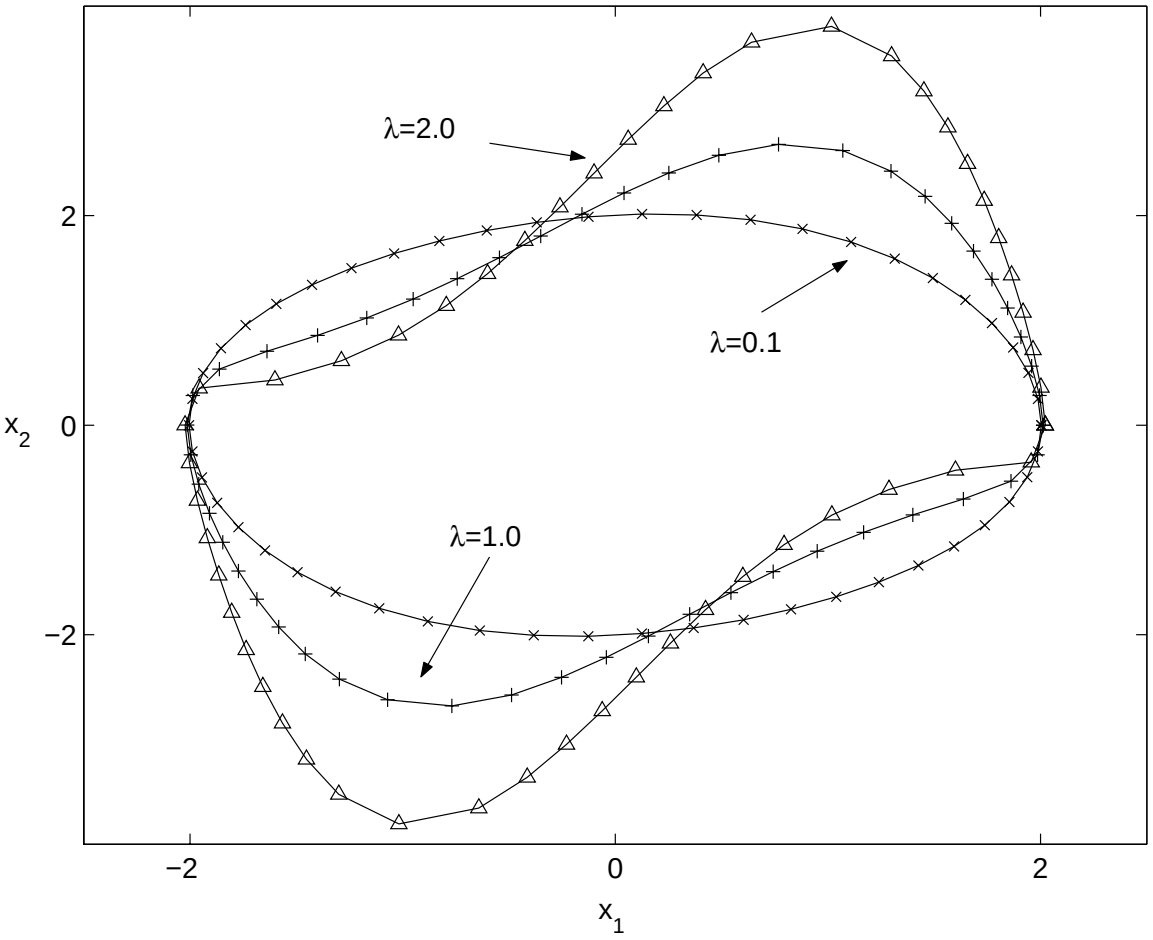

Figure 4.5: Continuation of van der Pol Oscillator with Re-distribution

The following figures show the results of the algorithm applied to a 50-point grid where the parameter grows from $\lambda = 0.1$ to $\lambda = 2.0$ with a step size of 0.05. To start the algorithm, the initial guess is

$$\overline{\mathbf{x}}(\phi_i) = \overline{\mathbf{x}}_i = 2.0 \begin{pmatrix} \cos(\phi_i) \\ \sin(\phi_i) \end{pmatrix} , \tag{4.6}$$

where $\phi_i = 2\pi i/50$, $i = 1, 2, \ldots, 50$.

The Jacobian in Newton's method comes from forward-differencing on r with a step size of 10^{-9}, and the cut off criterion for Newton's method is the same as for the peanut cycle: that the two-norm of the right-hand side (*i.e.*, $\|\mathbf{f}\|$ in the tables below) be less than 0.001.

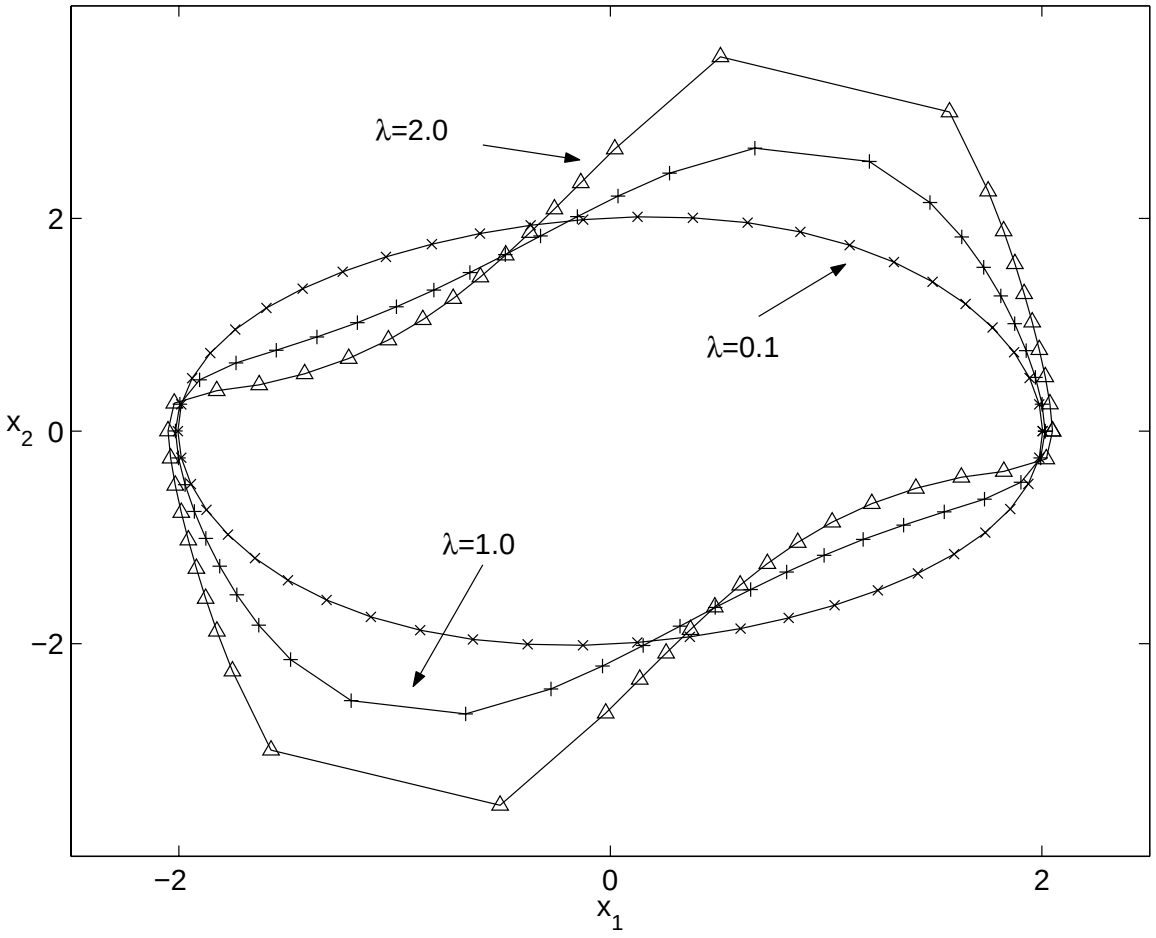

Figure 4.6: Continuation of van der Pol Oscillator without Re-distribution

Table 4.1: Newton Iteration: van der Pol Oscillator with Re-distribution

From λ	To λ	Iteration	$\|\mathbf{f}\|$	$\kappa(J)$	$\|\mathbf{y}\|$
–	0.1	1	0.70	190	0.28
		2	0.0016	190	0.0028
			1.2×10^{-7}		
0.95	1.0	1	0.36	90	0.15
		2	0.0012	92	0.0011
			2.0×10^{-6}		
1.95	2.0	1	0.55	160	0.15
		2	0.025	160	0.0026
			1.8×10^{-5}		

Figures 4.5 and 4.6 show the continuation of the limit cycle with and without re-distributing via arc length respectively. The curves in Figure 4.5 represent the solution at convergence, but before re-distribution at that value of λ. As before, the condition number estimator is "condest" in Matlab 6.0.

Arc length re-distribution clearly helps the algorithm in this case more so than with the peanut orbit. Its influence is probably due to the higher curvature observed here as opposed to the relatively mild bending in the peanut cycle. When the algorithm includes re-distribution at convergence at each λ step, the condition number (with respect to to the one-norm) of the (50×50) Jacobian ranges approximately from 80 to 190 and averages about 100. Without re-distribution, it ranges approximately from 65 to 120 and averages about 80. The initial Jacobian has a condition number of about 190, since the initial guess is not as good as it could be.

Tables 4.1 and 4.2 show some sample Newton iterations with and without re-distribution. The vector $\mathbf{y}$ is the correction at each Newton iteration. The first Newton iteration is of course identical in both cases, since no re-distribution has occurred yet.

Table 4.2: Newton Iteration: van der Pol Oscillator without Re-distribution

From λ	To λ	Iteration	$\|\mathbf{f}\|$	$\kappa(J)$	$\|\mathbf{y}\|$
0.95	1.0	1	0.31	71	0.12
		2	0.0054	72	7.8×10^{-4}
			9.9×10^{-7}		
1.95	2.0	1	0.23	113	0.076
		2	0.0028	115	5.1×10^{-4}
			3.0×10^{-7}		

4.1.3 Failure of the Method in the Plane

This section contains an example where the orthogonality condition does not work directly. The example is the planar vector field given in polar coordinates by

$$\begin{aligned} \dot{r} &= r\left(\lambda - r^2\right) \\ \dot{\theta} &= \sin\theta, \end{aligned} \tag{4.7}$$

or in Cartesian coordinates by

$$\begin{aligned} \dot{x}_1 &= x_1\left(\lambda - x_1 - x_2\right) - \frac{x_2^2}{\sqrt{x_1^2 + x_2^2}} \\ \dot{x}_2 &= x_2\left(\lambda - x_1 - x_2\right) + \frac{x_1 x_2}{\sqrt{x_1^2 + x_2^2}}. \end{aligned} \tag{4.8}$$

Linearization shows that the above system admits an attracting heteroclinic orbit of constant radius $\sqrt{\lambda}$ between a saddle at $(\sqrt{\lambda}, 0)$ and a sink at $(-\sqrt{\lambda}, 0)$. Figure 4.7 is a picture.

Numerical experimentation has shown that the orthogonality condition combined with the usual discretization scheme described in Section 3.2 does not work well on the system in Equation (4.7). The Jacobian is extremely ill-conditioned for a wide variety of distributions, and no amount of adjustment seems to help. Moreover, both the a_i's and the b_i's switch sign around the fixed points, which seems to offer no hope in evaluating stability.

Just because one discretization is ill-suited to heteroclinic cycles, however, does not mean that the orthogonality condition does not apply. There are in fact many ways

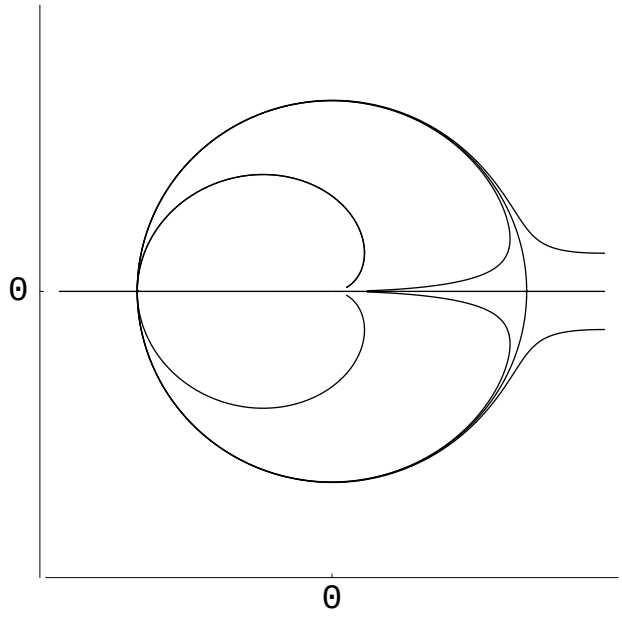

Figure 4.7: Heteroclinic Cycle in the Plane

to repair the discretization so that Equation (1.18) does not induce an ill-conditioned Jacobian.

For example, one might consider the cycle as two heteroclinic orbits, and construct them one at a time. Using a straight center-difference template, as in Equation (3.71), let N be the number of points on the orbit, and let $\{\overline{\mathbf{x}}_i\}$, $i = 1, 2, \ldots, N$ as the initial guess with $\overline{\mathbf{x}}_1 = (-\sqrt{\lambda}, 0)$, $\overline{\mathbf{x}}_N = (\sqrt{\lambda}, 0)$, and all others chosen to approximate the upper or lower orbit.

The normal vectors are rotations of the tangents,

$$\overline{\mathbf{n}}_i = R_{\pi/2} \frac{\overline{\mathbf{x}}_{i+1} - \overline{\mathbf{x}}_{i-1}}{\|\overline{\mathbf{x}}_{i+1} - \overline{\mathbf{x}}_{i-1}\|}, \qquad i = 2, 3, \ldots, N-1. \tag{4.9}$$

Let $\hat{\mathbf{x}}_i = \overline{\mathbf{x}}_i + r_i \overline{\mathbf{n}}_i$ and the system of equations in r is

$$\begin{aligned} r_1 \;&=\; r_N = 0 \\ \mathbf{\Phi}\left(\overline{\mathbf{x}}_i\right)^T R_{\pi/2} \frac{\hat{\mathbf{x}}_{i+1} - \hat{\mathbf{x}}_{i-1}}{\|\hat{\mathbf{x}}_{i+1} - \hat{\mathbf{x}}_{i-1}\|} &= 0\ , \qquad i = 2, 3, \ldots, N-1. \end{aligned} \tag{4.10}$$

The Jacobian in a Newton's method solution to Equation (4.10) is tri-diagonal. Figure 4.8 shows the results for $\lambda = 1.0$ to $\lambda = 3.0$ in steps of $\Delta\lambda = 0.1$. The

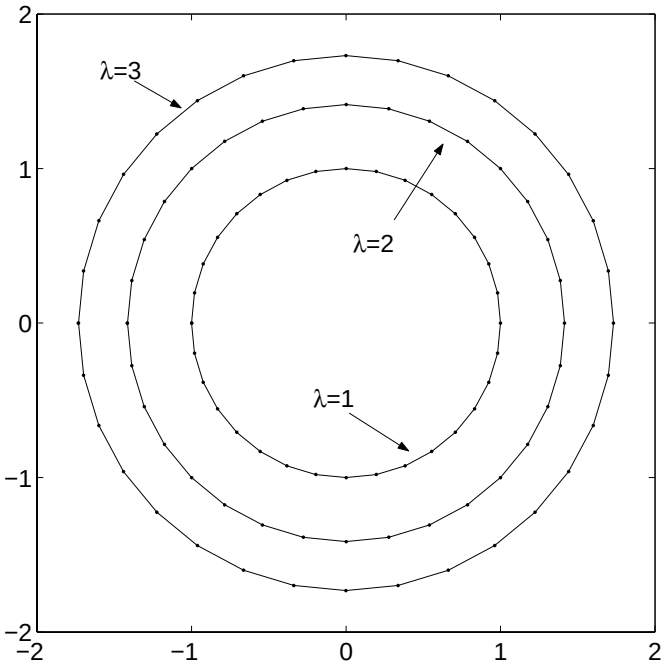

Figure 4.8: Solution of Heteroclinic Cycle in the Plane

curve contains 15 points on each of the upper and lower orbits, plus the fixed points. Computation time is minimal, and the condition number for the (17×17) Jacobian is about 12-13.

The above method is not the only way to apply the orthogonality condition to a heteroclinic orbit, and the reader probably can conceive of several more schemes with a few minutes' consideration.

The literature additionally contains many different methods for computing homo- and heteroclinic curves, with most using a boundary-value problem approach [5, 38]. One definite advantage to using the orthogonality condition is that it obviates the the conversion to an infinite-time boundary value problem. While it is not straightforward to apply the orthogonality condition to non-hyperbolic curve – as will often be the case for homoclinic orbits – some adaptations have been successful [24, 27, 28, 29, 30].

4.2 Example: Two-Tori in $\mathbb{R}^3$

This section contains three examples of the discretization developed in Section 3.2 applied to two-tori in $\mathbb{R}^3$. The first two examples demonstrate successful application of the method, while the third demonstrates how the method can fail when the torus contains closed, invariant sub-manifolds (in this case, two periodic orbits).

4.2.1 Two-Torus from Fluid Flow

Langford [22] proposes the following system of ODE as a simplification of equations describing fluid flow:

$$\begin{aligned}
\dot{x}_1 &= (\lambda - 3)x_1 - (1/4)x_2 + x_1\left[x_3 + (1/5)\left(1 - x_3^2\right)\right] \\
\dot{x}_2 &= (1/4)x_1 + (\lambda - 3)x_2 + x_2\left[x_3 + (1/5)\left(1 - x_3^2\right)\right] \\
\dot{x}_3 &= \lambda x_3 - \left(x_1^2 + x_2^2 + x_3^2\right) \ .
\end{aligned} \tag{4.11}$$

This vector field has a cylindrical symmetry that reveals how it gives rise to an invariant torus. The symmetry actually converts the field into a planar problem.

Using cylindrical coordinates with $x_1 = r\cos(\theta)$, $x_2 = r\sin(\theta)$, and $z = x_3$. Equation (4.11) becomes

$$\begin{aligned}
\dot{r} &= r\left(-z^2/5 + z + \lambda - 14/5\right) \\
\dot{z} &= z\left(\lambda - z\right) - r^2,
\end{aligned} \tag{4.12}$$

with $\dot{\theta} = 1/4$. Thus, it suffices to analyze the system in the right half-(r, z)-plane.

A sequence of bifurcations occurs in the planar system as λ grows:

- For $\lambda < 5 - \sqrt{11}$, the equilibria in (r, z) coordinates are $(0, 0)$ and $(0, \lambda)$. The origin is a saddle, and $(0, \lambda)$ is a stable node. There is a heteroclinic orbit along the z axis that connects the two points.

- At $\lambda = 5 - \sqrt{11}$, a stable equilibrium breaks off of the $(0, \lambda)$ branch. The location of this new equilibrium is $(\sqrt{a(\lambda - a)}, a)$, where $a = (5 - \sqrt{20\lambda - 31})/2$.

Note that this equilibrium corresponds to a periodic orbit in the full, three-dimensional system. Also, the equilibrium at $(0, \lambda)$ changes to a saddle and the heteroclinic connection persists.

- At $\lambda = 2$, the new branch undergoes a Hopf bifurcation. The planar system admits a new, stable periodic orbit, which corresponds to a stable invariant torus in the full system. The branch of equilibria at $(\sqrt{a(\lambda - a)}, a)$ is now unstable, as is the corresponding periodic orbit in the full system.

- At $\lambda \approx 2.02482$, the stable manifold of $(0, 0)$ intersects the unstable manifold of $(0, \lambda)$ and forms a heteroclinic cycle. The heteroclinic cycle absorbs the periodic orbit and destroys the torus.

- At $\lambda = 14/5$, the branch at $(0, 0)$ absorbs the branch at $(\sqrt{a(\lambda - a)}, a)$.

The destruction of the torus at $\lambda \approx 2.02482$ (which corresponds to the creation and immediate destruction of a heteroclinic cycle in the plane) is a global bifurcation, so an exact value of λ would be difficult to calculate. Figure 4.9 shows the progression of the reduced planar system.

Because the torus is attracting, one can produce a reasonable picture of it by choosing an initial condition and integrating forward, and indeed this is how the bifurcation value of $\lambda \approx 2.02482$ is approximated. Figure 4.10 shows the progression of the full system. For a more complete description of the torus, see [22].

The following figures show the results of Algorithm 3.2 applied to a 45×45 torus from $\lambda = 2.005$ to breakdown. To start the algorithm, the initial guess is

$$\overline{\mathbf{x}}((\phi_1)_i, (\phi_2)_j) = \overline{\mathbf{x}}_{i,j} = \begin{pmatrix} (0.95 + 0.35\cos(\phi_2)_j)\cos(\phi_1)_i \\ -(0.95 + 0.2\cos(\phi_2)_j)\sin(\phi_1)_i \\ 0.35\sin(\phi_2)_j + 1 \end{pmatrix}, \tag{4.13}$$

where $(\phi_1)_i = (\phi_2)_i = 2\pi(i-1)/45$. This guess then undergoes an arc length redistribution along each meridian before the continuation process begins, if arc length

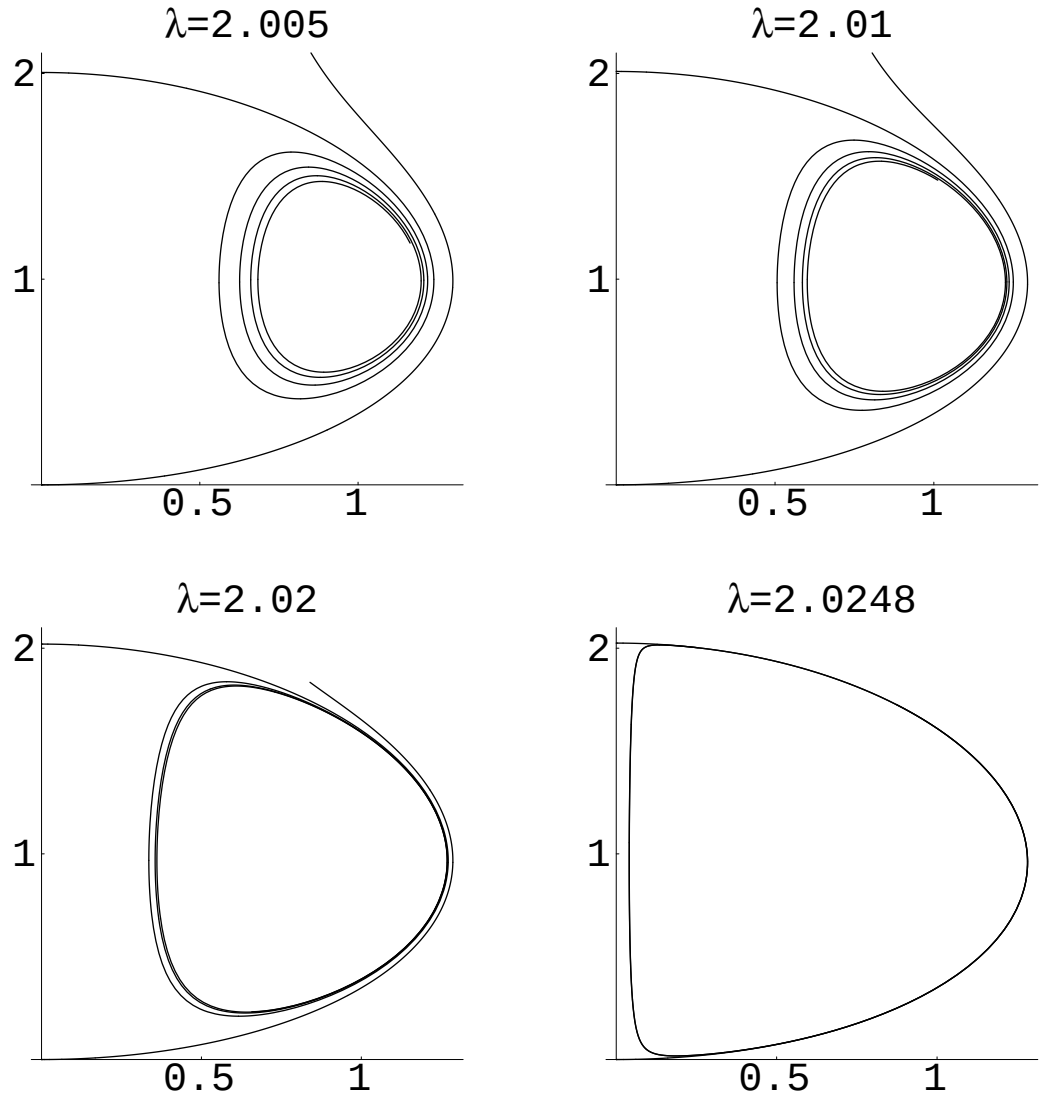

Figure 4.9: Progression of Reduced System

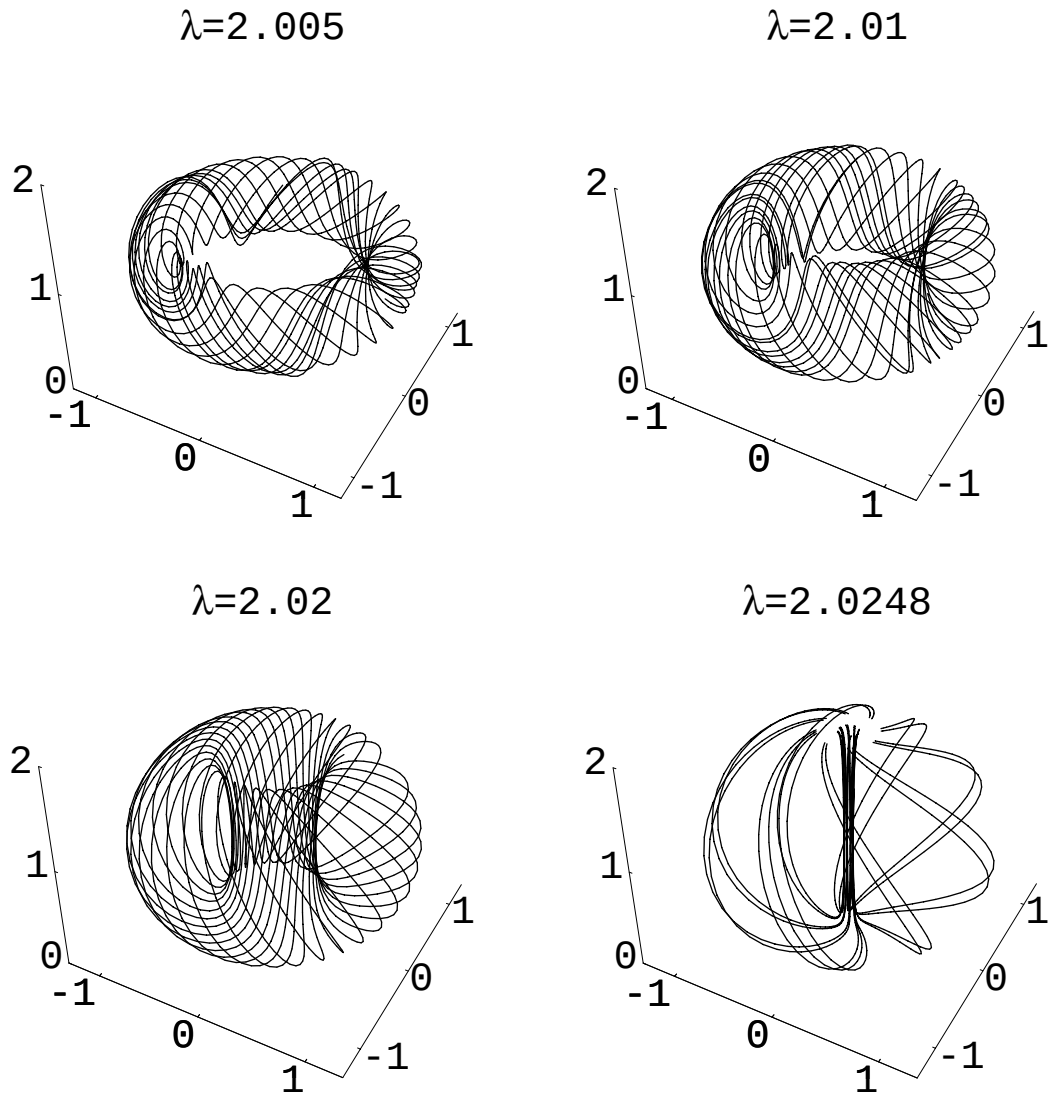

Figure 4.10: Progression of Full System

Table 4.3: Continuation Steps for Fluid-Flow Torus

λ Range	$\Delta\lambda$
2.005–2.02	0.005
2.021–2.024	0.001
2.0241–breakdown	0.0001

re-distribution is desired.

The Jacobian in Newton's method comes from forward-differencing on r with a step size of 10^{-8}, and the cut off criterion for Newton's method is that the two-norm of the right-hand side ($\|\mathbf{f}\|$) be less than 10^{-6}. The step size for the continuation process varies as shown in Table 4.3.

Because the torus is cylindrically symmetric about the x_3-axis, it is possible to re-distribute the points by arc length along each meridian to obtain a better spatial picture of the torus. The algorithm seems to be robust, however, and it seems to work with or without re-distribution. In fact, the algorithm is overly robust without re-distribution, since it will converge for parameter values up to about $\lambda = 2.025$, which is past the breakdown of the physical torus. This is probably a consequence of poor distribution of points that allows for extra solutions of the fundamental equations.

Figures 4.11 - 4.13 show the continuation process with arc length re-distribution along each meridian, and Figures 4.14 - 4.16 show it without re-distribution. As in the scalar case, the pictures in Figures 4.11 - 4.13 represent the solution at convergence but before re-distribution at each value of λ. The center lines in the exploded views represent arithmetical averages among all the points in a given meridian.

Again, the estimated condition number with respect to the one-norm comes from the algorithm in Matlab 6.0 [19]. When the algorithm includes re-distribution at convergence at each λ step, the condition number of the 2025×2025 Jacobian ranges approximately from 1500 to 25000 and averages about 4000. Without re-distribution, it ranges approximately from 2300 to 33000 and also averages about 5000.

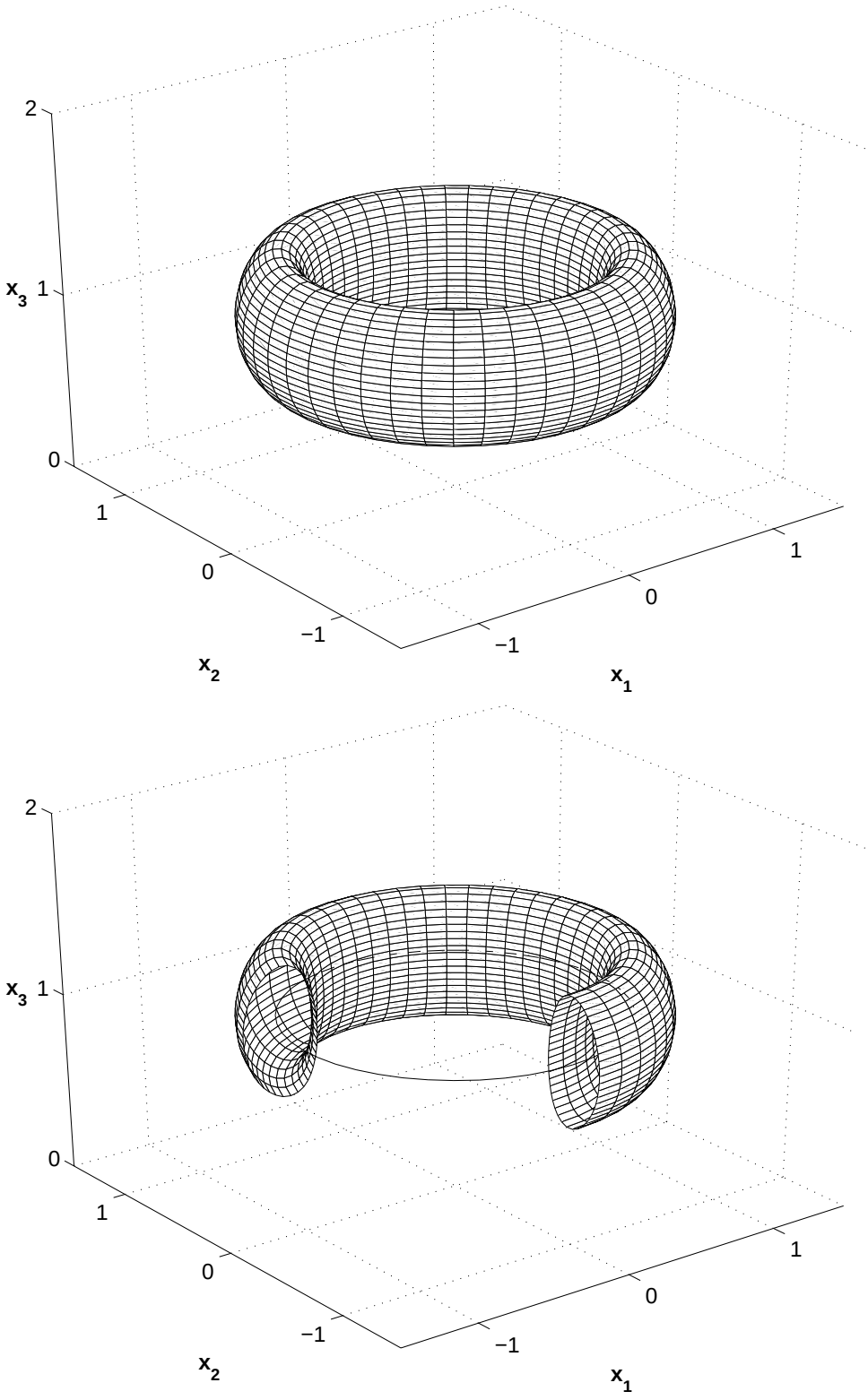

Figure 4.11: Fluid Flow Torus with Re-distribution; $\lambda = 2.005$

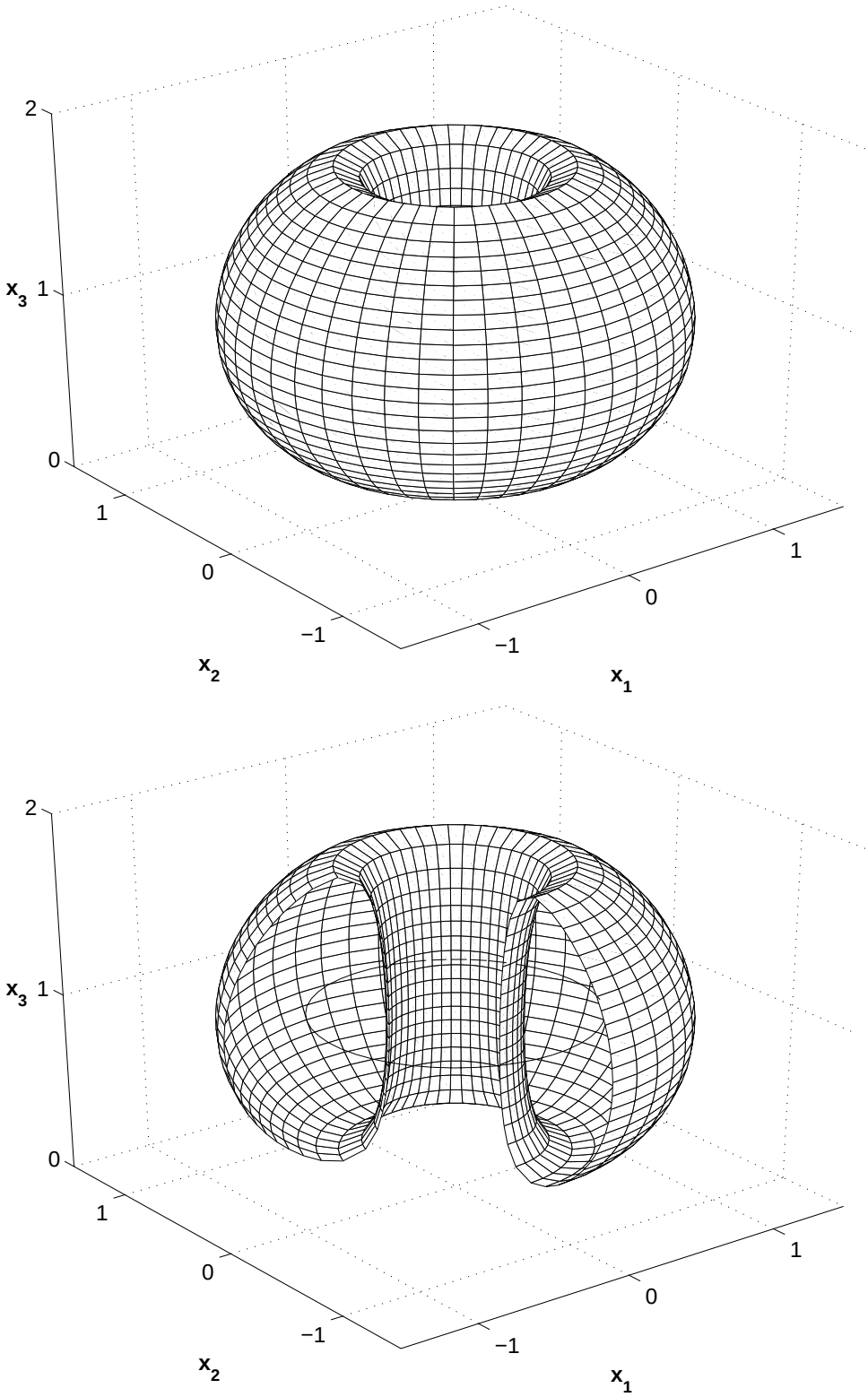

Figure 4.12: Fluid Flow Torus with Re-distribution; $\lambda = 2.020$

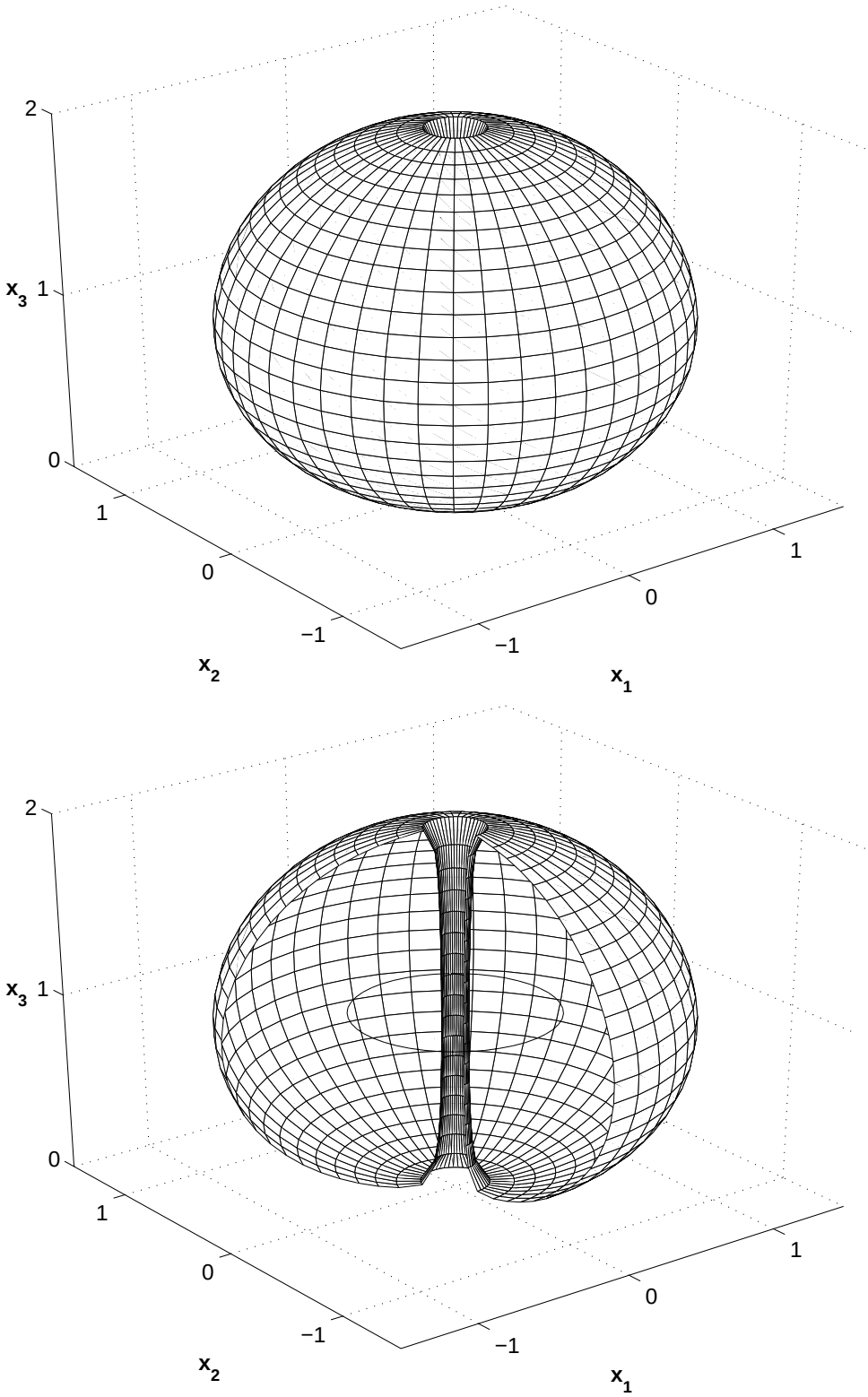

Figure 4.13: Fluid Flow Torus with Re-distribution; $\lambda = 2.024$

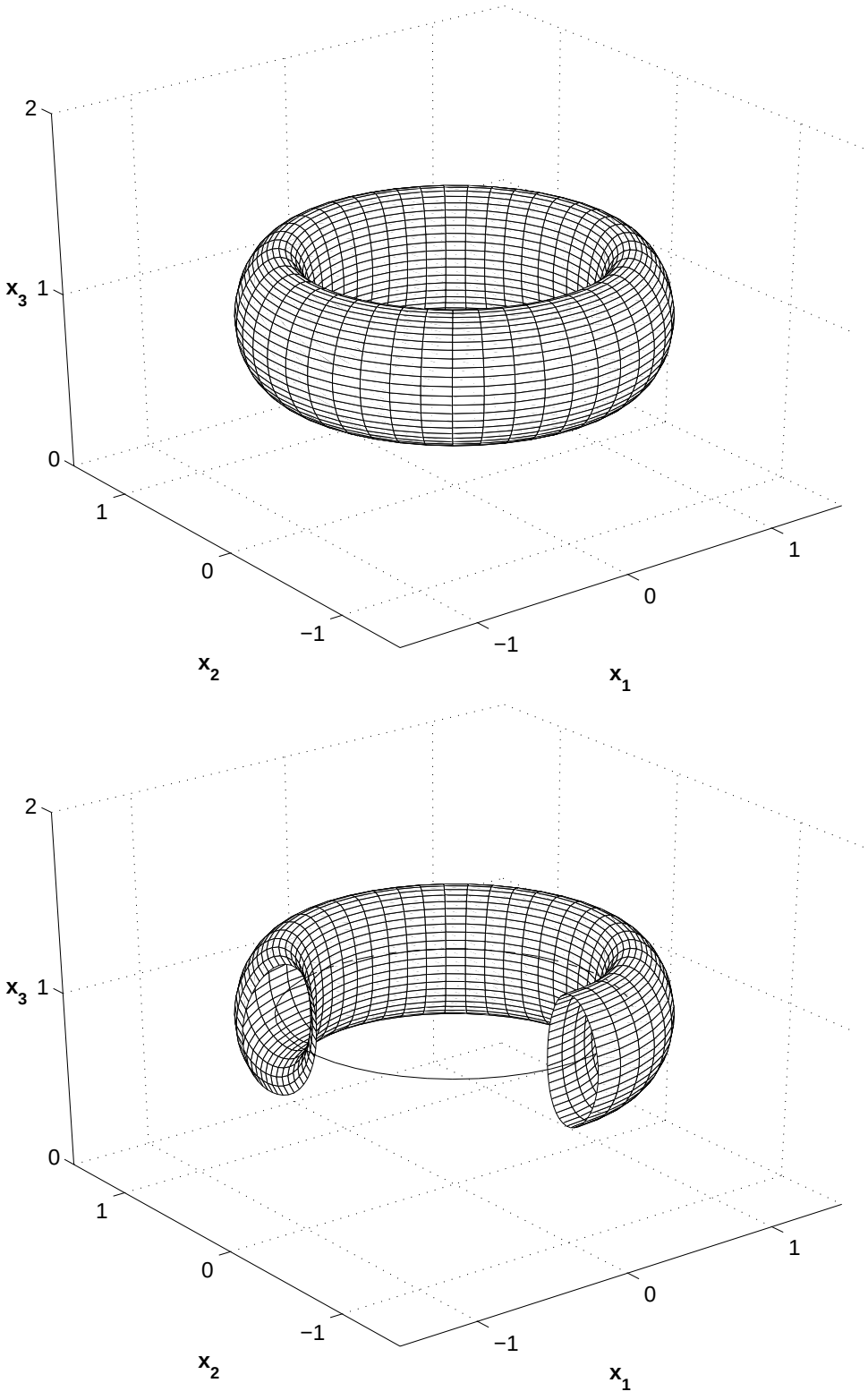

Figure 4.14: Fluid Flow Torus without Re-distribution; $\lambda = 2.005$

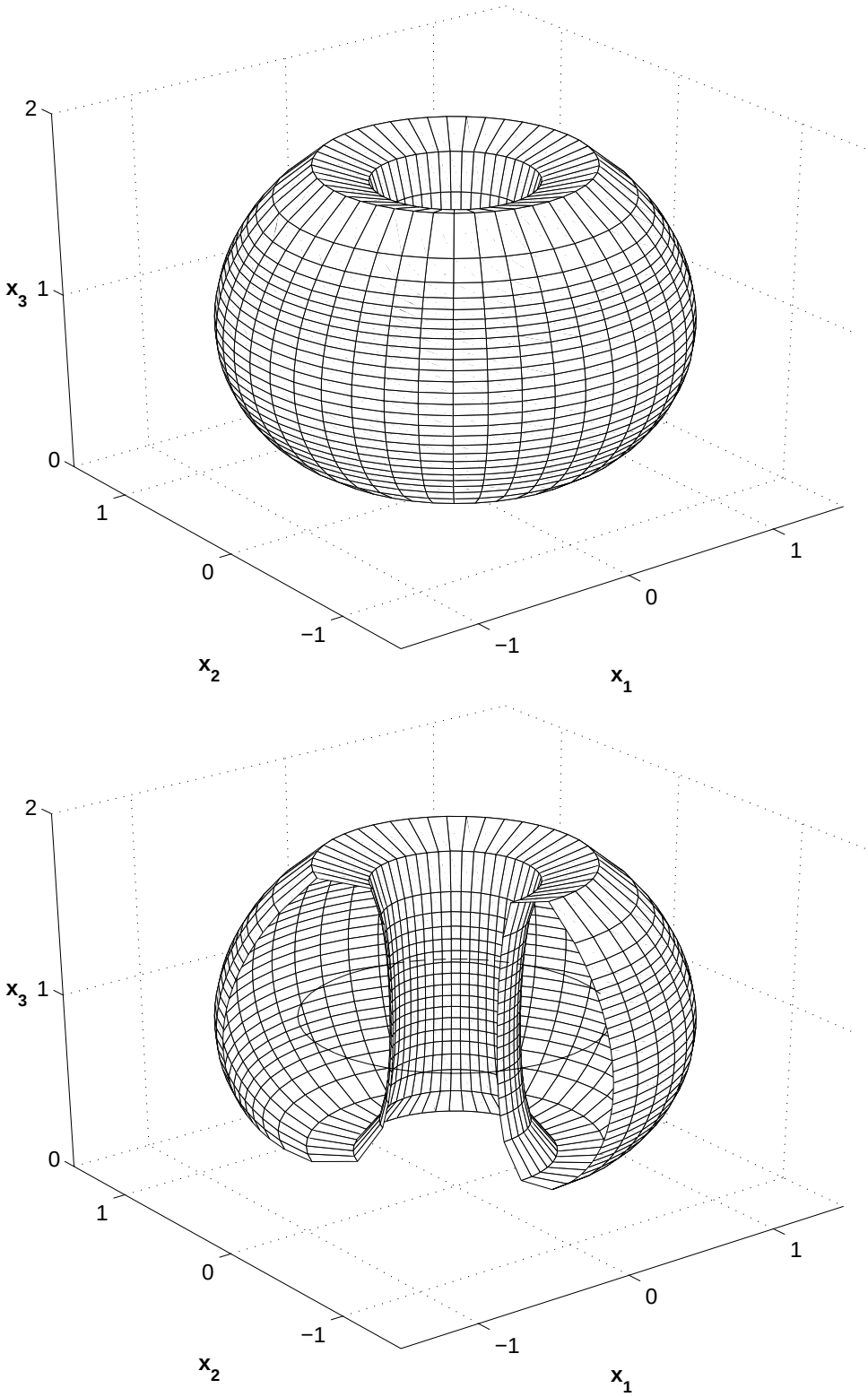

Figure 4.15: Fluid Flow Torus without Re-distribution; $\lambda = 2.020$

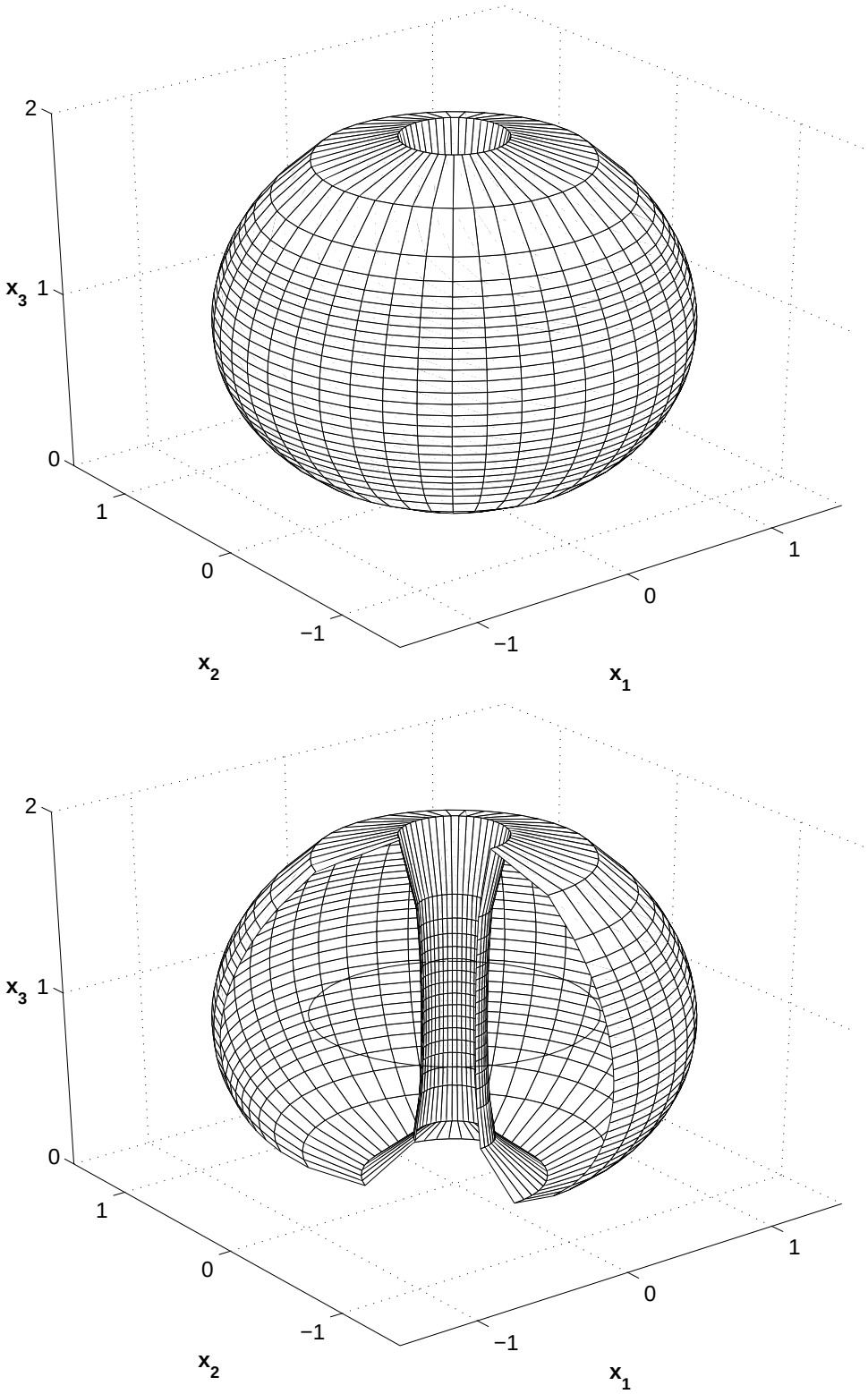

Figure 4.16: Fluid Flow Torus without Re-distribution; $\lambda = 2.0248$

Table 4.4: Newton Iteration: Fluid-Flow Torus with Re-distribution

From λ	To λ	Iteration	$\|\mathbf{f}\|$	$\kappa(J)$	$\|\mathbf{y}\|$
–	2.005	1	1.1	7200	0.72
		2	0.059	3000	0.20
		3	8.9×10^{-4}	3100	4.6×10^{-4}
			3.3×10^{-8}		
0.2015	2.020	1	0.39	4500	5.5
		2	1.1	6600	0.75
		3	0.031	5500	0.029
		4	1.3×10^{-4}	5600	2.8×10^{-4}
			3.4×10^{-9}		
2.0247	2.0248	1	0.071	1.0×10^4	0.75
		2	0.0083	1.2×10^4	0.18
		3	7.9×10^{-4}	1.5×10^4	0.016
		4	2.7×10^{-5}	1.5×10^4	1.3×10^{-4}
			1.6×10^{-9}		

See Tables 4.4 and 4.5 for condition numbers and corrections for some sample continuation steps. In these two tables, the naming convention is the same as in Section 4.1, so the right-hand side is $\mathbf{f}$, the vector containing the left hand side of Equation 3.43 at each (i, j). The vector $\mathbf{y}$ represents the correction at each Newton iteration, $\mathbf{y} = -J^{-1}\mathbf{f}$.

Computation time for the algorithm applied to a two-torus in $\mathbb{R}^3$ is still minimal. The largest computational expense is in generating the Jacobian, not solving the system, probably because the algorithm is implemented in Matlab 6.0, and there is no easy way to vectorize the generation of the Jacobian, which is intrinsically a local operation.

Regardless of the inefficiencies incurred by writing the code in a higher-level language, the Jacobian for a 45×45 torus still takes less than 15 seconds to generate on a modern computer. Writing the Jacobian-generation code in a lower-level language does significantly improve the performance of the algorithm for higher-dimensional tori – as shown later in Section 5.5 – but it is not necessary here.

Table 4.5: Newton Iteration: Fluid-Flow Torus without Re-distribution

From λ	To λ	Iteration	$\|\mathbf{f}\|$	$\kappa(J)$	$\|\mathbf{y}\|$
–	2.005	1	1.05	3700	0.72
		2	0.062	3400	0.21
		3	0.0011	3500	4.4×10^{-4}
			2.7×10^{-8}		
0.2015	2.020	1	0.23	3400	5.2
		2	0.64	4500	0.52
		3	0.021	5800	0.088
		4	1.6×10^{-4}	6200	1.4×10^{-4}
			1.3×10^{-9}		
2.0247	2.0248	1	0.0048	1.2×10^4	0.10
		2	2.5×10^{-4}	1.7×10^4	2.2×10^{-4}
			5.0×10^{-9}		

4.2.2 Two-Torus from Forced Oscillator

Another example of a two-torus embedded in $\mathbb{R}^3$ arises from the forced van der Pol oscillator,

$$\ddot{x} + \alpha\dot{x}(x^2 - 1) + x = \lambda\cos(\omega\theta), \tag{4.14}$$

which reduces to the first-order system [10, 17, 35]

$$\begin{aligned} \dot{x} &= y + \alpha x\left(1 - x^2/3\right) \\ \dot{y} &= -x + \lambda\cos(\omega\theta), \end{aligned} \tag{4.15}$$

where $\alpha > 0$, $\omega > 0$, and $\lambda\cos(\omega\theta)$ is the forcing term. In Equation (4.5), α is the continuation parameter, but now α is fixed and, in keeping with previous notation, λ is the continuation parameter.

The forced van der Pol oscillator admits an attracting periodic orbit for several values of the forcing term [18, 35]. Figure 4.17 shows examples of the periodic orbits when $\alpha = 0.4$ and $\lambda\cos(\omega\theta)$ ranges from -0.8 to 0.8.

The system generates an invariant torus through the addition a trivial third angular dimension, $\dot{\theta} = 1$. It is also necessary to shift the system by a certain fixed value, say $x \leftarrow x - 5$, to prevent the torus from overlapping itself when the periodic

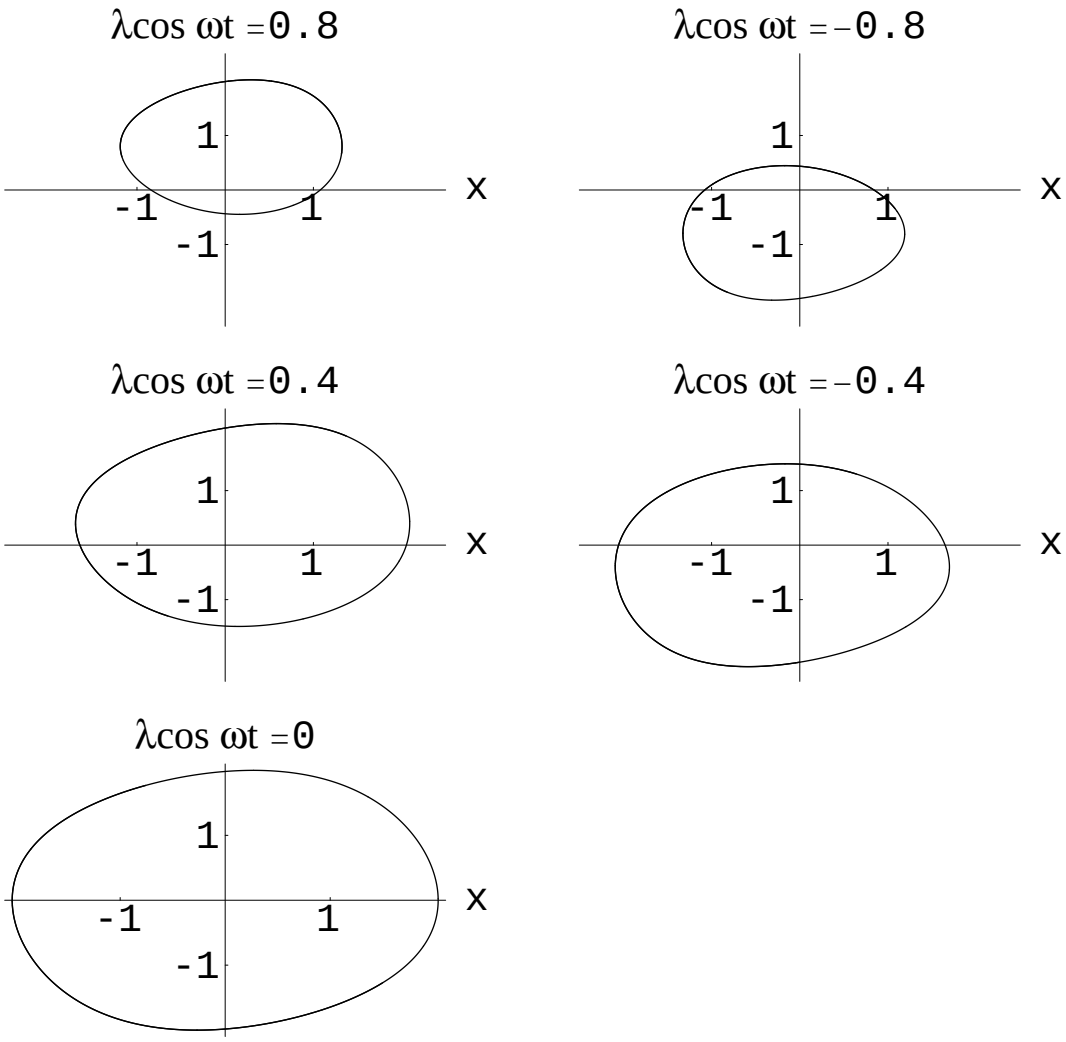

Figure 4.17: Examples of Periodic Orbits in Forced van der Pol Equations

orbit spins around the vertical axis. The new system is

$$\begin{aligned}\dot{x} &= y - 5 + \alpha x\left(1 - x^2/3\right)\\ \dot{y} &= -x + \lambda\cos(\omega\theta)\\ \dot{\theta} &= 1.\end{aligned} \tag{4.16}$$

A simple coordinate transformation takes advantage of the periodicity of θ and compacts the system into a torus. With $x_1 = y\cos(\omega\theta)$, $x_2 = y\sin(\omega\theta)$, and $x_3 = x$, the system becomes

$$\begin{aligned}\dot{x}_1 &= \frac{\lambda x_1^2}{x_1^2 + x_2^2} - \frac{x_1 x_3}{\sqrt{x_1^2 + x_2^2}} - \omega x_2\\ \dot{x}_2 &= \frac{\lambda x_1 x_2}{x_1^2 + x_2^2} - \frac{x_2 x_3}{\sqrt{x_1^2 + x_2^2}} + \omega x_1\\ \dot{x}_3 &= \sqrt{x_1^2 + x_2^2} - 5 + \alpha x_3\left(1 - x_3^2/3\right).\end{aligned} \tag{4.17}$$

This system is substantially different from the last example because it is not rotationally symmetric. Also, it is a standard example, so it provides a way to check the orthogonality condition with the current discretization against previous work [10, 12, 21, 29, 35, 36]. Because the torus is attracting, a simple forward integration exhibits a rough view of the torus, just as in Figure 4.10. Figures 4.18 and 4.19 show the progression of the torus in λ for $\alpha = 0.4$ and for $\omega = \sqrt{0.84}$ and $\omega = \sqrt{0.78}$ respectively. These are standard parameter values in the literature [10, 29, 38].

The torus actually persists for larger values of λ in both cases, but it becomes increasingly difficult to get an image of the torus from simple integration.

The following figures show the results of Algorithm 3.2 applied to the van der Pol torus, first with $\omega = \sqrt{0.84}$ and then with $\omega = \sqrt{0.78}$. In both cases, the initial guess at $\lambda = 0$ is

$$\overline{\mathbf{x}}((\phi_1)_i, (\phi_2)_j) = \overline{\mathbf{x}}_{i,j} = \begin{pmatrix} (5 + 2\cos(\phi_2)_j)\cos(\phi_1)_i \\ -(5 + 2\cos(\phi_2)_j)\sin(\phi_1)_i \\ 2\sin(\phi_2)_j \end{pmatrix}, \tag{4.18}$$

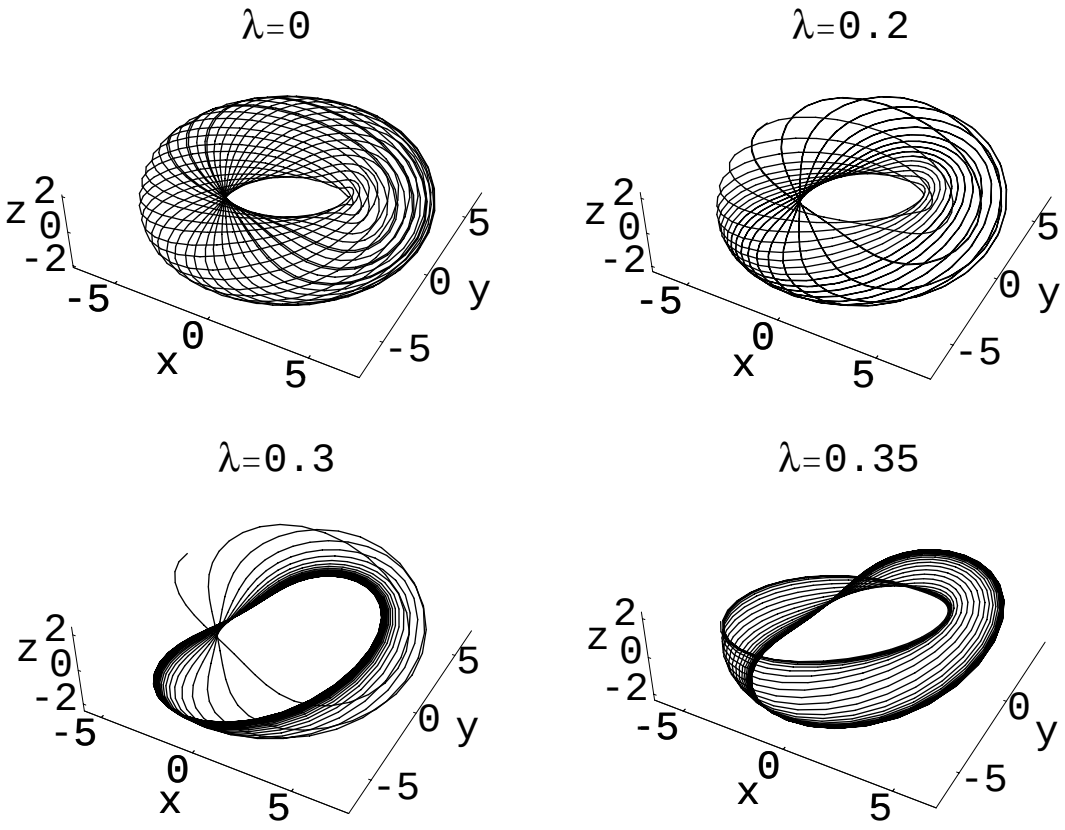

Figure 4.18: Progression of Full van der Pol System, $\omega = \sqrt{0.84}$

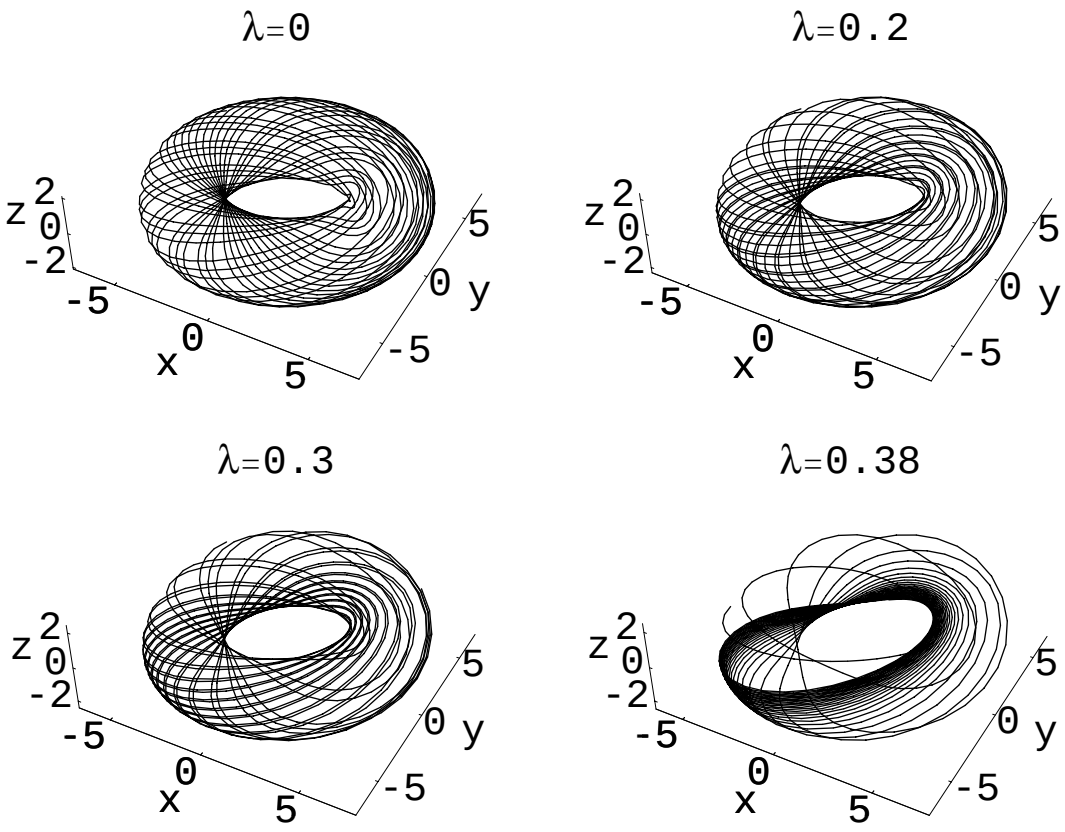

Figure 4.19: Progression of Full van der Pol System, $\omega = \sqrt{0.78}$

where $(\phi_1)_i = 2\pi(i-1)/N_i$ and $(\phi_1)_j = 2\pi(j-1)/N_j$. If desired, this initial guess then undergoes an arc length re-distribution along each meridian before the continuation process begins.

The Jacobian in Newton's method comes from forward-differencing on r with a step size of 10^{-8}, and the cut off criterion for Newton's method is that the two-norm of the right-hand side ($\|\mathbf{f}\|$) be less than 10^{-6}.

As in the previous torus, arc-length re-distribution along each meridian does improve the discretization. Unlike the previous torus, however, the deformation of the torus actually *requires* some sort of re-distribution, at least for part of the continuation process for one particular value of ω. Practical experience shows that for $\omega = \sqrt{0.84}$, a good strategy is to re-distribute at convergence up until some set λ value, then finish the continuation without re-distribution.

Figures 4.20–4.22 show the continuation process from $\lambda = 0.0$ through $\lambda \approx 0.342407$ when $\omega = \sqrt{0.84}$ with a grid of $N_i = N_j = 45$. The points are re-distributed along each meridian between steps for $\lambda \leq 0.30$. Above that value, the torus does not undergo re-distribution between steps. Figure 4.20 is the result at convergence, but before re-distribution.

The step size for the continuation process is dynamic, starting at 0.1 and halving every time the Newton process does not converge within a specified number of iterations – with some extra correction to allow for larger steps in the beginning. This causes the step size to shrink quickly near breakdown, as shown in Figure 4.23.

Condition numbers for the Jacobian calculated using the one-norm condition estimator [19] vary greatly, from about 600 near $\lambda = 0$, to about 10^6 for $\lambda > 0.325$. Table 4.6 contains some examples.

Note that this method extends the torus farther than some graph transform methods [12], probably because it does not rely so heavily on attractivity properties. It may be possible to extend the torus even further by experimenting with different

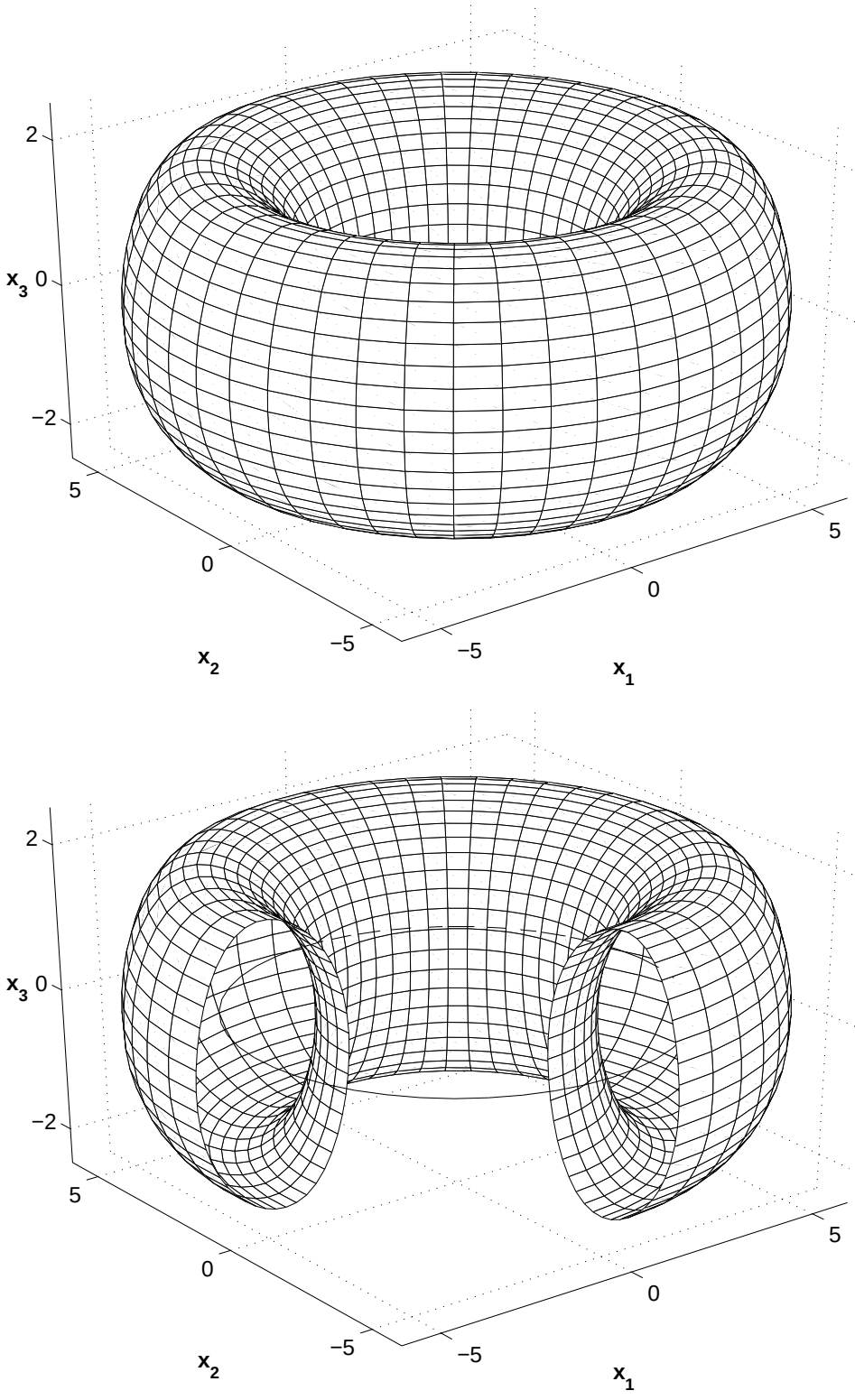

Figure 4.20: Forced van der Pol Torus; $\lambda = 0$

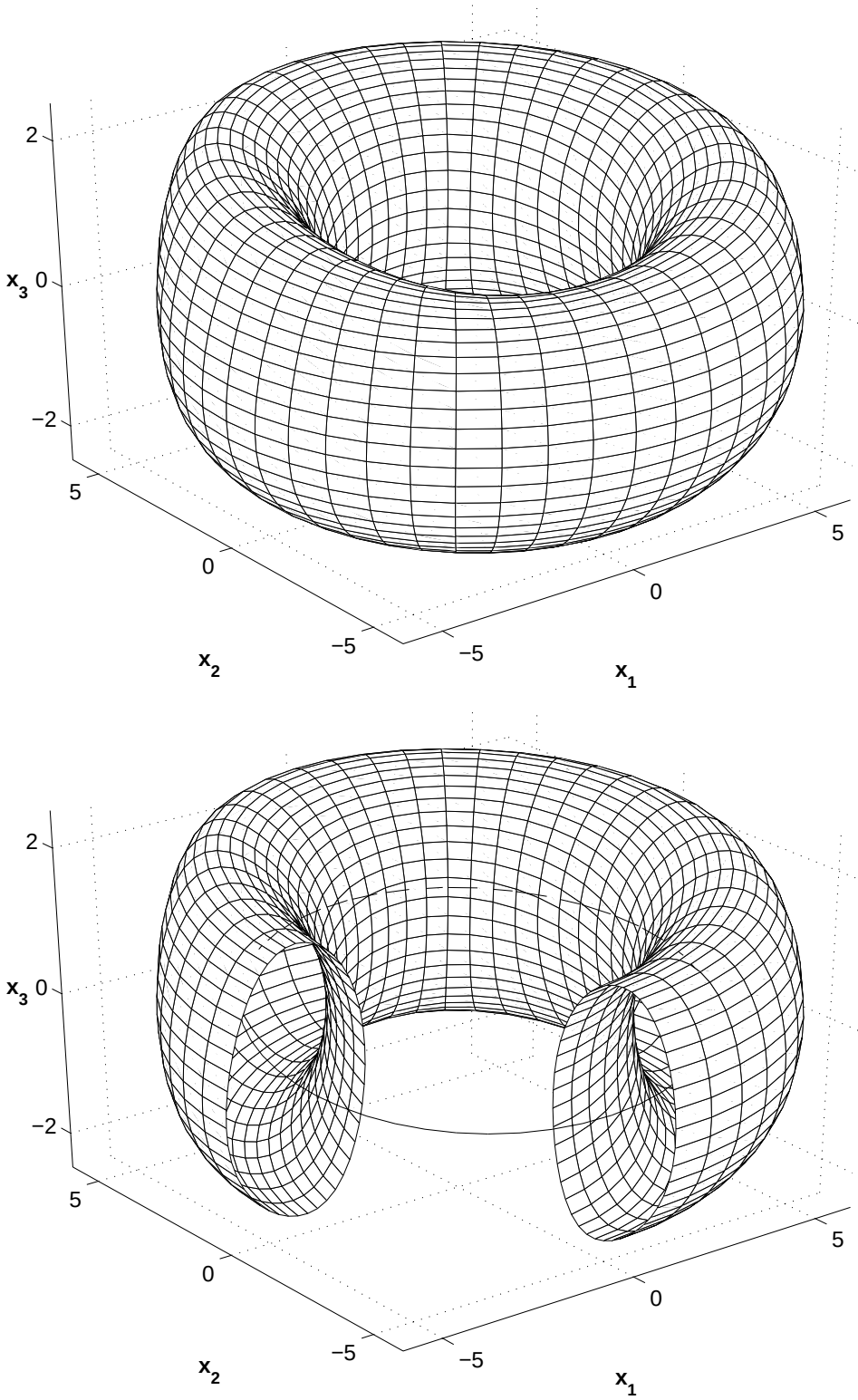

Figure 4.21: Forced van der Pol Torus; $\omega = \sqrt{0.84}$, $\lambda = 0.325$

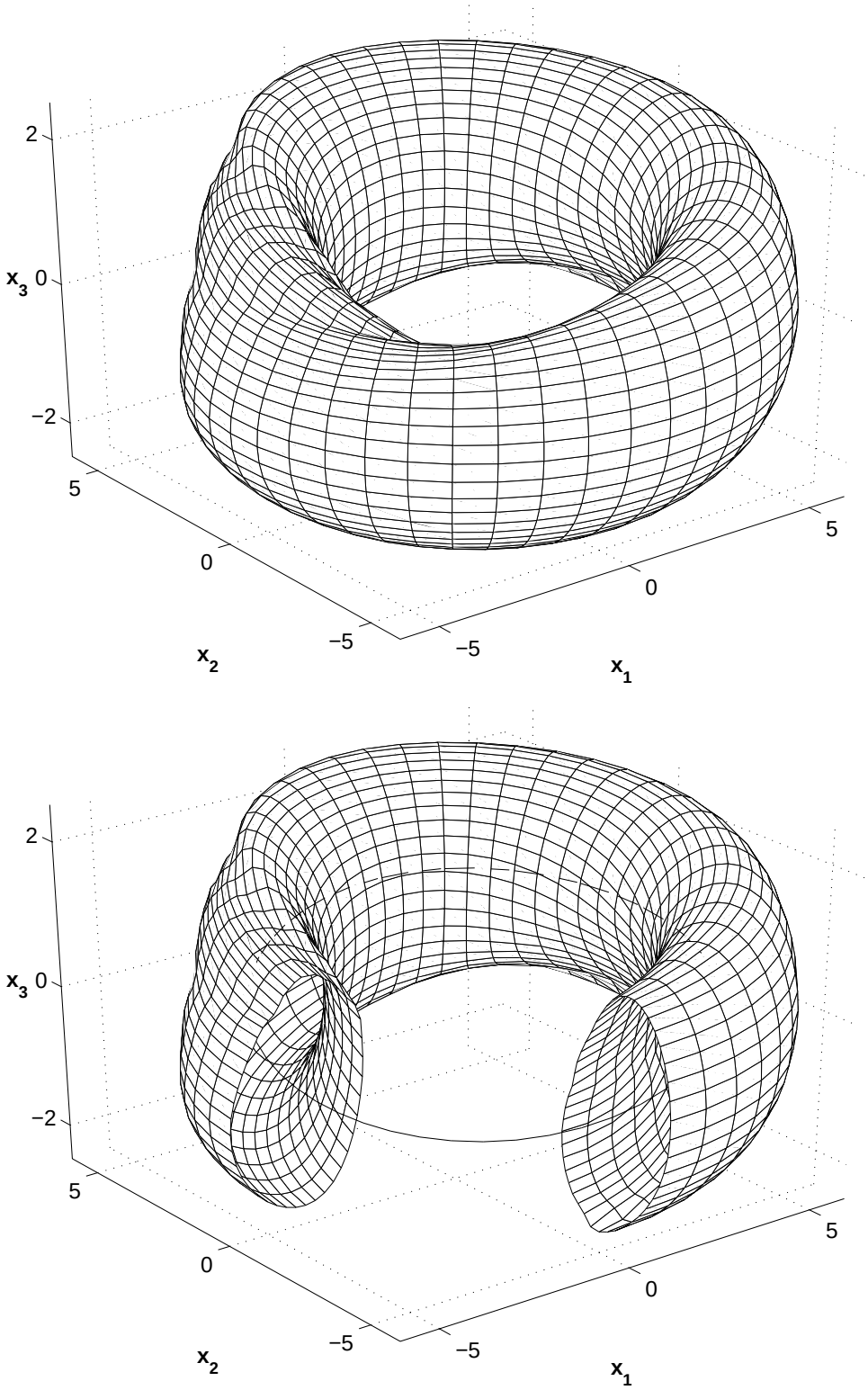

Figure 4.22: Forced van der Pol Torus; $\omega = \sqrt{0.84}$, $\lambda \approx 0.342407$

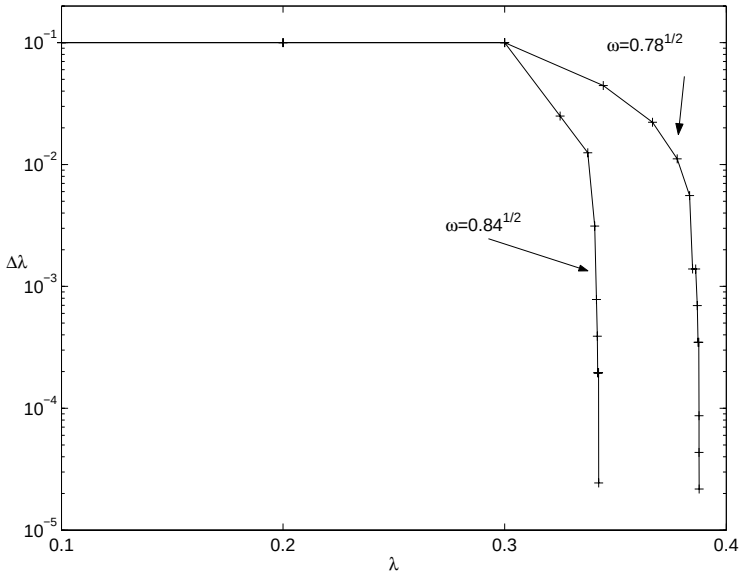

Figure 4.23: Continuation Steps for Forced van der Pol Torus

Table 4.6: Newton Iteration: Forced van der Pol Torus with $\omega = \sqrt{0.84}$

From λ	To λ	Iteration	$\|\mathbf{f}\|$	$\kappa(J)$	$\|\mathbf{y}\|$
–	0.0	1	5.9	620	2.7
		2	0.11	680	0.13
		3	1.9×10^{-4}	680	2.9×10^{-4}
			8.3×10^{-10}		
0.30	0.325	1	0.65	8.9×10^{5}	2.9
		2	0.11	2.7×10^{5}	0.98
		3	0.012	3.0×10^{5}	0.082
		4	9.6×10^{-5}	3.0×10^{5}	3.9×10^{-4}
			2.4×10^{-9}		
0.342383	0.342407	1	5.2×10^{-4}	3.1×10^{6}	0.17
		2	0.0019	4.3×10^{6}	0.051
		3	8.1×10^{-5}	5.3×10^{6}	0.0072
		4	2.8×10^{-6}	5.5×10^{6}	1.6×10^{-4}
			1.1×10^{-9}		

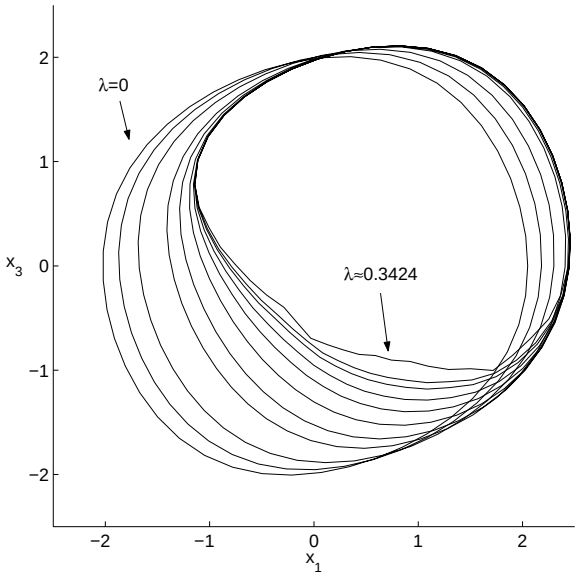

Figure 4.24: Forced van der Pol Torus; $\omega = \sqrt{0.84}$

choices of N_i and N_j and different cut-off thresholds for re-distribution, but the torus appears to be very near breakdown above $\lambda \approx 0.3424$.

Figure 4.24 shows one section of the torus at $\phi_1 = 0$ ($\theta = 0$) and approximate λ values of 0, 0.1, 0.2, 0.3, 0.325, 0.3375, 0.3406, 0.3414, 0.3418, 0.3420, and the final 0.3424. (*cf.* [10]).

Figures 4.25 – 4.27 show the continuation process through $\lambda \approx 0.3845$ when $\omega = \sqrt{0.78}$ with $N_i = 401$ and $N_j = 101$. (The result at $\lambda = 0$ is of course identical to the result for $\omega = \sqrt{0.84}$ in Figure 4.20.) The torus does not undergo any re-distribution between λ steps. The figures contains only a few representative points, since a full 401×101 grid would be too dense. The condition numbers of the Jacobian are comparable to the case of $\omega = \sqrt{0.84}$.

The reason for the drastic increase in the number of points at $\omega = \sqrt{0.78}$ is that the technique is much less stable, probably due to a difference in breakdown mechanism between $\omega = \sqrt{0.84}$ and $\omega = \sqrt{0.78}$. In the latter case, a fixed point is developing on the torus near breakdown [1, 12], and the method is unstable when a grid point is near an equilibrium. See the next section for a discussion of the effect

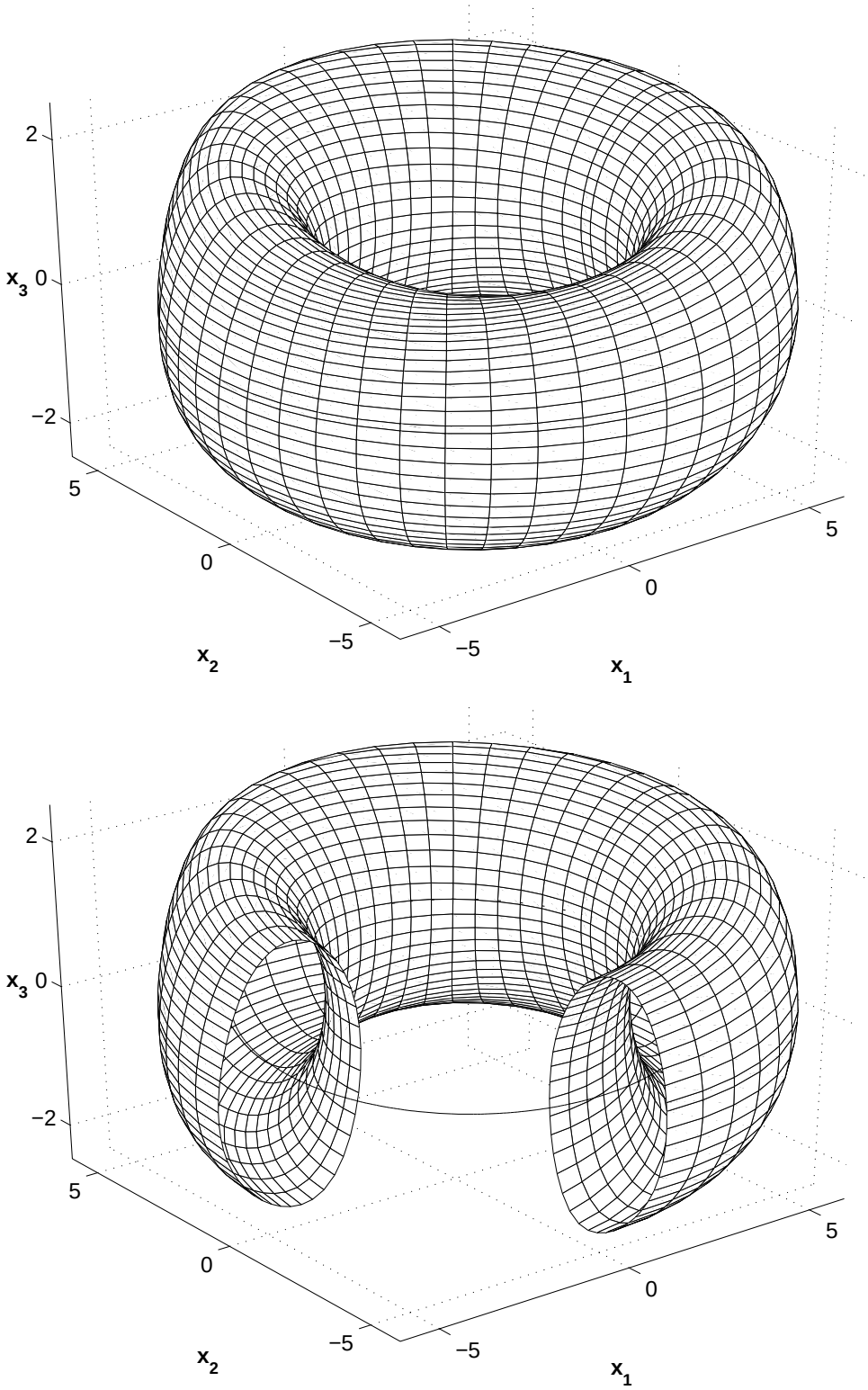

Figure 4.25: Forced van der Pol Torus; $\omega = \sqrt{0.78}$, $\lambda = 0.3445$

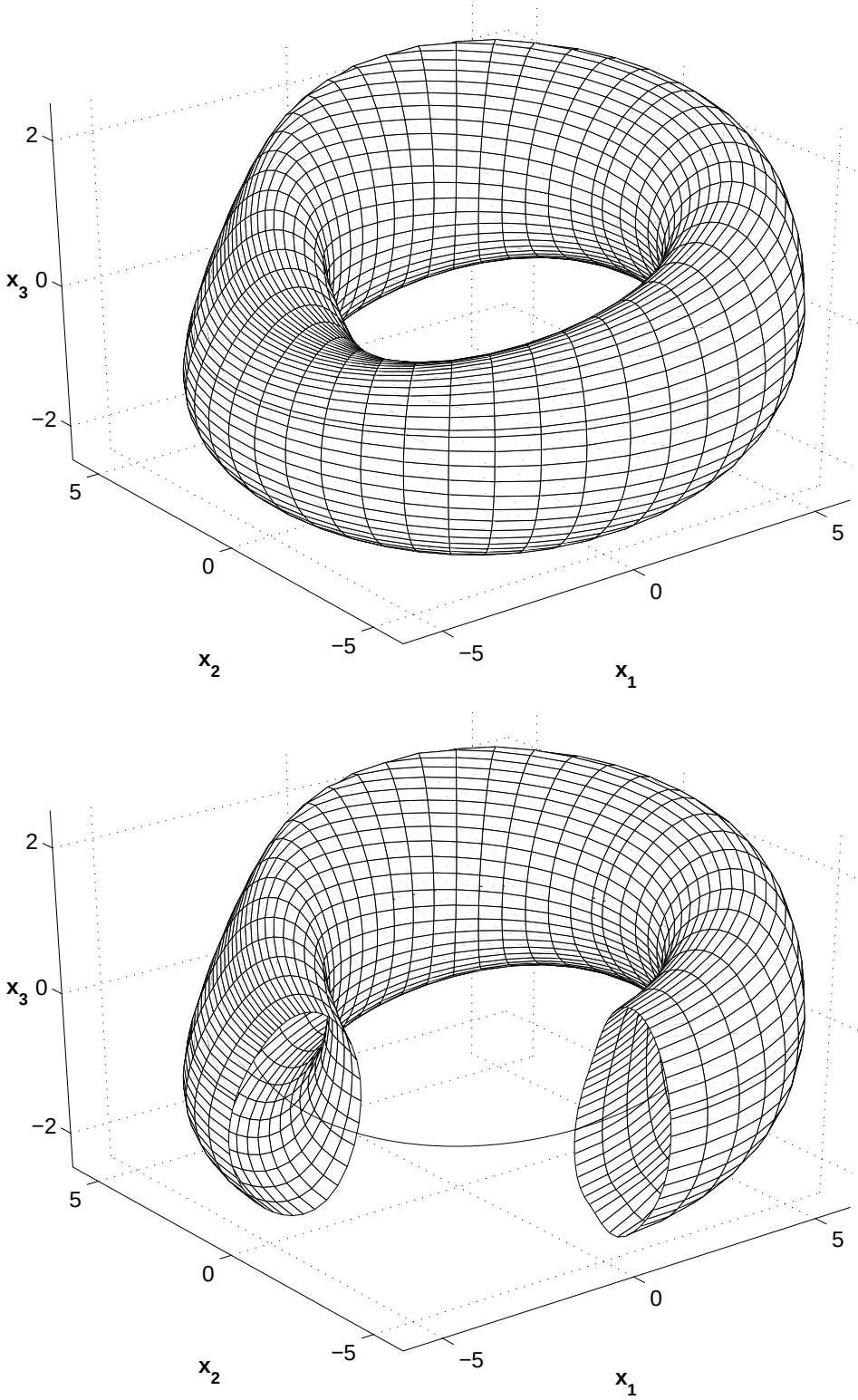

Figure 4.26: Forced van der Pol Torus; $\omega = \sqrt{0.78}$, $\lambda \approx 0.3848$

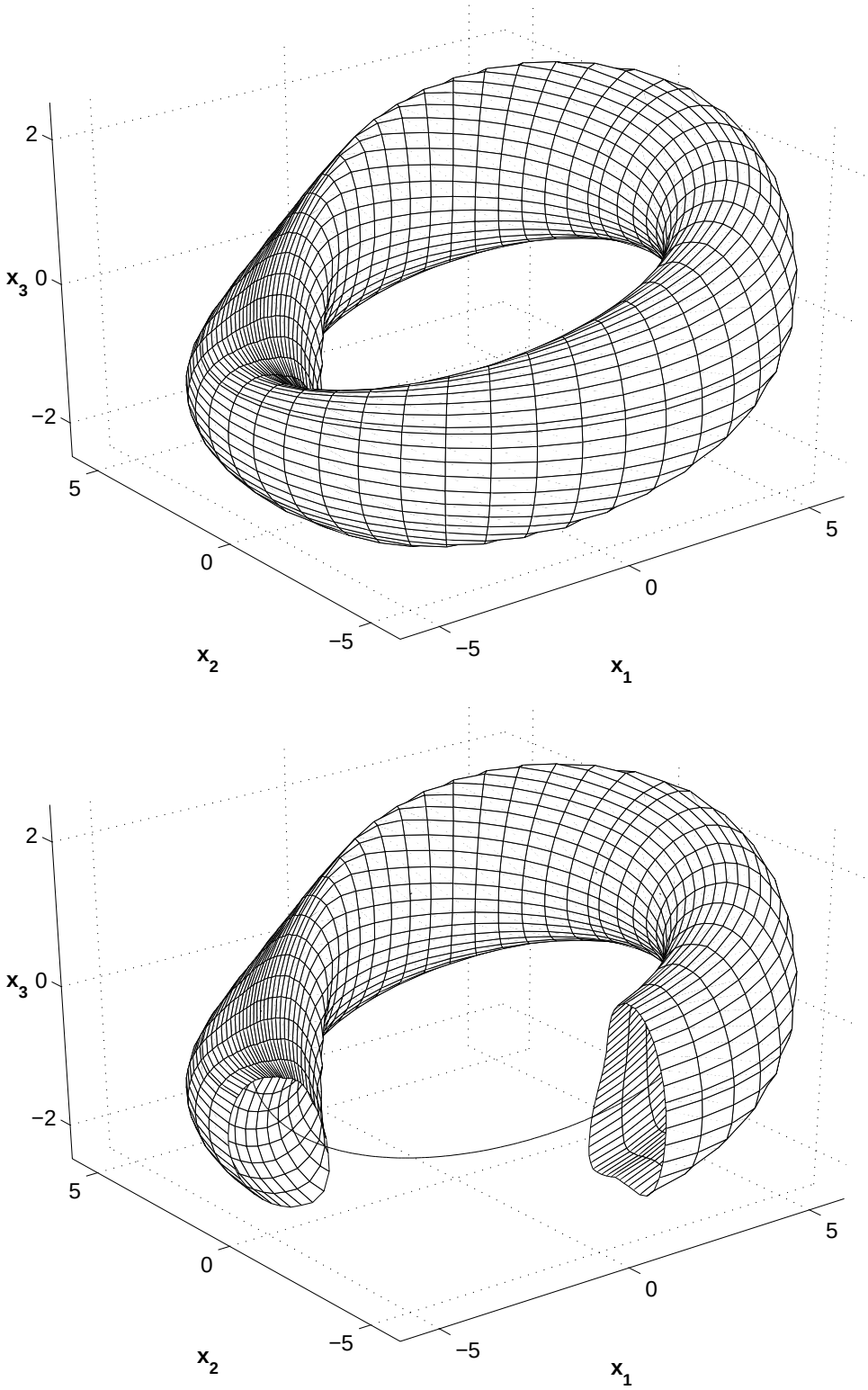

Figure 4.27: Forced van der Pol Torus; $\omega = \sqrt{0.78}$, $\lambda \approx 0.38776$

Table 4.7: Newton Iteration: Forced van der Pol Torus, $\omega = \sqrt{0.78}$

From λ	To λ	Iteration	$\|\mathbf{f}\|$	$\kappa(J)$	$\|\mathbf{y}\|$
–	0.0	1	27	9200	11
		2	0.47	6400	0.56
		3	7.9×10^{-4}	6500	0.0013
			3.6×10^{-9}		
0.30	0.3445	1	4.5	1.1×10^{4}	20
		2	1.0	1.3×10^{4}	6.5
		3	0.12	1.6×10^{4}	0.49
		4	8.0×10^{-4}	1.7×10^{4}	0.0017
			1.3×10^{-8}		
0.38774	0.387761	1	0.0020	1.1×10^{6}	1.6
		2	0.18	2.3×10^{6}	0.28
		3	0.062	1.5×10^{6}	0.24
		4	0.032	1.7×10^{6}	0.080
		5	0.0032	1.7×10^{6}	0.0040
		6	2.4×10^{-5}	1.7×10^{6}	4.2×10^{-5}
		*	1.8×10^{-9}		

of invariant sub-manifolds on the stability of the method.

Even disregarding the existence of a fixed point, the obvious pinching of the torus indicates that it is losing smoothness. Increased resolution, particularly in the direction of time (θ), seems to stabilize it somewhat, as it permits tighter calculations near the pinched ares. Other methods have reported difficulty when $\omega = \sqrt{0.78}$ as well [10].

Figure 4.28 shows one section of the torus at $\phi_1 = 0$ ($\theta = 0$) and approximate λ values of 0, 0.1, 0.2, 0.3, 0.3445, 0.3668, 0.3779, 0.3834, 0.3848, 0.3862, 0.3869, 0.3873, 0.3876, and the final 0.3878 (*cf.* [10, 38]).

4.2.3 Complications with Method for Two-Torus in $\mathbb{R}^3$

In the analysis of Section 3.3, one of the concerns was the existence of closed, invariant sub-manifolds such as periodic orbits, the idea being that such manifolds are the natural extension of fixed points that create problems for one-tori in the plane. This

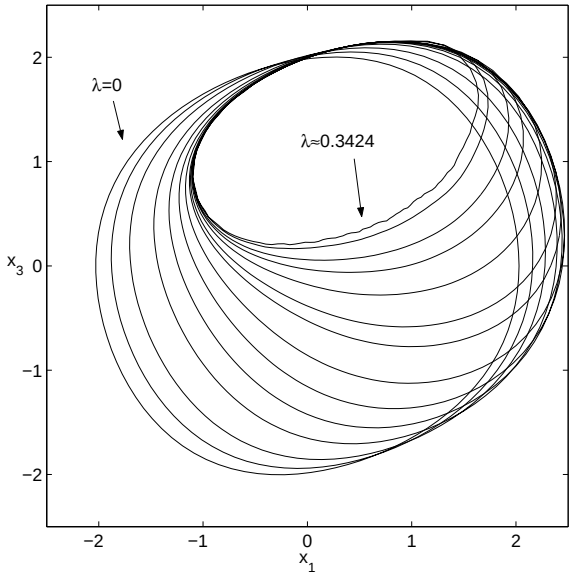

Figure 4.28: Forced van der Pol Torus; $\omega = \sqrt{0.78}$

section contains an example of an invariant two-torus in $\mathbb{R}^3$ with two periodic orbits, for which the method seems to be unconditionally unstable if the discretization aligns with one or more of the orbits.

The construction of the torus proceeds along the same lines as in Section 4.1.3. It starts with the usual attracting oscillator in Equation (2.10), which in Cartesian coordinates is

$$\begin{aligned} \dot{x} &= \lambda x - y - x\left(x^2 + y^2\right) \\ \dot{y} &= x + \lambda y - y\left(x^2 + y^2\right). \end{aligned} \tag{4.19}$$

To create a torus from a simple oscillator about the origin, it is necessary to shift the periodic orbit to the right by a fixed factor, say 3, and then add a rotational dimension, $\dot{\theta} = \sin\theta$. The new system is

$$\begin{aligned} \dot{x} &= \lambda(x-3) - y - (x-3)\left((x-3)^2 + y^2\right) \\ \dot{y} &= (x-3) + \lambda y - y\left((x-3)^2 + y^2\right) \\ \dot{\theta} &= \sin\theta. \end{aligned} \tag{4.20}$$

The standard cylindrical coordinate transformations of $x_1 = x\cos\theta$, $x_2 = x\sin\theta$,

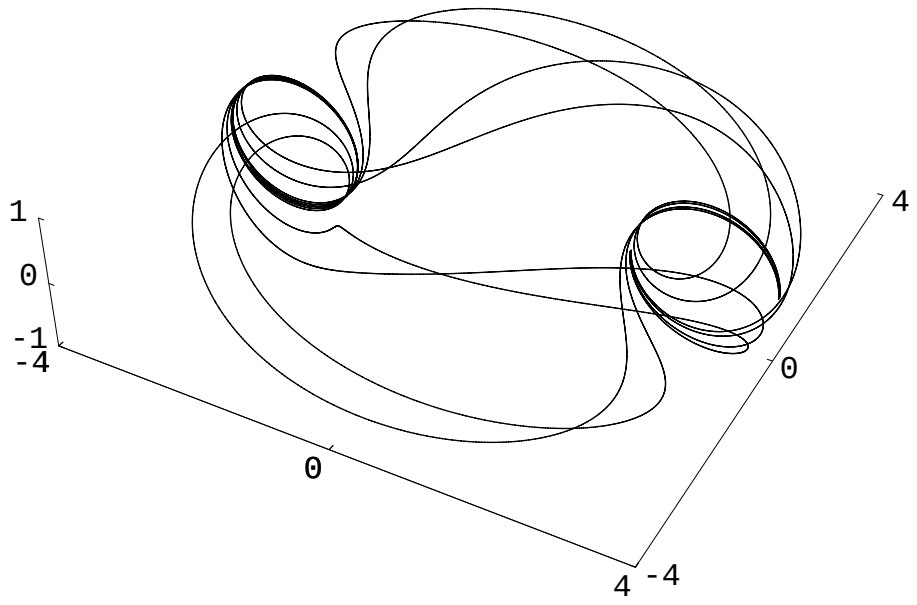

Figure 4.29: Torus with Two Periodic Orbits, $\lambda = 1$

and $x_3 = y$ convert Equation (4.20) to

$$\begin{aligned}
\dot{x}_1 &= \frac{x_1\left(\sqrt{x_1^2+x_2^2}-3\right)}{\sqrt{x_1^2+x_2^2}}\left(\lambda - -\left(\sqrt{x_1^2+x_2^2}-3\right)^2 + x_3^2\right) - \frac{x_2^2+x_1x_3}{\sqrt{x_1^2+x_2^2}} \\
\dot{x}_2 &= \frac{x_2\left(\sqrt{x_1^2+x_2^2}-3\right)}{\sqrt{x_1^2+x_2^2}}\left(\lambda - -\left(\sqrt{x_1^2+x_2^2}-3\right)^2 + x_3^2\right) + \frac{x_1x_2-x_2x_3}{\sqrt{x_1^2+x_2^2}} \qquad (4.21) \\
\dot{x}_3 &= \left(\sqrt{x_1^2+x_2^2}-3\right) + \lambda x_3 - x_3\left(\left(\sqrt{x_1^2+x_2^2}-3\right)^2 + x_3^2\right).
\end{aligned}$$

This vector field admits a two-torus with two periodic orbits. Both periodic orbits lie in the x_1-x_3 plane. The unstable one is centered at $(3, 0, 0)$, and the stable one is centered at $(-3, 0, 0)$. The torus itself is globally attracting, so forward integration gives a rough picture of it. Figure 4.29 shows the two periodic orbits with eight connecting orbits.

As mentioned, this section show the results of two different types of initial guesses.

The first one is a modification of the ones used in previous sections:

$$\overline{\mathbf{x}}((\phi_1)_i, (\phi_2)_j) = \overline{\mathbf{x}}_{i,j} = \begin{pmatrix} (3 + 2\cos(\phi_2)_j)\cos(\phi_1)_i \\ -(3 + 2\cos(\phi_2)_j)\sin(\phi_1)_i \\ 2\sin(\phi_2)_j + 1 \end{pmatrix}, \tag{4.22}$$

where $(\phi_1)_i = 2\pi(i-1)/N_i$ and $(\phi_2)_j = 2\pi(j-1)/N_j$.

This choice of $\overline{\mathbf{x}}$ has the property that at least one ϕ_1-section (*i.e.*, a collection of points where ϕ_1 is constant) lines up exactly along one of the periodic orbits. Specifically, all the points $\overline{\mathbf{x}}_{1,j}$ lie on the repelling periodic orbit, and, if N_i is even, then the points $\overline{\mathbf{x}}_{N_i/2+1,j}$ lie on the attracting orbit.

If N_i is even, then the condition number of the Jacobian is markedly higher than if N_j is odd, although the method is poorly conditioned in general regardless of N_i. The condition number algorithm [19] estimates a condition number for the Jacobian on the order of 10^{12} for the Jacobian of a 46×45 torus and 10^{13} for a 100×101 torus. In neither case does the Newton iteration converge at $\lambda = 1$.

The same algorithm estimates a condition number on the order of 10^9 for a 45×45 torus and 10^{10} for a 101×101 torus. The method will in fact continue the torus from $\lambda = 1.0$ up to $\lambda = 1.8$ for a 45×45 torus in steps of $\Delta\lambda = 0.1$, but it is unclear how reliable these results are, due to the high condition numbers.

Given that the discretization seems to have difficulty when a section lines up with a periodic orbit, the next obvious initial guess to try is the same as in Equation (4.22), but with a diagonally slanted meridian. Changing the definitions of ϕ_1 and ϕ_2 is the simplest way to induce a slant into the initial guess.

Let $(\phi_2)_j = 2\pi(j-1)/N_j$ as before. Shifting the definition of one of the angles by a set factor of the other is the simplest way to produce a slanted picture, so now let $(\phi_1)_i = 2\pi(i-1)/N_i + \sin(\phi_2)_j/5$. The extra term generates a torus whose meridians no longer lie in the vertical plane. See Figure 4.30.

This new initial guess does improve the performance marginally, but not so much

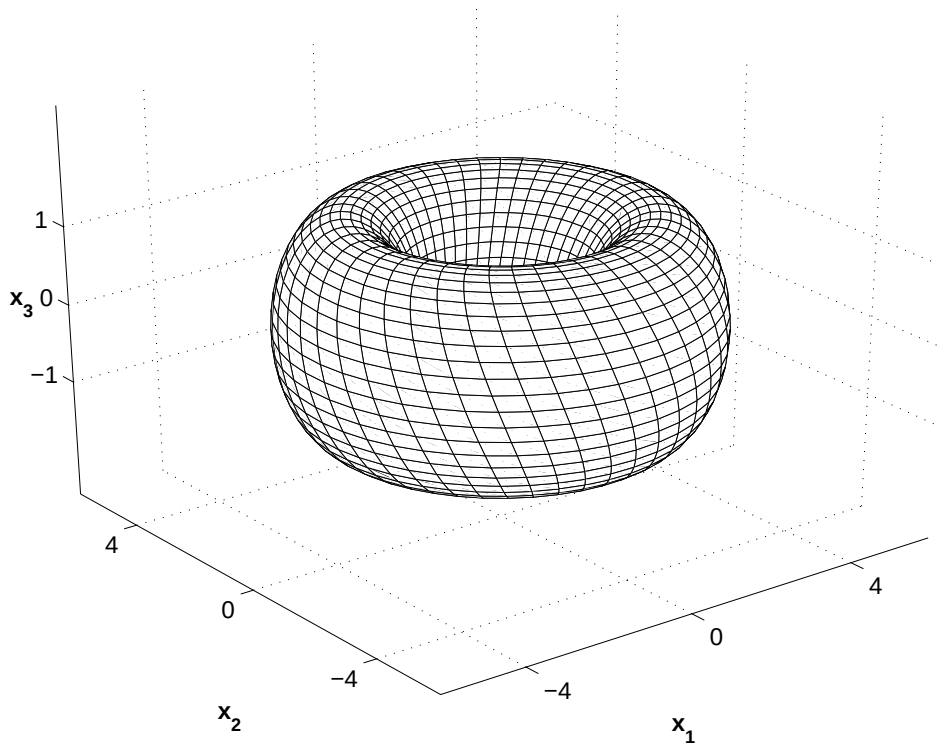

Figure 4.30: Continued Torus with Two Periodic Orbits, $\lambda = 2.0$

that the method is completely reliable. The condition number of the Jacobian for a 45×45 torus is about 1.5×10^6 at $\lambda = 1.0$, but it climbs above 10^9 near $\lambda = 2.0$ when using increments of $\Delta\lambda = 0.1$. Figure 4.30 shows the result of the continuation process for a 45×45 torus at $\lambda = 2.0$. No re-distribution is necessary here, since the torus grows symmetrically.

As expected, the oddness/evenness of N_i does not matter so much with a slanted torus. Table 4.8 shows the estimated condition numbers for this torus for a variety of numerical experiments. All condition number estimates come from the standard algorithm computed for the *first* Newton iteration before convergence at the λ value. A "–" in the table indicates where the method could not continue. The slanted, larger tori could not continue past $\lambda = 1.7$ with $\Delta\lambda = 0.1$.

Table 4.8: Condition Numbers for Example with Periodic Orbits

		$\kappa(J)$	
Initial Guess	$N_i \times N_j$	$\lambda = 1.0$	$\lambda = 2.0$
Vertical	45×45	2.8×10^8	–
	46×45	3.3×10^{12}	–
	45×46	2.9×10^8	–
	101×101	8.1×10^{10}	–
	102×101	8.3×10^{13}	–
	101×102	8.3×10^{10}	–
Slanted	45×45	1.6×10^6	6.6×10^8
	46×45	4.3×10^6	4.6×10^8
	45×46	1.9×10^6	5.1×10^8
	101×101	6.2×10^7	–
	102×101	8.0×10^7	–
	101×102	1.2×10^8	–

CHAPTER V

ORTHOGONALITY CONDITION: GENERAL CASE

The special cases described and implemented in Chapters 3 and 4 rely on special properties of $\mathbb{R}^2$ or $\mathbb{R}^3$. This chapter extends the orthogonality condition to general p-tori in $\mathbb{R}^n$ in a way that is similar, though not identical, to the technique proposed by Moore [29]. It also contains an analysis of some of the numerical issues involved, notably answering questions about the structure of the Jacobian in the Newton iterations and the best methods for solving the sparse system in higher dimensions.

Finally, this chapter introduces a physical example of a three-torus embedded in $\mathbb{R}^8$ that arises from a system of indirectly coupled oscillators. Numerical results show the continuation of the torus to a parameter value near breakdown.

5.1 General Algorithm

When trying to implement Equation (1.16) for a general p-torus embedded in $\mathbb{R}^n$, the first challenge is to construct a new, smooth set of traveling normal vectors on the surface of each torus. Local tangent vectors are relatively easy to approximate through natural extensions of the box discretizations described in earlier chapters, but given a set of p independent tangent vectors in $\mathbb{R}^{p+q}$, there is no obvious method for constructing an orthonormal set of q normal vectors, at least not smoothly along the entire torus. In lower dimensions, natural rotations and cross-products provide updated normal vectors based on tangent directions, but in higher dimensions the algorithm becomes more complicated.

As usual, the search is for a p-torus in $\mathbb{R}^n$ with $q = n - p$. Let $\overline{\mathbf{x}}(\boldsymbol{\phi})$ be a

guess for the torus with $\boldsymbol{\phi} = (\phi_1, \phi_2, \ldots, \phi_p)$ being p periodic coordinates, and let $\overline{Q}(\boldsymbol{\phi})$ be a smooth, moving set of normal vectors on the graph of $\overline{\mathbf{x}}$. Then the sought-after torus in local coordinates is $\hat{\mathbf{x}}(\boldsymbol{\phi}) = \overline{\mathbf{x}}(\boldsymbol{\phi}) + \overline{Q}(\boldsymbol{\phi})\mathbf{r}(\boldsymbol{\phi})$, where $\mathbf{r}(\boldsymbol{\phi}) = (r_1(\boldsymbol{\phi}), r_2(\boldsymbol{\phi}), \ldots, r_q(\boldsymbol{\phi}))$.

Now let the initial guess and normal vectors be discrete with N_k points along each ϕ_k direction, $k = 1, 2, \ldots, p$. References for $\overline{\mathbf{x}}$, $\hat{\mathbf{x}}$, $\mathbf{r}$, and $\overline{Q}$ are $\overline{\mathbf{x}}_{i_1,i_2,\ldots,i_p}$, $\hat{\mathbf{x}}_{i_1,i_2,\ldots,i_p}$, and $\overline{Q}_{i_1,i_2,\ldots,i_p}$ respectively by convention. Periodicity indicates that arithmetic in the indexing is modulo N_k in the kth position, meaning that $N_k + 1 = 1$ for all $k = 1, 2, \ldots, p$.

Tangent vectors come from the box scheme, and the natural extension works as follows. For a limit cycle, each box is a line segment with two vertices: $\hat{\mathbf{x}}_i$ and $\hat{\mathbf{x}}_{i+1}$, and the tangent vector is the difference between the vertices.

For a two-torus, each box is a square with four vertices: $\hat{\mathbf{x}}_{i,j}$, $\hat{\mathbf{x}}_{i+1,j}$, $\hat{\mathbf{x}}_{i,j+1}$, and $\hat{\mathbf{x}}_{i+1,j+1}$, and the two tangent vectors are averages. That is to say, the first tangent direction is $\hat{\mathbf{x}}_-^{(1)} = \left(\hat{\mathbf{x}}_{i+1,j} - \hat{\mathbf{x}}_{i,j} + \hat{\mathbf{x}}_{i+1,j+1} - \hat{\mathbf{x}}_{i,j+1}\right)/2$, the second tangent direction is $\hat{\mathbf{x}}_-^{(2)} = \left(\hat{\mathbf{x}}_{i,j+1} - \hat{\mathbf{x}}_{i,j} + \hat{\mathbf{x}}_{i+1,j+1} - \hat{\mathbf{x}}_{i+1,j}\right)/2$, and the normal vector is $\hat{\mathbf{x}}_-^{(1)} \times \hat{\mathbf{x}}_-^{(2)}$, normalized. (As mentioned in Section 3.2, this average gives the same normal direction as the previous definitions of $\hat{\mathbf{x}}_-^{(1)}$ and $\hat{\mathbf{x}}_-^{(2)}$.)

In general, then, a single box in a p-torus has 2^p vertices, and the p tangent directions are averages. Let $\mathcal{V}$ be the vertices of a box,

$$\mathcal{V} = \left\{\hat{\mathbf{x}}_{j_1,j_2,\ldots,j_p}\right\}, \tag{5.1}$$

where each j_k ranges from i_k to $i_k + 1$, forming the 2^p vertices.

This box defines q numbers in the function that should be set to zero in the orthogonality condition. In other words, the orthogonality condition with a box scheme in *any* dimension gives a set of equations of the form of Equation (3.3), where $\hat{\mathbf{x}}_{1/2}$ and $Q_{1/2}$ represent the position and set of normal vectors respectively at the center of the box.

Calculating the position at the center of the box is a straightforward averaging of all the vertices and evaluation of the vector field at that point. The normal vectors are trickier.

Let $\mathbf{y}_k$ and $\mathbf{z}_k$ be the sums of all vertices with i_k+1 and i_k respectively in the kth position, that is

$$\mathbf{y}_k = \sum \{\mathbf{x} \in \mathcal{V} \quad | \quad \mathbf{x} = \hat{\mathbf{x}}_{\bullet,\bullet,\ldots,i_k+1,\ldots,\bullet}\}, \tag{5.2}$$

$$\mathbf{z}_k = \sum \{\mathbf{x} \in \mathcal{V} \quad | \quad \mathbf{x} = \hat{\mathbf{x}}_{\bullet,\bullet,\ldots,i_k,\ldots,\bullet}\}, \tag{5.3}$$

where the i_k+1 or i_k occur in the kth position. Then a set of approximate tangent directions at the center of the box lies in the columns of W, where

$$W = \begin{pmatrix} \mathbf{y}_1 - \mathbf{z}_1 & \mathbf{y}_2 - \mathbf{z}_2 & \cdots & \mathbf{y}_p - \mathbf{z}_p \end{pmatrix}. \tag{5.4}$$

Now the task is to use W to extract normal vectors in such a way that the resulting set of normal vectors move smoothly over all possible W's. One possible way to achieve this is to use information from the original normal vectors, $\overline{Q}$.

Moore actually opts for a quasi-Newton iteration on a tangency condition [29], so his method does not require an explicit computation of the Q's during the convergence process. Any method based on the orthogonality condition must nevertheless generate a new set of $\overline{Q}$'s *after* convergence, so Moore proposes a method for generating a smooth, moving basis for the normal space based on the "orthogonal Procrustes problem."

Essentially, this method requires a rotation from the baseline normal vectors, $\overline{Q}$, into the updated normal vectors, Q, by means of orthogonal matrices, subject to norm-minimization constraints. The constraint at each point, $i_1, i_2, \ldots, i_p$, is to minimize

$$\sum_{k=1}^{p} \left\| \overline{Q}_{i_1,i_2,\ldots,i_p} Q_{i_1,i_2,\ldots,i_p} - \overline{Q}_{i_1-1,i_2,\ldots,i_k-1,\ldots,i_p} \right\|^2 \cdot \left\| \overline{Q}_{i_1,i_2,\ldots,i_p} Q_{i_1,i_2,\ldots,i_p} - \overline{Q}_{i_1,i_2,\ldots,i_k+1,\ldots,i_p} \right\|^2, \tag{5.5}$$

where $Q_{i_1,i_2,\ldots,i_p}$ is an orthogonal matrix, and all the $\overline{Q}$'s have columns that span the orthogonal complement of their respective normal spaces. Gauss-Seidel iteration on this constraint converges to a smooth, moving system of normal vectors. See [15] for an explanation of the general orthogonal Procustes problem.

This method would be capable of generating the Q's, but the following approach seems more natural and may require less computation.

Let $\overline{Q}$ be the sum of all the $\overline{Q}$'s associated with the vertices in $\mathcal{V}$,

$$\overline{Q}_{1/2} = \sum_{\hat{\mathbf{x}}_{j_1,j_2,\ldots,j_p} \in \mathcal{V}} \overline{Q}_{j_1,j_2,\ldots,j_p}. \tag{5.6}$$

As long as none of the columns of $\overline{Q}_{1/2}$ lie in the image of W, then the operator $\begin{pmatrix} W & \overline{Q} \end{pmatrix}$ is non-singular.

Orthonormalizing the columns of the operator therefore gives a splitting into the tangent and normal spaces. A standard QR decomposition yields,

$$\begin{pmatrix} W & \overline{Q}_{1/2} \end{pmatrix} = UR = \begin{pmatrix} T & Q_{1/2} \end{pmatrix} R, \tag{5.7}$$

where W is as in Equation (5.4), $\overline{Q}_{1/2}$ is as in Equation (5.6), R is upper-triangular with positive diagonal entries, U is unitary (orthogonal in the real case), and the first p columns of U (*i.e.*, T) span the tangent space, while the last q columns (*i.e.*, $Q_{1/2}$) span the normal space.

Note that this calculation of $Q_{1/2}$ yields a smooth moving set over the whole torus, subject to closeness constraints. A multi-step process implements Equation (3.3) in each box:

Algorithm 5.1 *Applying orthogonality condition*

1. Calculate the average $\hat{\mathbf{x}}_{1/2}$ at the center of the box by averaging all the vertices of the box.

2. Calculate $\mathbf{\Phi}\left(\hat{\mathbf{x}}_{1/2}, \lambda\right)$.

3. Calculate the tangent vectors using Equation (5.4), and calculate the average normal vectors using Equation (5.6).

4. Perform a QR decomposition as in Equation (5.7) to get Q, the normal vectors at the center of the box.

5. The projection $\mathbf{\Phi}\left(\hat{\mathbf{x}}, \lambda\right)^T Q_{1/2} = \mathbf{0}$ gives q equations at each box.

The "biased" QR decomposition used to calculate Q may also provide an updated $\overline{Q}$ for a new λ value after convergence. For example, consider the point $\overline{\mathbf{x}}_{i_1,i_2,\ldots,i_p}$ with normal vectors $\overline{Q}_{i_1,i_2,\ldots,i_p}$, and let $\hat{\mathbf{x}}$ be the updated torus that satisfies the orthogonality condition. To get the new normal vectors, it is necessary to construct new tangent vectors at $\overline{\mathbf{x}}_{i_1,i_2,\ldots,i_p}$ using – among other possibilities – center differences:

$$W = \begin{pmatrix} \left(\hat{\mathbf{x}}_{i_1+1,i_2,\ldots,i_p} - \hat{\mathbf{x}}_{i_1-1,i_2,\ldots,i_p}\right) & \cdots & \left(\hat{\mathbf{x}}_{i_1,i_2,\ldots,i_p+1} - \hat{\mathbf{x}}_{i_1,i_2,\ldots,i_p-1}\right) \end{pmatrix}, \tag{5.8}$$

then the updated normals come from a QR decomposition just as in Equation (5.7),

$$\begin{pmatrix} W & \overline{Q}_{i_1,i_2,\ldots,i_p} \end{pmatrix} = \begin{pmatrix} T & Q_{i_1,i_2,\ldots,i_p} \end{pmatrix} R$$
$$\overline{Q}_{i_1,i_2,\ldots,i_p} \leftarrow Q_{i_1,i_2,\ldots,i_p}. \tag{5.9}$$

It is now possible to write down the algorithm for a general p-torus in $\mathbb{R}^n$.

Algorithm 5.2 *Continuing T^p in $\mathbb{R}^n$.*

1. Start with a given λ, and a discrete $\overline{\mathbf{x}}$ and $\overline{Q}$ as above.

2. Obtain $q \cdot N_1 \cdot N_2 \cdots N_p$ equations using Algorithm 5.1.

3. Solve the equations using Newton's method with a numerically approximated Jacobian. The unknowns are the individual components of the $\mathbf{r}$'s

4. Upon convergence, if this is the final value of λ, stop the algorithm.

5. Otherwise, update $\lambda = \lambda + \Delta\lambda$, and set $\overline{\mathbf{x}} = \hat{\mathbf{x}}$ (or some other guess)

6. If desired, re-distribute the points in $\overline{\mathbf{x}}$.

7. Re-compute the $\overline{Q}$'s using the QR decomposition technique in Equations (5.8) and (5.9). If the points have been re-distributed, then make sure that the old normal vectors, $\overline{Q}$, are close enough that the QR decomposition technique is still valid.

8. Return to Step 1

5.2 Numerical Issues

In Algorithms 3.1 and 3.2, the most time-consuming task is generating the Jacobian for use in Newton's method iterations. This is true for Algorithm 5.2 as well in the case of two-tori embedded in lower-dimensional real spaces.

For higher-dimensional tori and tori with very large codimensions, however, the actual solution of the linear system takes more time than the generation of the Jacobian. In addition, the system grows to a size that makes it impractical to fill in large portions of the Jacobian during the course of the solution. It is therefore necessary to use creative solution techniques that sacrifice computational efficiency in order to save memory.

Consider, for example, the equations and Jacobian matrices involved in the continuation of a p-torus in $\mathbb{R}^n$, with points $N_1, N_2, \ldots, N_p$ in each respective direction. Let $\mathbf{f}$ be a vector containing the quantities to be set to zero, and let the points of the torus be ordered lexicographically according $i_p, i_{p-1}, \ldots, i_1$. (See the definition of $\mathbf{f}$ below.) If one arbitrarily associates the box with vertices $\mathcal{V}$ in Equation (5.1) with

the numbering $i_1, i_2, \ldots, i_p$, just to have some ordering on $\mathbf{f}$, then $\mathbf{f}$ looks like

$$\mathbf{f} = \begin{pmatrix} \left(\mathbf{\Phi}\left(\hat{\mathbf{x}}, \lambda\right)^T Q\right)(1,1,\ldots,1,1) \\ \left(\mathbf{\Phi}\left(\hat{\mathbf{x}}, \lambda\right)^T Q\right)(1,1,\ldots,1,2) \\ \vdots \\ \left(\mathbf{\Phi}\left(\hat{\mathbf{x}}, \lambda\right)^T Q\right)(1,1,\ldots,2,1) \\ \left(\mathbf{\Phi}\left(\hat{\mathbf{x}}, \lambda\right)^T Q\right)(1,1,\ldots,2,2) \\ \vdots \\ \left(\mathbf{\Phi}\left(\hat{\mathbf{x}}, \lambda\right)^T Q\right)(N_1, N_2, \ldots, N_p) \end{pmatrix}, \tag{5.10}$$

where the index in parentheses sets the box, $\hat{\mathbf{x}}$ is the average of the vertices of the box, and Q comes from Equation (5.7) applied to the box.

Each line constitutes q equations, for a total of $q \cdot N_1 \cdot N_2 \cdots N_p$. The corresponding unknowns are the radial coordinates, $\mathbf{r}_{i_1,i_2,\ldots,i_p}$. For future reference, let

$$\mathbf{r} = \begin{pmatrix} \left(\mathbf{r}_{1,1,\ldots,1}\right)^T & \left(\mathbf{r}_{1,1,\ldots,2}\right)^T & \cdots & \left(\mathbf{r}_{N_1,N_2,\ldots,N_p}\right)^T \end{pmatrix}^T. \tag{5.11}$$

If J is the Jacobian,

$$J = \begin{pmatrix} \partial\mathbf{f}/\partial(r_1)_{1,1,\ldots,1} & \partial\mathbf{f}/\partial(r_2)_{1,1,\ldots,2} & \cdots & \partial\mathbf{f}/\partial(r_q)_{N_1,N_2,\ldots,N_p} \end{pmatrix}, \tag{5.12}$$

then the system of equations to be solved at each Newton iteration is $J\mathbf{y} = -\mathbf{f}$. A simple forward-difference in each $\mathbf{r}$ component gives a reasonable numerical approximation of the Jacobian.

Each box of the torus depends on 2^p different vertices, each of which can move in q directions. Thus, each row or column of the Jacobian contains at most $q \cdot 2^p$ nonzero entries, and the whole Jacobian contains at most $q^2 \cdot 2^p \cdot N_1 \cdot N_2 \cdots N_p$ nonzero entries.

Moreover, the nonzero entries are well-organized. The overall structure of the Jacobian is periodic block bi-diagonal as in Definition 3.7, where now each block is itself periodic block bi-diagonal, and so on to p nested levels of the structure. The lowest block structure comprises full square components that are q elements on a side.

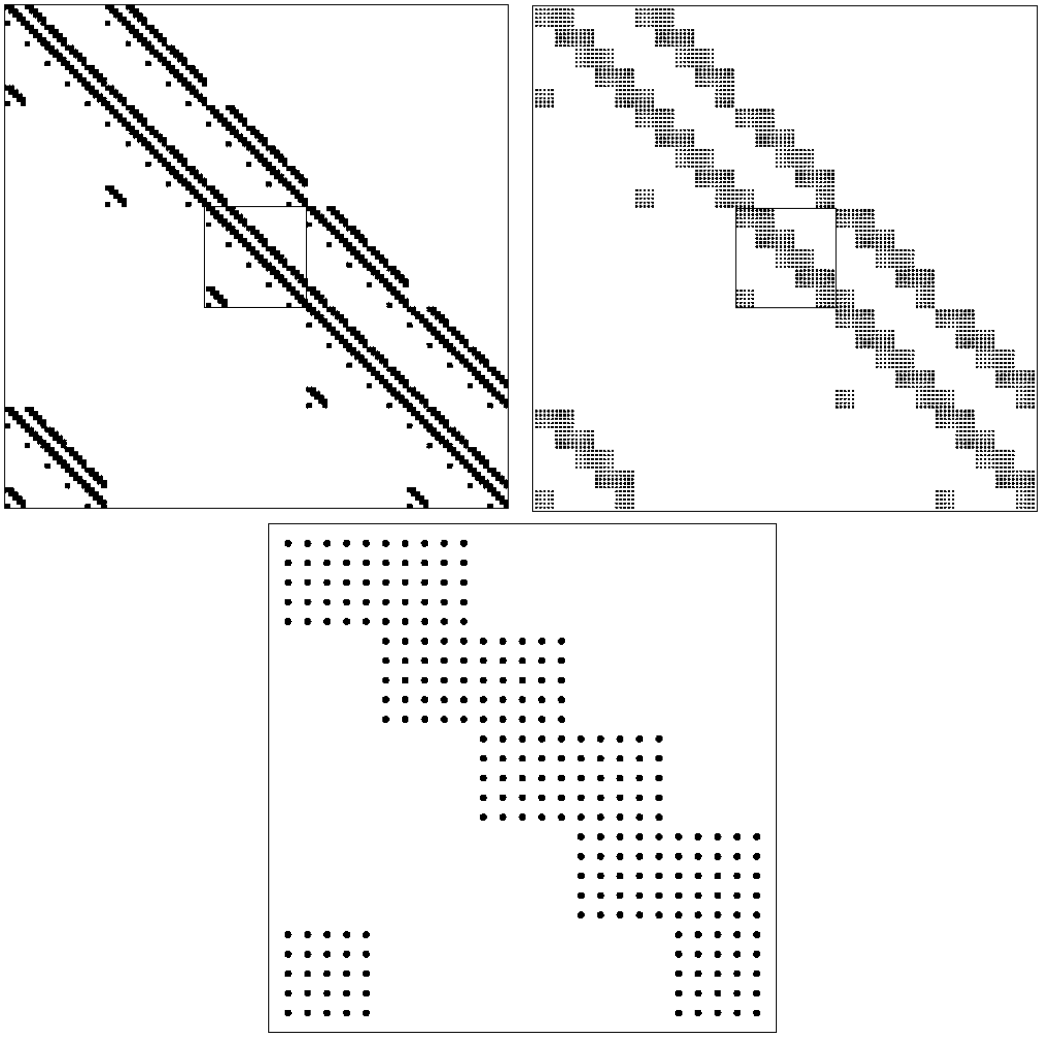

Figure 5.1: Sparsity Plots of Jacobian

Figure 5.1 shows the sparsity structure of a $5 \times 5 \times 5$ three-torus in $\mathbb{R}^8$. The box in each picture indicates the zoom region for the next picture.

As mentioned in previous sections, it is not at all easy to tell whether the Jacobian is well-conditioned in higher-dimensional cases. The conditioning may depend on several factors, including the number of points used and whether the torus has any invariant sub-manifolds.

Even if the Jacobian has a well-understood sparsity pattern and is well-conditioned, it is still not obvious how to solve $J\mathbf{y} = -\mathbf{f}$. The main constraint on direct

solution methods is not computation time, but rather memory.

Consider, for example, a solution technique that operates on the highest level blocks (the A's and B's). The periodic, block bi-diagonal sparsity pattern of the Jacobian indicates that some sort of block Gaussian elimination would be the fastest way to solve the system. Algorithm 5.3 shows how to accomplish this without pivoting.

Algorithm 5.3 *Solving the system* $J\mathbf{y} = \mathbf{f}$.

- *Simultaneously form two items in a loop:*

$$C = I - (-1)^{N_1} B_{N_1}^{-1} A_{N_1} B_{N_1-1}^{-1} A_{N_1-1} \cdots B_1^{-1} A_1, \text{ and} \tag{5.13}$$

$$\tilde{\mathbf{f}} = B_{N_1}^{-1}\mathbf{f}_{N_1} - B_{N_1}^{-1} A_{N_1} B_{N_1-1}^{-1}\mathbf{f}_{N_1-1} + \ldots + (-1)^{N_1} B_{N_1}^{-1} A_{N_1} B_{N_1-1}^{-1} \cdots A_2 B_1^{-1}\mathbf{f}_1. \tag{5.14}$$

- *Solve* $C\mathbf{y}_1 = \tilde{\mathbf{f}}$. *Condition I of Proposition 3.3 guarantees that this is numerically well-scaled and well-conditioned.*

- *Substitute forward. For* $i = 1, 2, \ldots, N_1 - 1$, *calculate* $\mathbf{y}_{i+1} = B_i^{-1} A_i \mathbf{y}_i$.

(This algorithm can form the long products in Equations (5.13) and (5.14) recursively, if desired.)

Unfortunately, each one of the blocks A_i and B_i has a full inverse. The total number of elements in any given block is $(q \cdot N_2 \cdot N_3 \cdots N_p)^2$, a number that is potentially much larger than the number of nonzero elements in the whole Jacobian. Thus, any viable solution technique cannot fill too many blocks, lest the computer run out of memory. Pivoting, either block or scalar, is therefore impossible, and Algorithm 5.3 represents the only known direct solution technique that satisfies memory constraints for reasonably large three-tori because in practice it only requires two full blocks.

Scaling presents an even more imposing barrier for direct solution techniques. If, for $i = 1, 2, \ldots, N_p$, $\left\|A_i^{-1} B_i\right\| \gg 1$, $\left\|B_i^{-1} A_i\right\| \gg 1$, and N_p is large then the Gaussian

elimination produces poorly-scaled chains of operators. Poor scaling also diminishes the estimate of the inverse norm given in Proposition 3.3.

Iterative methods therefore promise to be superior to direct methods when they are available. Numerical experimentation has shown that the Generalized Minimum Residual algorithm (GMRES) works well for this particular system, *if* it receives a good pre-conditioner. (In this thesis, the term "residual" refers to the quantity, $\|J\mathbf{y} - \mathbf{f}\|$.)

Recall that a pre-conditioner is a matrix, M, that modifies the system to make it more amenable to the particular iterative technique used to solve it. In particular, if the original system is $J\mathbf{y} = \mathbf{f}$, then the pre-conditioned system is $M^{-1}J\mathbf{y} = M^{-1}\mathbf{f}$. The pre-conditioner should be chosen in such a way that solving systems with M is relatively easy and $M^{-1}J$ is "close" to the identity. Unfortunately, what constitutes closeness is not always clear. The field of iterative solution techniques is well-developed, and multiple references [4, 15, 16] discuss the GMRES algorithm and pre-conditioners.

The choice of pre-conditioner is not obvious. If Condition I of Proposition 3.3 holds, and if the bounds m and n in the proposition are not too large, then a reasonable pre-conditioner is

$$M = \begin{pmatrix} 0 & B_1 & 0 & \cdots & 0 \\ 0 & 0 & B_2 & \cdots & 0 \\ \vdots & \vdots & \ddots & \vdots & \vdots \\ 0 & 0 & \cdots & 0 & B_{N_1-1} \\ B_{N_1} & 0 & \cdots & 0 & 0 \end{pmatrix}. \tag{5.15}$$

As the continuation process moves along, the operators $B_i^{-1}A_i$ typically grow larger in norm, the pre-conditioner loses its effectiveness and GMRES ceases to converge. When that happens, a direct solution technique such as the one in Algorithm 5.3 is necessary. Section 5.5 contains an example of where standard decompositions

fail and it becomes necessary to use both GMRES and Algorithm 5.3. Numerical experimentation shows that GMRES with the pre-conditioner in Equation (5.15) works well for a while, but it breaks down before Algorithm 5.3, which necessitates using the direct solution technique after a certain parameter value.

Other iterative techniques do not seem to work as well as GMRES. Some of the iterations tried during the course of numerical experiments include Gauss-Seidel, Jacobi, Successive Over-Relaxation, Bi-Conjugate Gradient, and Stabilized Bi-Conjugate Gradient [16] – all in straight or block form, and with many different pre-conditioners.

One should note finally that the pre-conditioner in Equation (5.15) and the method of Algorithm 5.3 apply best when the Jacobian satisfies Condition I of Proposition 3.3. If the Jacobian satisfies Condition II, then there is an analogous pre-conditioner and direct substitution algorithm.

5.3 General Method Applied to Two-Torus in $\mathbb{R}^4$

One very common example in the literature of a two-torus embedded in $\mathbb{R}^4$ is a system of two strongly coupled oscillators [7, 10, 29, 35],

$$\begin{aligned}
\dot{x}_1 = &\quad \alpha x_2 + x_1\left(1 - x_1^2 - x_2^2\right) - \lambda\left(x_1 + x_2 - x_3 - x_4\right) \\
\dot{x}_2 = &-\alpha x_1 + x_2\left(1 - x_1^2 - x_2^2\right) - \lambda\left(x_1 + x_2 - x_3 - x_4\right) \\
\dot{x}_3 = &\quad \alpha x_4 + x_3\left(1 - x_3^2 - x_4^2\right) + \lambda\left(x_1 + x_2 - x_3 - x_4\right) \\
\dot{x}_4 = &-\alpha x_3 + x_4\left(1 - x_3^2 - x_4^2\right) + \lambda\left(x_1 + x_2 - x_3 - x_4\right),
\end{aligned} \tag{5.16}$$

where $\alpha > 0$ is fixed. For comparison to previous studies, let $\alpha = 0.55$.

At $\lambda = 0$, the system consists of two uncoupled, planar oscillators that trivially form a torus. Each oscillator comprises an attracting periodic orbit of unit radius and period $2\pi/\alpha$. As λ increases, the torus is still globally attracting, but two independent periodic orbits appear on its surface: one attracting, the other repelling. This is easy to observe by breaking down the coupling in Equation (5.16).

If $x_1 = x_3$, and $x_2 = x_4$, then the coupling terms are zero, and there is a single periodic orbit that descends from

$$\begin{aligned} \dot{x}_1 = &\quad \alpha x_2 + x_1\left(1 - x_1^2 - x_2^2\right) \\ \dot{x}_2 = &-\alpha x_1 + x_2\left(1 - x_1^2 - x_2^2\right). \end{aligned} \tag{5.17}$$

Thus, the plane defined by $x_1 = x_3$ and $x_2 = x_4$ contains an attracting periodic orbit of unit radius. Similarly, if $x_1 = -x_3$, and $x_2 = -x_4$, then the coupling terms reduce to $2\lambda(x_1 + x_2)$, and there is a single, repelling periodic orbit that descends from

$$\begin{aligned} \dot{x}_1 = &\quad \alpha x_2 + x_1\left(1 - x_1^2 - x_2^2\right) - 2\lambda(x_1 + x_2) \\ \dot{x}_2 = &-\alpha x_1 + x_2\left(1 - x_1^2 - x_2^2\right) - 2\lambda(x_1 + x_2). \end{aligned} \tag{5.18}$$

Thus, the plane defined by $x_1 = -x_3$ and $x_2 = -x_4$ contains a repelling periodic orbit of unit radius, and – given the difficulties of Section 4.2.3 – it pays to be cautious about the discretization.

The second periodic orbit develops fixed points at $\lambda = \alpha/2$, but the torus actually breaks down before that when it loses its attractivity at $\lambda \approx 0.2605$ [11, 35]. See [1] for a full analysis of this problem for various values of α.

Algorithm 5.2 applies directly to this continuation problem. The initial $\overline{\mathbf{x}}$ at $\lambda = 0$ is the obvious

$$\overline{\mathbf{x}}\left((\phi_1)_i, (\phi_2)_j\right) = \overline{\mathbf{x}}_{i,j} = \begin{pmatrix} \cos(\phi_1)_i & \sin(\phi_1)_i & \cos(\phi_2)_j & \sin(\phi_2)_j \end{pmatrix}^T, \tag{5.19}$$

and the initial normal vectors are

$$\overline{Q}_{i,j} = \begin{pmatrix} \cos(\phi_1)_i & \sin(\phi_1)_i & 0 & 0 \\ 0 & 0 & \cos(\phi_2)_j & \sin(\phi_2)_j \end{pmatrix}^T, \tag{5.20}$$

where, as usual, $(\phi_1)_i = 2\pi(i-1)/N_i$ and $(\phi_2)_j = 2\pi(j-1)/N_j$.

At first glance, it seems that the method might not work well for this torus because it is entirely composed of periodic orbits at $\lambda = 0$, and the method in the two special

cases analyzed in Chapter 4 does not seem to adapt well to tori with closed sub-invariants. Fortunately, the method is well-conditioned initially, and the only problem comes about when the discretization lines up at positive λ values with at least one of the two planar periodic orbits described above. The stable behavior at $\lambda = 0$ is probably due to the non-genericity of most of the periodic orbits, since all but two of them disappear for $\lambda > 0$.

The method is sensitive to the choice of number of discretization points according to the following observations:

1. If N_i and N_j are both even, then the Jacobian is generally ill-conditioned at $\lambda = 0$.

2. If $N_i = N_j$ and both are odd, then the Jacobian is well-conditioned at first, but then grows to a very large number for the first iteration at $\lambda > 0$ (order 10^{11} for a 45×45 torus).

3. if $N_i = N_j \pm 1$, then the Jacobian is generally well-conditioned, and the method has no problem continuing the torus to bifurcation.

The first observation is probably related to the already observed ill-conditioning in the method for an even-even two-torus in $\mathbb{R}^3$. Proving that even numbers induce multiple solutions in the general algorithm would be extremely complicated, since the cross product and all its elegant derivative properties are no longer available, but the general idea should be the same.

The second observation is probably related to the difficulties encountered in the example of Section 4.2.3. If $N_i = N_j$, then the grid lines up exactly along at least one of the two periodic orbits described in Equations (5.17) and (5.18). One simple way to prevent this is to choose N_i to be slightly different from N_j, which explains the third observation.

Table 5.1: Continuation Steps for Directly Coupled Oscillators

λ Range	$\Delta\lambda$
0.0–0.25	0.05
0.251–0.255	0.001
0.2555–breakdown	0.0005

The Jacobian during the Newton iterations is periodic block bi-diagonal. Each sub-block is periodic block bi-diagonal with full 2×2 blocks. Thus, the Jacobian is $2N_iN_j \times 2N_iN_j$ with $16N_iN_j$ possible nonzero entries, and each high-level block contains $4N_j^2$ entries when full. This memory requirement is well within the reach of standard direct solution techniques and condition number estimators for the required N_i's and N_j's, so there is no need to resort to the more complicated techniques outlined in Section 5.2.

As with the two-tori in $\mathbb{R}^3$, computation time is minimal. The largest expense is the generation of the Jacobian, and much of this is probably due to the use of `Matlab` instead of a lower-level language to perform all of the local (and hence looped) derivative approximations.

Practice has shown that for a 45×46 torus, a good correction strategy is to re-distribute according to arc length along each longitude (*i.e.*, sections of the form $\overline{\mathbf{x}}_{i,t}$, where t is constant), and then independently re-distribute along each meridian. The strategy is best applied after convergence, up through $\lambda = 0.25$, with no re-distribution before the iterations at $\lambda = 0$. After $\lambda = 0.25$, the torus does not undergo any further re-distribution. Table 5.1 shows how $\Delta\lambda$ decreases as the torus approaches breakdown.

Figures 5.2 and 5.3 show the continuation process from $\lambda = 0.0$ to $\lambda = 0.2605$. In each figure, the vertical axis is artificial and represents a sweep in either ϕ_1 or ϕ_2. Figures for $\lambda \leq 0.25$ show the result at convergence, but before re-distribution.

Figures 5.4 and 5.5 show essentially the same information with the intersections of

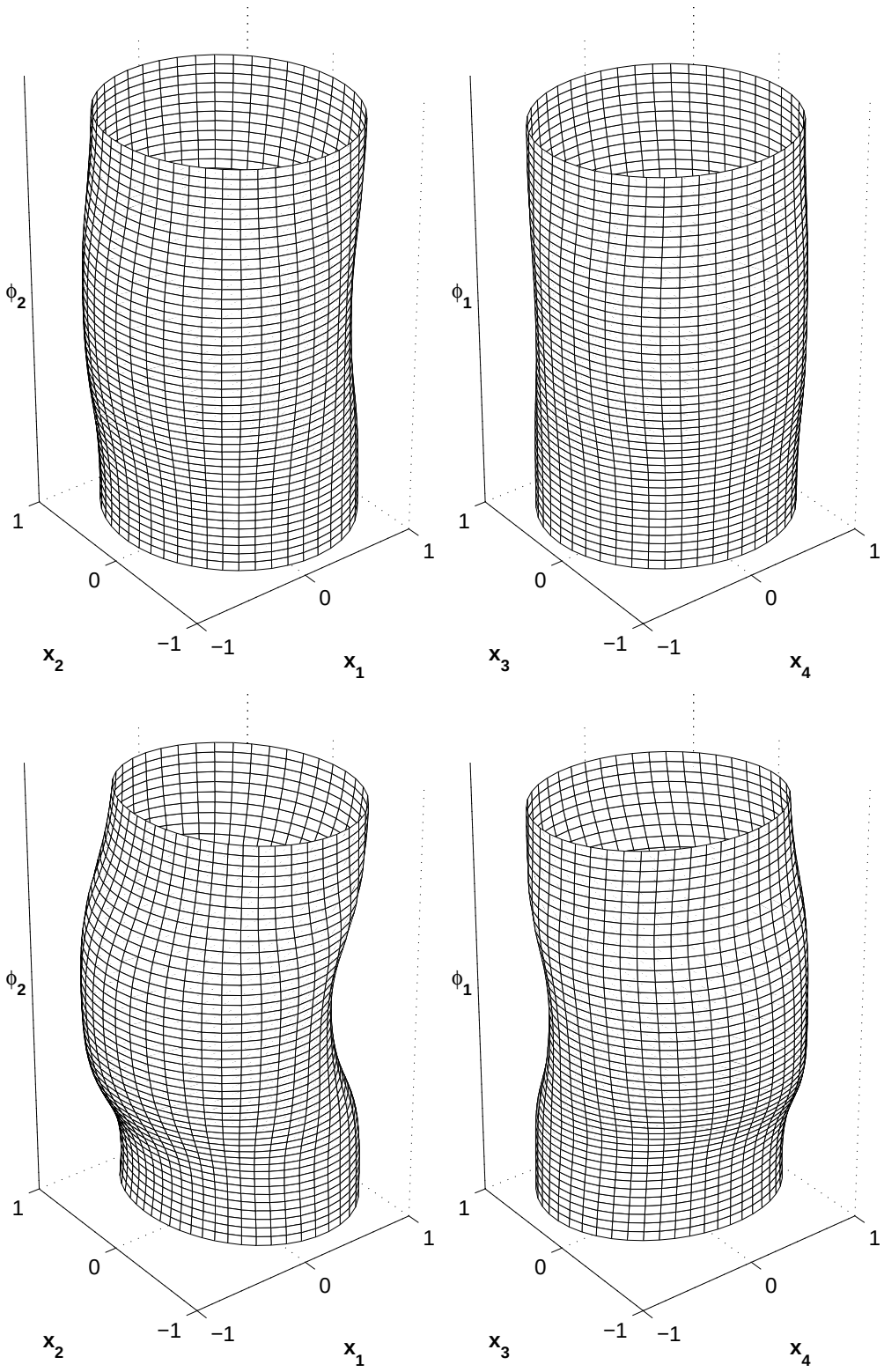

Figure 5.2: Directly Coupled Oscillators; $\lambda = 0.1$ (top) and 0.2

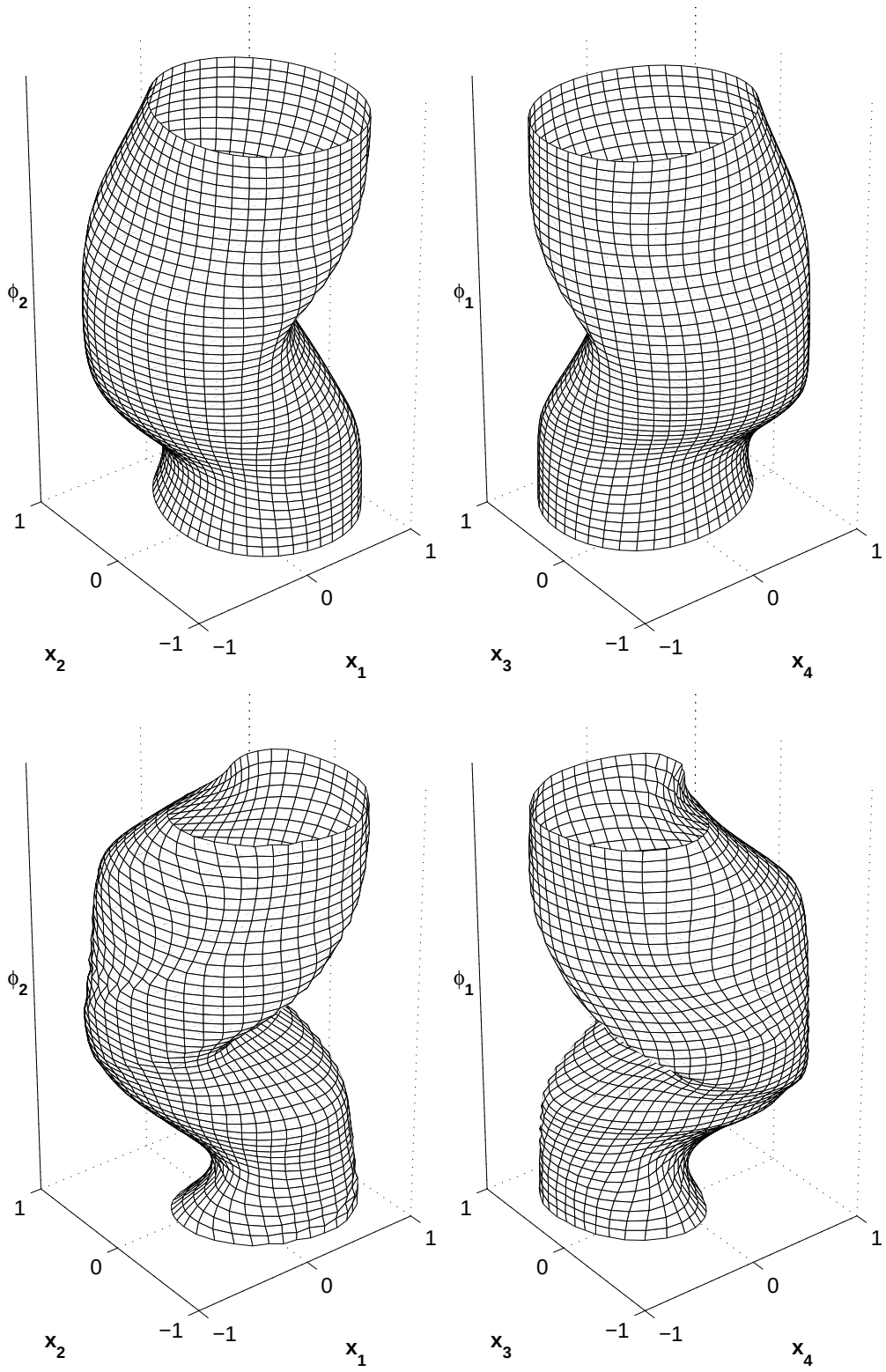

Figure 5.3: Directly Coupled Oscillators; $\lambda = 0.25$ (top) and 0.2605

two hyperplanes highlighted. The solid line corresponds to the $x_1 = x_3$ and $x_2 = x_4$ plane, so it should indicate the stable periodic orbit outlined in Equation (5.17). Similarly, the dashed line corresponds to the $x_1 = -x_3$ and $x_2 = -x_4$ plane, so it should indicate the unstable periodic orbit outlined in Equation (5.18).

Calculating the planar intersections is not itself a simple task. The strategy used to generate the lines on Figures 5.4 and 5.5 is three-fold:

- Find grid lines where the desired plane intersects the torus.
- Calculate two linear interpolation coefficients, one based on $\hat{x}_1 \pm \hat{x}_3$, and the other based on $\hat{x}_2 \pm \hat{x}_4$ (where the sign depends on the plane).
- Use the average of those two coefficients to place a point on the plot.

For example, let $\hat{\mathbf{x}}_{i,j}$ and $\hat{\mathbf{x}}_{i+1,j}$ be two points such that $(\hat{\mathbf{x}}_1)_{i,j} - (\hat{\mathbf{x}}_3)_{i,j}$ and $(\hat{\mathbf{x}}_1)_{i+1,j} - (\hat{\mathbf{x}}_3)_{i+1,j}$ are of opposite sign, and $(\hat{\mathbf{x}}_1)_{i,j} - (\hat{\mathbf{x}}_3)_{i,j}$ and $(\hat{\mathbf{x}}_1)_{i+1,j} - (\hat{\mathbf{x}}_3)_{i+1,j}$ are of opposite sign as well. Then the assumption is that there is a point in the $x_{1,3} = x_{2,4}$ plane on the grid line connecting the two points.

The two coefficients are

$$s_1 = \left((\hat{x}_1)_{i,j} - (\hat{x}_3)_{i,j}\right) / \left[\left((\hat{x}_1)_{i,j} - (\hat{x}_3)_{i,j}\right) - \left((\hat{x}_1)_{i+1,j} - (\hat{x}_3)_{i+1,j}\right)\right], \text{ and} \quad (5.21)$$

$$s_2 = \left((\hat{x}_2)_{i,j} - (\hat{x}_4)_{i,j}\right) / \left[\left((\hat{x}_2)_{i,j} - (\hat{x}_4)_{i,j}\right) - \left((\hat{x}_2)_{i+1,j} - (\hat{x}_4)_{i+1,j}\right)\right]. \quad (5.22)$$

The average, $s = (s_1 + s_2)/2$, is the actual coefficient used, so the point to be plotted is $(1 - s)\,\hat{\mathbf{x}}_{i,j} + s\hat{\mathbf{x}}_{i+1,j}$.

Unfortunately, the intersection between the $x_{1,3} = -x_{2,4}$ plane and the torus seems to become non-transverse at breakdown, so only a few points satisfy the first condition of the interpolation procedure above. The bottom pictures in Figure 5.5 therefore show the discrete points for which the difference between components changes sign.

Table 5.2 shows the entire Newton process for three different parameter values. Even with relatively large step sizes, it is clear that the method is stable.

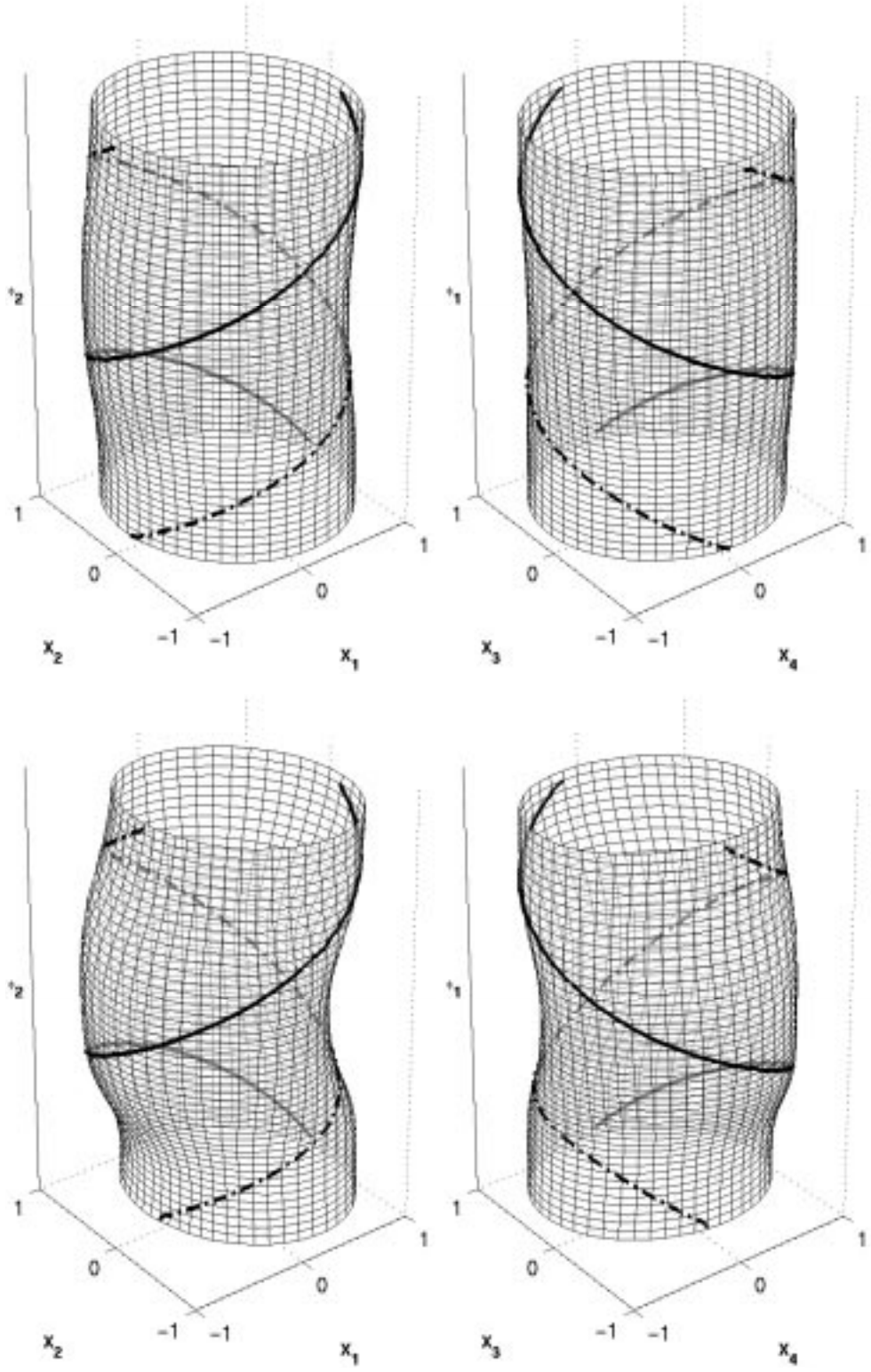

Figure 5.4: Oscillators with Planar Intersections; $\lambda = 0.1$ (top) and 0.2

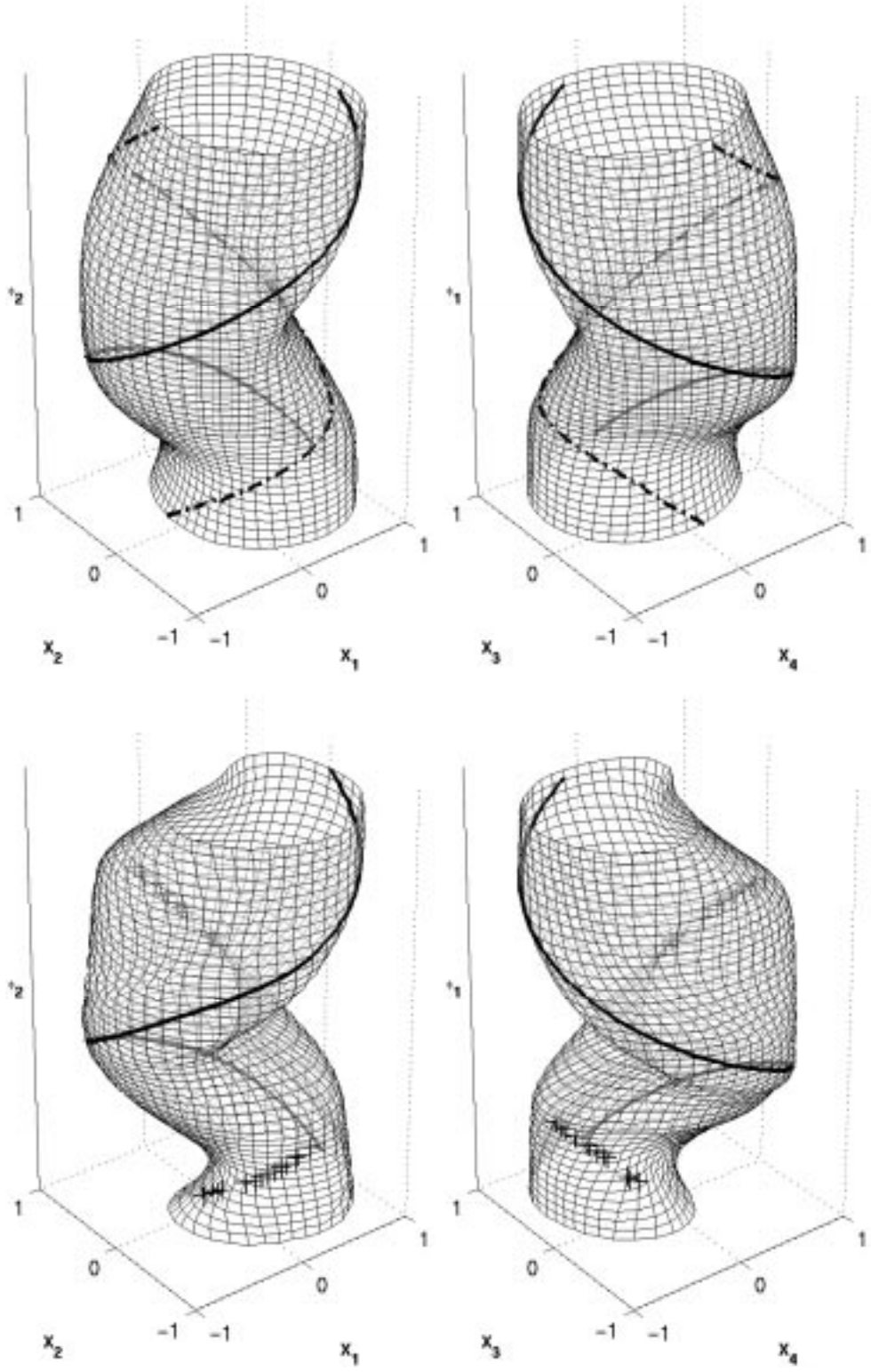

Figure 5.5: Oscillators with Planar Intersections; $\lambda = 0.25$ (top) and 0.2605

Table 5.2: Newton Iteration: Directly Coupled Oscillators

From λ	To λ	Iteration	$\|\mathbf{f}\|$	$\kappa(J)$	$\|\mathbf{y}\|$
0.05	0.1	1	4.8	490	2.6
		2	0.51	510	0.36
		3	0.011	530	0.0072
		4	5.0×10^{-6}	520	2.9×10^{-6}
			9.9×10^{-13}		
0.2	0.25	1	3.7	1800	4.1
		2	0.90	6600	2.5
		3	0.61	2.0×10^{5}	1.2
		4	0.19	2.6×10^{5}	0.15
		5	0.0037	2.6×10^{5}	0.0014
		6	1.3×10^{-6}	2.6×10^{5}	9.3×10^{-7}
			2.9×10^{-13}		
0.26	0.2605	1	0.029	3.5×10^{5}	1.2
		2	0.14	5.6×10^{5}	0.29
		3	0.014	5.8×10^{5}	0.045
		4	5.0×10^{-4}	5.8×10^{5}	0.0019
			8.6×10^{-7}		

5.4 Example of a Three-Torus

In order to test a numerical technique properly, it is necessary to develop an example that is comprehensible and direct without being trivial. The example should also be related to a physical application, so that it does not seem contrived and irrelevant. Fortunately, planar oscillators abound in nature, and it is possible to construct a large variety of flow-invariant tori by coupling them together either directly or indirectly. This section describes an instance of the latter case – where planar oscillators influence each other indirectly through a medium that can store potential energy. (The previous section describes an example of direct coupling.)

Such indirect coupling can occur in many applications, with one of the most obvious being multiple systems of mechanical devices coupled through a spring-resistance medium, or RLC circuits coupled through an RC medium. Other applications of this type of system include time-dependent chemical reactions [33] and suspensions of cells

in passive media [32, 33].

Typically, the strength of coupling depends on a parameter, λ, where $\lambda = 0$ indicates a completely uncoupled problem. At $\lambda = 0$, each oscillator exists without any outside effects, and there is an obvious torus. The question of persistence of the torus as the coupling increases is mostly answered in some simple cases [39].

Consider a system of p oscillators, each embedded in dimension m. Let $\dot{\mathbf{x}}_i = \mathbf{\Phi}_i(\mathbf{x}_i)$, $i = 1, 2, \ldots, p$ be p autonomous systems, each with a periodic solution, $\mathbf{y}_i(t)$ with minimal period, τ_i. Let the systems be coupled indirectly through another m-dimensional system, $\dot{\mathbf{x}}_0 = \mathbf{\Phi}_0(\mathbf{x}_0)$. Specifically, let the coupling be

$$\begin{aligned} \dot{\mathbf{x}}_i &= \mathbf{\Phi}_i(\mathbf{x}_i) + \lambda P(\mathbf{x}_0 - \mathbf{x}_i), \qquad i = 1, 2, \ldots, p, \\ \dot{\mathbf{x}}_0 &= \alpha_0 P\left(\frac{1}{p}\sum_{i=1}^{p} \mathbf{x}_i - \mathbf{x}_0\right), \end{aligned} \tag{5.23}$$

where α_0 is a number greater than zero, and P is an $m \times m$ matrix.

At $\lambda = 0$, the oscillators are uncoupled, and the system has an invariant p-torus of the form,

$$\begin{aligned} \mathbf{x}_i &= \mathbf{y}_i(\phi_i) \qquad i = 1, 2, \ldots, p, \\ \mathbf{x}_0 &= \frac{\alpha_0}{p}\sum_{i=1}^{p}\left\{\left(I - e^{-\alpha_0\tau_i P}\right)^{-1}\int_0^{\tau_i} e^{\alpha_0(s-\tau_i)P}\mathbf{y}_i(\phi_i + s)\,ds\right\}, \end{aligned} \tag{5.24}$$

where $\boldsymbol{\phi} = (\phi_1, \phi_2, \ldots, \phi_p)$ is any set of periodic coordinates parameterizing the p-torus. See [39] for a derivation of Equation (5.24).

The following analysis assumes three conditions about the system in Equation (5.23):

- The vector fields, $\mathbf{\Phi}_i$, are at least three times continuously differentiable,
- The eigenvalues of P have positive real parts, and
- Each system $\dot{\mathbf{x}}_i = D\mathbf{\Phi}(\mathbf{y}_i)\,\mathbf{x}_i$ has 1 as a simple multiplier, with the remaining multipliers having modulus less than 1.

Under these conditions, Watanabe and Othmer [39] have proven that the invariant torus persists for sufficiently small $\lambda > 0$. Actually, their proof is more general, as this is just a special case in a class of persistent flow-invariant tori [34, 39, 40].

Now the task is to construct a three-torus embedded in $\mathbb{R}^8$ using the information above. Let P be the identity and $\alpha_0 = 1$. Three simple oscillators in the form of Equation (4.19) will do. That equation, with slightly different notation, is given by Equation (5.17).

If ϕ is a standard angular coordinate, then the periodic solutions of Equation (5.17) are $\mathbf{x}(\phi) = \sqrt{\alpha}\,(\cos\phi, \sin\phi)$. The following eight-equation vector field therefore admits an invariant three-torus at $\lambda = 0$:

$$\begin{aligned}
\dot{x}_1 &= x_1 - x_2 - x_1\left(x_1^2 + x_2^2\right) + \lambda\,(x_7 - x_1)\\
\dot{x}_2 &= x_1 + x_2 - x_2\left(x_1^2 + x_2^2\right) + \lambda\,(x_8 - x_2)\\
\dot{x}_3 &= x_3 - x_4 - x_3\left(x_3^2 + x_4^2\right) + \lambda\,(x_7 - x_3)\\
\dot{x}_4 &= x_3 + x_4 - x_4\left(x_3^2 + x_4^2\right) + \lambda\,(x_8 - x_4)\\
\dot{x}_5 &= x_5 - x_6 - x_5\left(x_5^2 + x_6^2\right) + \lambda\,(x_7 - x_5)\\
\dot{x}_6 &= x_5 + x_6 - x_6\left(x_5^2 + x_6^2\right) + \lambda\,(x_8 - x_6)\\
\dot{x}_7 &= (x_1 + x_3 + x_5)\,/3 - x_7\\
\dot{x}_8 &= (x_2 + x_4 + x_6)\,/3 - x_8.
\end{aligned} \tag{5.25}$$

Equation (5.24) gives the exact solution of the torus (in component form), at $\lambda = 0$ in standard angular coordinates $\boldsymbol{\phi} = (\phi_1, \phi_2, \phi_3)$ as

$$\begin{aligned}
\mathbf{x}(\boldsymbol{\phi}) = \Big(&\cos\phi_1\ ,\ \sin\phi_1\ ,\ \cos\phi_2\ ,\ \sin\phi_2\ ,\ \cos\phi_3\ ,\ \sin\phi_3\ ,\\
&\frac{1}{6}\sum_{i=1}^{3}(\cos\phi_i + \sin\phi_i)\ ,\ \frac{1}{6}\sum_{i=1}^{3}(-\cos\phi_i + \sin\phi_i)\Big).
\end{aligned} \tag{5.26}$$

The system of Equation (5.25) satisfies the three conditions mentioned above, so the torus persists for sufficiently small $\lambda > 0$.

Now that the existence and form of the torus is established, the next task is to compute a smooth, moving, orthonormalized system of normal vectors at $\lambda = 0$. Three vectors are obvious. They are

$$\begin{aligned}
\mathbf{n}_1(\boldsymbol{\phi}) &= \begin{pmatrix} \cos\phi_1 & \sin\phi_1 & 0 & 0 & 0 & 0 & 0 & 0 \end{pmatrix}^T, \\
\mathbf{n}_2(\boldsymbol{\phi}) &= \begin{pmatrix} 0 & 0 & \cos\phi_2 & \sin\phi_2 & 0 & 0 & 0 & 0 \end{pmatrix}^T, \text{ and} \\
\mathbf{n}_3(\boldsymbol{\phi}) &= \begin{pmatrix} 0 & 0 & 0 & 0 & \cos\phi_3 & \sin\phi_3 & 0 & 0 \end{pmatrix}^T.
\end{aligned} \tag{5.27}$$

The next two normal vectors are more difficult to find. One way to calculate them is to stack the three normal vectors above, together with the derivatives of Equation (5.26) in a matrix, then do Gaussian elimination. This process gives

$$\mathbf{n}_4(\boldsymbol{\phi}) = \begin{pmatrix} \sin\phi_1\mu_1 \\ -\cos\phi_1\mu_1 \\ \sin\phi_2\mu_2 \\ -\cos\phi_2\mu_2 \\ \sin\phi_3\mu_3 \\ -\cos\phi_3\mu_3 \\ 1 \\ 0 \end{pmatrix} \quad \text{and} \quad \mathbf{n}_5(\boldsymbol{\phi}) = \begin{pmatrix} (\nu_1 - \mu_1\xi)\sin\phi_1 \\ (-\nu_1 + \mu_1\xi)\cos\phi_1 \\ (\nu_2 - \mu_2\xi)\sin\phi_2 \\ (-\nu_2 + \mu_2\xi)\cos\phi_2 \\ (\nu_3 - \mu_3\xi)\sin\phi_3 \\ (-\nu_3 + \mu_3\xi)\cos\phi_3 \\ -\xi \\ 1 \end{pmatrix}, \tag{5.28}$$

where the constants represent collections,

$$\mu_i = (\cos\phi_i - \sin\phi_i)/6, \tag{5.29}$$

$$\nu_i = (\cos\phi_i + \sin\phi_i)/6, \text{ and} \tag{5.30}$$

$$\xi = \sum_{i=1}^{3} \mu_i\nu_i \Big/ \left(1 + \sum_{i=1}^{3} \mu_i^2\right). \tag{5.31}$$

The vectors $\mathbf{n}_1$-$\mathbf{n}_5$ in Equations (5.27) and (5.28) form a smooth, orthogonal set of moving vectors that is normal to the graph of the original, uncoupled torus. In practice, one should normalize the last two vectors, $\mathbf{n}_4$ and $\mathbf{n}_5$, so the set will be

orthonormal. It is now possible to apply Algorithm 5.2 to the three torus. Results follow in the next section.

5.5 Numerical Resolution of the Three-Torus

Due to memory constraints, the resolution of the numerical results is not as fine as it is for one- and two-tori in Chapter 4. The following results and analysis come from calculations on a $27 \times 28 \times 29$ torus. Experimentation shows that at least two of the choices of number of discretization points must be odd for the method to have any chance at stability, a result that agrees with the previous conjecture in Section 3.3 that says that least $p - 1$ of the angular directions should have odd numbers of discretization points.

Because the codimension is 5, the number of equation to solve is 1.1×10^5, and the total number of possible nonzero entries in the Jacobian is 4.4×10^6. More importantly, however, each high-level block (A_i or B_i) contains 1.6×10^7 entries, which causes Algorithm 5.3 to run slowly and consume memory.

Therefore, GMRES is the preferred solution algorithm when available. Numerical experiments have shown that the following GMRES options are reasonable when solving for the three-torus of the previous section. See [16] for an explanation of the different options used in implementing GMRES.

- Maximum iterations: 30
- Maximum restarts: 5 (so 150 total iterations maximum)
- Pre-conditioner: Equation (5.15)
- Cut-off tolerance: Either 1×10^{-3} or the minimum of $\sqrt{N_1 N_2 N_3} \times 10^{-5} / \left(\sqrt{5}\,\|\mathbf{f}\|\right)$ and $1/2$, whichever is larger.

The program always tries GMRES at least once at each Newton iteration, then defers to Algorithm 5.3 if GMRES does not converge successfully.

The Newton iterations stop successfully if either $\|\mathbf{y}\|$ or $\|\mathbf{f}\|$ are smaller than $\sqrt{N_1 N_2 N_3} \times 10^{-5}$. They stop unsuccessfully if Algorithm 5.3 fails or if the iterations do not stop successfully within ten steps.

In the particular continuation computation show below, a constant step size suffices to continue the torus to near breakdown. In other computations on the same torus, however, it has been useful to employ a correction strategy, where after an unsuccessful Newton attempt, λ reverts to the previous λ plus half the previous step increment, and the iterations start anew. In other words, if the Newton iterations do not converge for $\lambda = \lambda_0 + \Delta\lambda$, then the program tries again for $\lambda = \lambda_0 + \Delta\lambda/x$, where x is some number greater than 1 (typically $x = 2$). This is similar to the strategy used for the forced van der Pol torus in Section 4.2.2.

The following figures and tables illustrate the continuation process for the $27 \times 28 \times 29$ three-torus from $\lambda = 0$ to $\lambda = 0.46$ in constant steps of $\Delta\lambda = 0.02$. It is not known if the torus persists for significantly larger λ values, since there is no bifurcation analysis available as in previous examples.

Table 5.3 is similar to previous tables in that it shows some sample Newton iterations at chosen λ's, but it contains more information because the solution process is more complicated.

In the heading of table, "#" refers to the iteration number, and $\|\mathbf{f}\|$ and $\|\mathbf{y}\|$ are the same as before. If GMRES is successful, then the next two columns show the outer iteration (*i.e.*, the number of restarts plus 1), and the inner iteration (*i.e.*, the iteration, after restart) at convergence. The next column shows the residual: $\|J\mathbf{y} - \mathbf{f}\|$.

Memory requirements prohibit condition number estimates for the entire Jacobian, but, if GMRES is unsuccessful – and hence Algorithm 5.3 is the method of choice in solving the equation – then the last column ($\kappa(\bullet)$) shows the condition number of the long operator chain in Equation (5.13).

Table 5.3: Newton Iteration: Three-Torus

From λ	To λ	#	$\|\mathbf{f}\|$	$\|\mathbf{y}\|$	Out	In	Residual	$\kappa(\bullet)$
–	0.02	1	3.2	1.7	1	4	0.0020	–
		2	0.031	0.016	1	4	2.9×10^{-4}	–
			2.9×10^{-4}					
0.38	0.40	1	3.6	3.1	1	22	0.0032	–
		2	0.11	0.15	3	15	6.6×10^{-4}	–
			8.2×10^{-4}					
0.42	0.44	1	3.4	3.4	3	21	0.0032	–
		2	0.14	0.55	–	–	–	1.1×10^4
			0.0019					
0.44	0.46	1	3.4	3.9	–	–	–	1.6×10^4
		2	0.17	2.1	–	–	–	3.4×10^4
		3	0.0068	0.027	5	7	6.6×10^{-4}	–
			6.6×10^{-4}					

Visualizing a three-dimensional torus in $\mathbb{R}^8$ is not easy. The following figures are an attempt to convey the increasing curvature of the torus as λ increases, but they do not, and cannot, show all the points of the torus in a reasonable number of steps. They are similar to Figures 5.2 and 5.3, in that they show two coordinates in the plane, while the vertical dimension is artificial and represents a change in fixed-angular-coordinate sections as one of the coordinates increases. The difference now is that there are many such graphs available due to the additional angular coordinate.

For example, consider a graph with x_1 and x_2 in the horizontal plane and ϕ_2 on the vertical. Each horizontal slice represents a section as ϕ_1 increases with fixed ϕ_1 and ϕ_3. Therefore, for each different λ, there are N_3 different graphs available: one for each possible ϕ_3.

Figure 5.6 illustrates the concept. It shows the x_1,x_2 coordinates extended along ϕ_2 at $\lambda = 0.44$ for four different values of ϕ_3.

Figure 5.7 illustrates the continuation process along one slice. It shows the x_1,x_2 coordinates extended along ϕ_3 at $\lambda = 0.2$, 0.3, 0.42,and 0.46 at constant $\phi_2 = 0$.

Figure 5.8 is similar, except that x_7 and x_8 are the horizontal coordinates extended

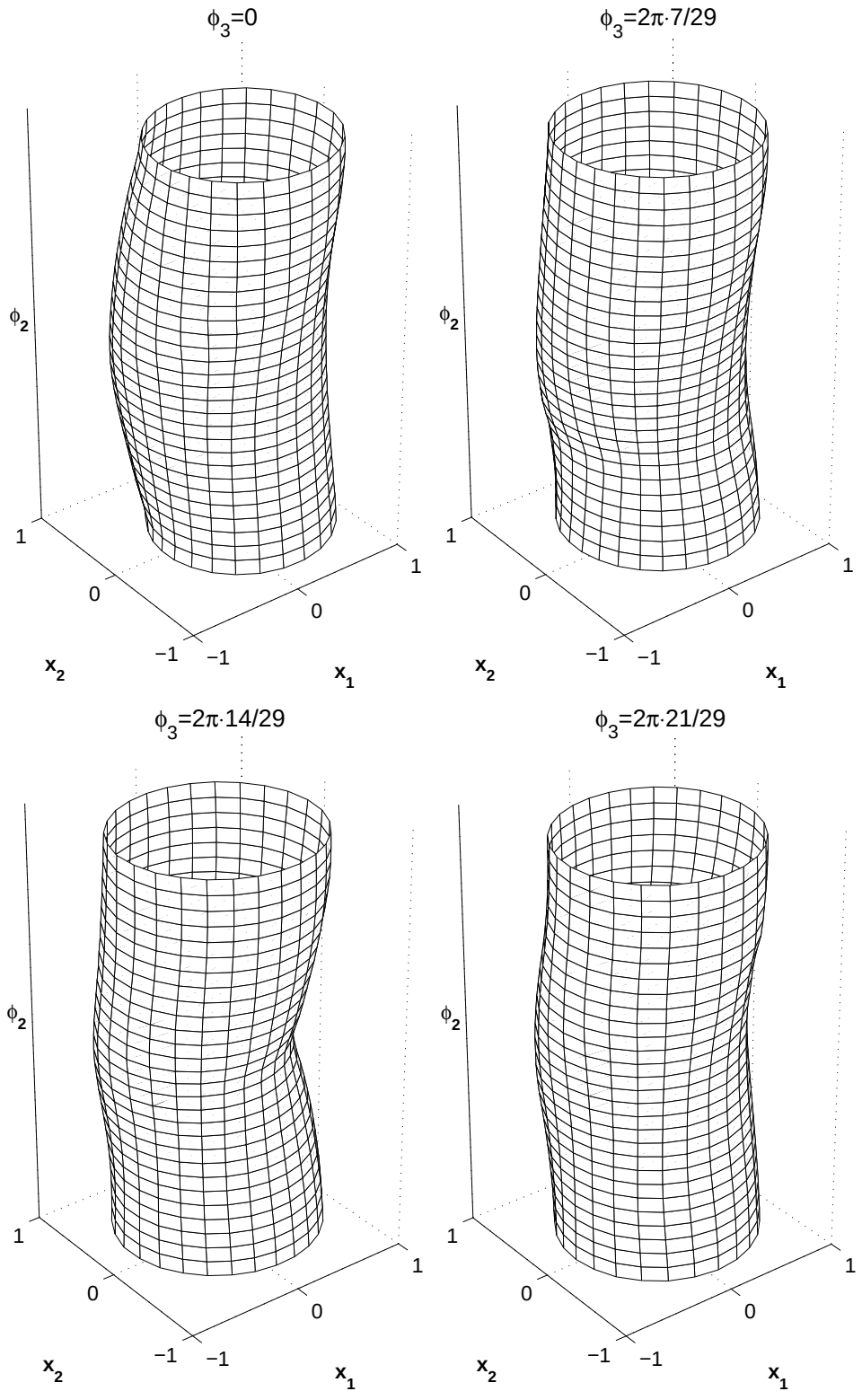

Figure 5.6: Representative Slices of the Three-Torus at $\lambda = 0.44$

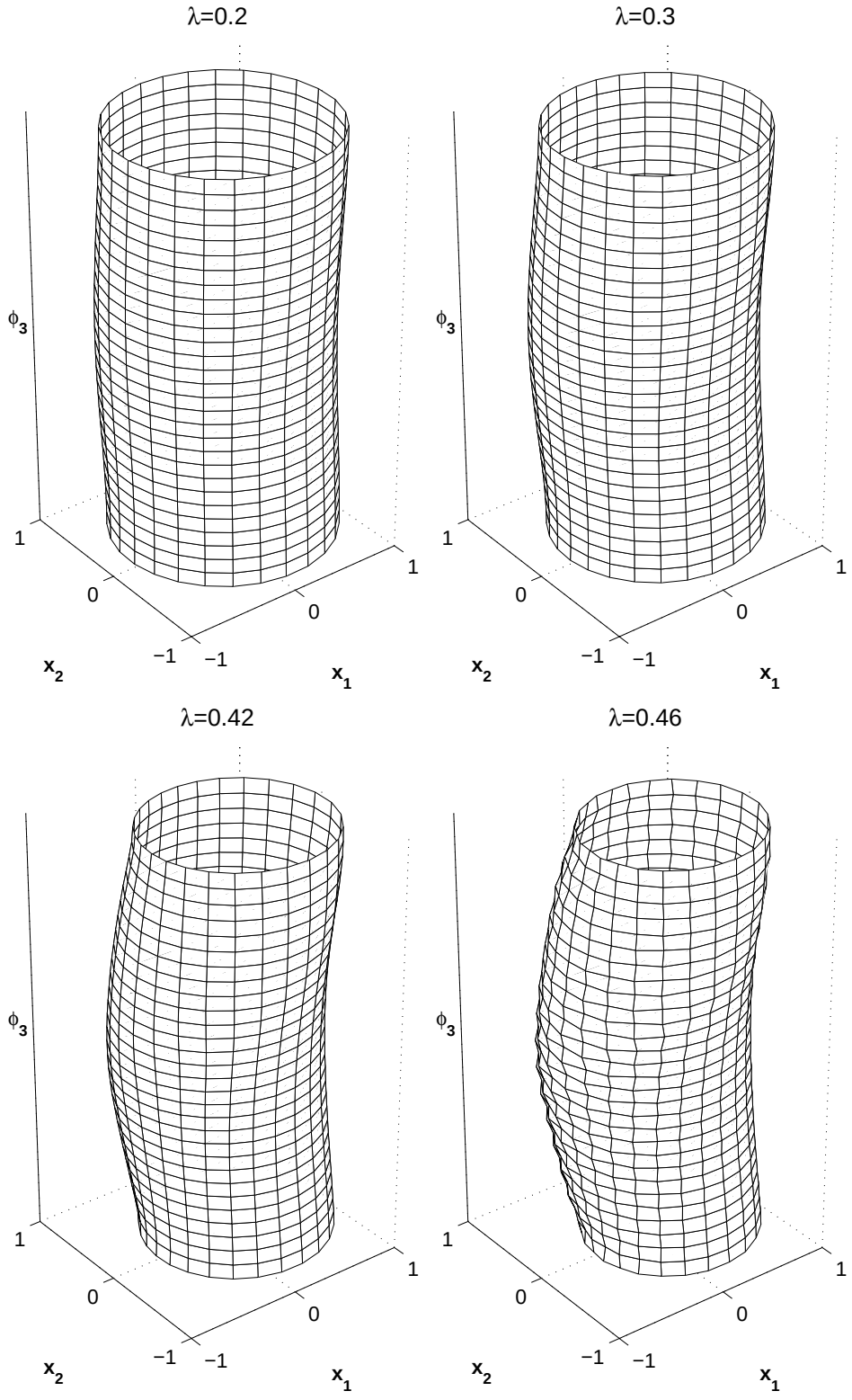

Figure 5.7: Continuation of One Slice of the Three-Torus

along ϕ_1, with ϕ_2 constant at zero. The scale in the horizontal direction is smaller. This figure shows that the torus is becoming pinched, and hence loses smoothness, which is a potential breakdown mechanism.

As discussed previously, it is unknown whether the torus persists far beyond the observed breakdown point of $\lambda = 0.46$. Non-smooth surfaces are clearly developing in the solution at $\lambda = 0.46$, but this may be due to a breakdown in the solution method rather than a breakdown in the torus. Nevertheless, the orthogonality technique seems to provide a reasonable picture of the continuation process for a significant increase in λ, which is an improvement over other techniques that require too much computation time to examine a three-torus, even one as coarsely represented as the current example.

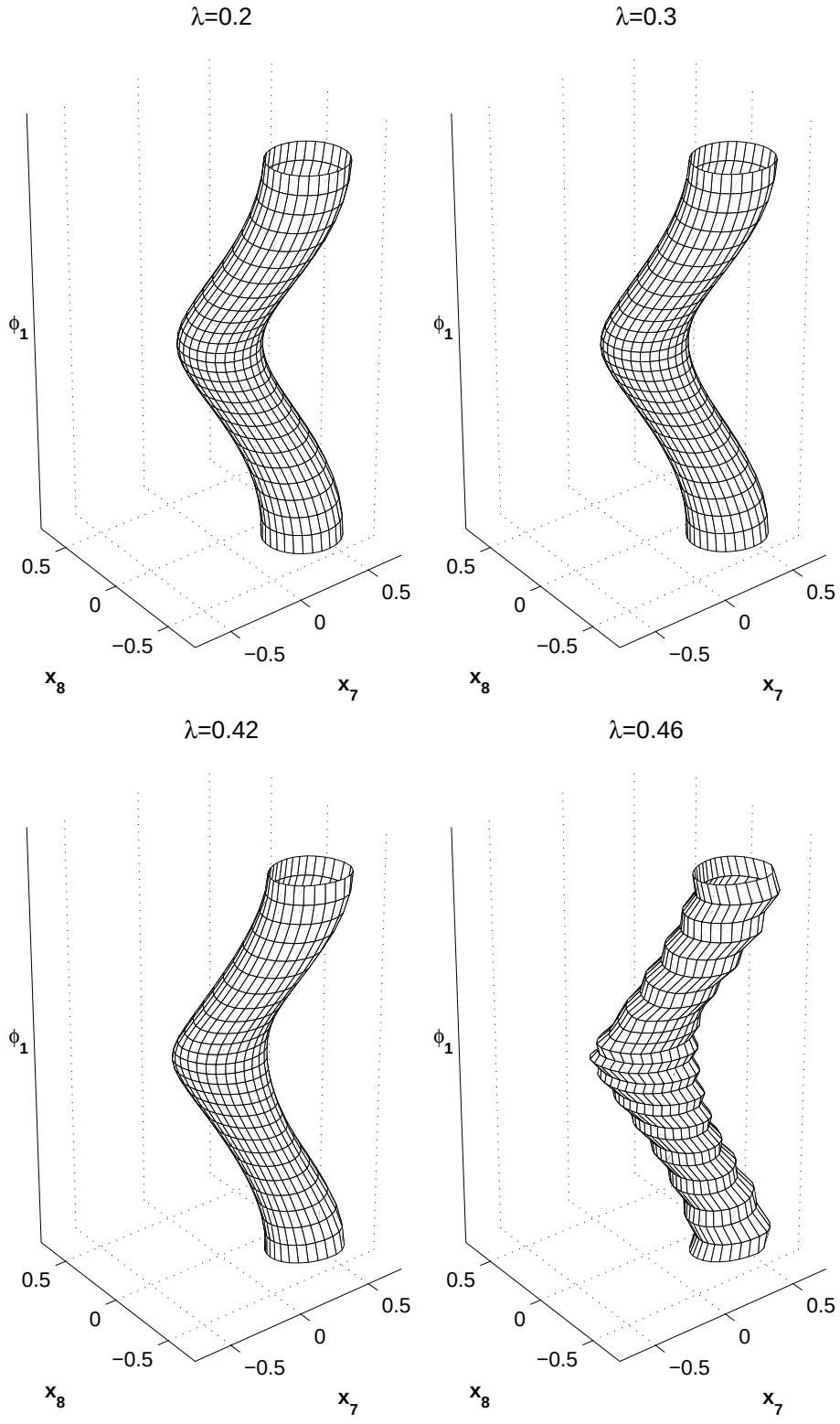

Figure 5.8: Continuation of Coupling Medium in Three-Torus

REFERENCES

[1] Aronson, D. G., Doedel, E. J., and Othmer, H. G., "An analytical and numerical study of the bifurcations in a system of linearly-coupled oscillators," *Physica D*, vol. 25, no. 1–3, pp. 20–104, 1987.

[2] Ascher, U. M., Mattheij, R. M., and Russell, R. D., *Numerical Solution of Boundary Value Problems for Ordinary Differential Equations*. Prentice Hall Series in Computational Mathematics, Englewood Cliffs, New Jersey: Prentice Hall, 1988.

[3] Ascher, U. M. and Russell, R. D., "Reformulation of boundary value problems into standard form," *SIAM Review*, vol. 23, no. 2, pp. 238–254, 1981.

[4] Berman, A. and Plemmons, R. J., *Nonegative Matrices in the Mathematical Sciences*. SIAM Classics in Applied Mathematics, Philadelphia: Society for Industrial and Applied Mathematics, 1994.

[5] Beyn, W. J., "The numerical computation of connecting orbits in dynmical systems," *IMA Journal of Numerical Analysis*, vol. 9, no. 3, pp. 379–405, 1990.

[6] Broer, H. W., Osinga, H. M., and Vegter, G., "Algorithms for computing normally hyperbolic invariant manifolds," *Zietschrift für Angewandte Mathematik und Physik*, vol. 48, no. 3, pp. 480–524, 1997.

[7] Dieci, L. and Bader, G., "Solution of the systems associated with invariant tori approximation ii: Multigrid methods," *SIAM Journal of Scientific Computing*, vol. 15, no. 6, pp. 1375–1400, 1994.

[8] Dieci, L. and Bader, G., "Block iterations and compactification for periodic block dominant systems associated to invariant tori approximation," *Applied Numerical Mathematics*, vol. 17, pp. 251–274, 1995.

[9] Dieci, L. and Eirola, T., "Numerical dynamical systems." Class notes, May 2001.

[10] Dieci, L. and Lorenz, J., "Computation of invariant tori by the method of characteristics," *SIAM Journal of Numerical Analysis*, vol. 32, no. 5, pp. 1436–1474, 1995.

[11] Dieci, L. and Lorenz, J., "Lyapunov-type numbers and torus breakdown: Numerical aspects and a case study," *SIAM Journal of Scientific and Statistical Computing*, vol. 14, no. 1–3, pp. 79–103, 1997.

[12] Dieci, L., Lorenz, J., and Russell, R. D., "Numerical calcuation of invariant tori," *SIAM Journal of Scientific and Statistical Computing*, vol. 12, no. 3, pp. 607–647, 1991.

[13] Fenichel, N., "Persistence and smoothness of invariant manifolds for flows," *Indiana University Mathematics Journal*, vol. 21, pp. 193–226, 1971.

[14] Ge, T. and Leung, Y. T., "Construction of invariant torus using toepliz jacobian matrices / fast fourier transform approach," *Nonlinear Dynamics*, vol. 15, no. 3, pp. 283–305, 1998.

[15] Golub, G. H. and Loan, C. F. V., *Matrix Computations*. Baltimore: Johns Hopkins University Press, third ed., 1996.

[16] Greenbaum, A., *Iterative Methods for Solving Linear Systems*. SIAM Frontiers in Applied Mathematics, Philadelphia: Society for Industrial and Applied Mathematics, 1997.

[17] Guckenheimer, J. and Holmes, P., *Nonlinear Oscillations, Dynamical Systems, and Bifurcations of Vector Fields*. No. 42 in Springer Series in Applied Mathematical Sciences, New York: Springer-Verlag, 1985.

[18] Hale, J., *Ordinary Differential Equations*. Malabar, Florida: Krieger Publishing Company, second ed., 1980.

[19] Higham, N. J. and Tisseur, F., "A block algorithm for matrix 1-norm estimation, with an application to 1-norm pseudospectra," *SIAM Journal of Matrix Analysis and Applications*, vol. 21, no. 4, pp. 1185–1201, 2000.

[20] Kosinski, A., *Differential Manifolds*, vol. 138 of *Pure and Applied Mathematics*. San Diego: Academic Press, Inc., 1993.

[21] Krauskopf, B. and Osinga, H. M., "Investigating torus bifurcations in the forced van der pol oscillator," in *Numerical Methods for Bifurcation Problems and Large-Scale Dynamical Systems*, vol. 119 of *IMA Volumes in Mathematics and its Applications*, (New York), pp. 199–208, IMA, Springer, 2000.

[22] Langford, W. F., "Numerical studies of torus bifurcations," *International Series of Numerical Mathematics*, vol. 70, pp. 285–294, 1984.

[23] Langford, W. F., "Periodic and steady-state mode interactions lead to tori," *SIAM Journal of Applied Mathematics*, vol. 70, no. 1, pp. 22–48, 1984.

[24] Liu, L., Moore, G., and Russell, R. D., "Computation and continuation of homoclinic and heteroclinic orbits with arclengh parameterization," *SIAM Journal of Scientific Computing*, vol. 18, no. 1, pp. 69–93, 1997.

[25] Matsumoto, T., Chua, L., and Tokunaga, R., "Chaos via torus breakdown," *IEEE Transactions on Circuits and Systems*, vol. CAS-34, no. 3, pp. 240–253, 1987.

[26] Mingyou, H., Küpper, T., and Masbaum, N., "Computation of invariant tori by the fourier methods," *SIAM Journal of Scientific Computing*, vol. 18, no. 3, pp. 918–942, 1997.

[27] Moore, G., "Computation and parameterization of periodic and connecting orbits," *IMA Journal of Numerical Analysis*, vol. 15, no. 2, pp. 245–263, 1995.

[28] Moore, G., "Geometric methods for computing invariant manifolds," *Applied Numerical Mathematics*, vol. 17, no. 3, pp. 319–331, 1995.

[29] Moore, G., "Computation and parameterisation of invariant curves and tori," *SIAM Journal of Numerical Analysis*, vol. 33, no. 6, pp. 2333–2358, 1996.

[30] Moore, G. and Hubert, E., "Algorithms for constructing stable manifolds of stationary solutions," *IMA Journal of Numerical Analysis*, vol. 19, no. 3, pp. 375–424, 1999.

[31] Osinga, H. M., *Computing Invariant Manifolds – Variations of the Graph Transform*. PhD dissertation, University of Groningen, 1996.

[32] Othmer, H. G., "Synchronization, phase-locking and other phenomena in coupled cells," in *Temporal Order* (Rensing, L. and Jaeger, N. I., eds.), no. 23 in Springer Series in Synergetics, pp. 130–143, Heidelberg: Springer-Verlag, 1985.

[33] Othmer, H. G., ed., *Nonlinear Oscillations in Biology and Chemistry*. New York: Springer-Verlag, 1986.

[34] Othmer, H. G. and Watanabe, M., "On the collapse of resonance structure in a three-parameter family of coupled oscillators," *Rocky Mountain Journal of Mathematics*, vol. 18, no. 2, pp. 403–433, 1988.

[35] Reichelt, V., "Computing invariant tori and circles in dynamical systems," in *Numerical Methods for Bifurcation Problems and Large-Scale Dynamical Systems*, vol. 119 of *IMA Volumes in Mathematics and its Applications*, (New York), pp. 407–437, IMA, Springer, 2000.

[36] Trummer, M. R., "Spectral methods in computing invariant tori," *Applied Numerical Mathematics*, vol. 34, no. 2–3, pp. 275–292, 2000.

[37] Valkering, T. A., Hooijer, C. L. A., and Kroon, M. F., "Dynamics of two capacitively coupled josephson junctions in the overdamped limit," *Physica D*, vol. 135, no. 1–2, pp. 137–153, 2000.

[38] Veldhuizen, M. V., "A new algorithm for the numerical approximation of an invariant curve," *SIAM Journal of Scientific and Statistical Computing*, vol. 8, no. 6, pp. 951–962, 1987.

[39] Watanabe, M. and Othmer, H. G., "Persistence of invariant tori in systems of coupled oscillators i: Regular and singular problems," *Differential and Integral Equations*, vol. 2, no. 2, pp. 331–368, 1991.

[40] Watanabe, M. and Othmer, H. G., "Persistence of invariant tori in systems of coupled oscillators ii: Degenerate problems," *SIAM Journal of Mathematical Analysis*, vol. 22, no. 6, pp. 1584–1630, 1991.

[41] Wiggins, S., *Normally Hyperbolic Invariant Manifolds in Dynamical Systems*. New York: Springer-Verlag, 1994.

VITA

Bryan Rasmussen received B.S.E. and M.S.E. degrees in Mechanical Engineering from the University of Alabama in Huntsville in Spring, 1997 and Spring, 1999 respectively. He has professional experience in engineering and applied mathematics, including an undergraduate cooperative education stint at Marshall Space Flight Center in Huntsville, Alabama; a three-month stay at ONERA in Palaiseau, France; a three-month internship at Sandia National Laboratories in Livermore, California; and various research and teaching assistantships throughout graduate school. He married his wife, Amanda in May of 2000. They live in Dunwoody, Georgia with two cats, and by the time this thesis is disseminated, their first child will have been born.